Connected In Vitro Tissue Models for Oral Drug Delivery

Jepsen, Morten Leth

Publication date:
2019

Document Version
Publisher's PDF, also known as Version of record

Connected *In Vitro* Tissue Models for Oral Drug Delivery

By Morten Leth Jepsen

Supervisor: Martin Dufva
Co-supervisors: Line Hagner Nielsen and Anja Boisen

December 2019

PhD Thesis

Technical University of Denmark
Department of Health Technology

The Danish Research Foundation and Villum Foundation's Center for Intelligent Drug Delivery and Sensing Using Microcontainers and Nanomechanics (IDUN)

Preface

The research included in this thesis was carried the Technical University of Denmark at the department of Health Technology (former Nanotechnology). Some of the research was carried out at the Division of Cellular Medicine, School of Medicine, Dundee University during a two months external stay. The PhD project was supervised by Martin Dufva and co-supervised by Line Hagner Nielsen and Anja Boisen. The work was carried out from December 2016 to December 2019.

This PhD project was funded by the Danish National Research Foundation (DNRF122) and Villum Fonden (Grant No. 9301) for Intelligent Drug Delivery and Sensing Using Microcontainers and Nanomechanics (IDUN) and was a part of the IDUN project.

Kgs. Lyngby,
14th December 2019
Morten Leth Jepsen

Acknowledgements

First, I want to thank my supervisors Martin, Line, and Anja for their support and guidance. Line for always telling to go with my ideas and trust in the research directions I believe in. Martin for teaching me to accept the situation and look ahead for the next experiment. Anja for creating a good work environment in the IDUN group. I believe that their guidance has helped me grow both as a person and as a scientist. I am thankful for been giving the chance to pursue my own ideas.

I want to thank my family and friends for their love and support. Julie for her unwavering love and support and for always waiting at home with a smile when I arrived after long days at DTU.

I want to thank the two groups I have been a part of here at DTU both the IDUN group and the FAST group. I have had a great time with all the wonderful group members of these two groups. I will miss coming to work and chatting with everyone. I want to thank Chiara, Juliane, Stine, and Varadarajan, who have been the best of friends. I was fortunate to have the chance of working with Chiara for the last experiments and to have the joy of sharing office with Stine. I would like to thank Chiara, Juliane, Stine, and Rolf for correcting my writing.

I also want to thanks my students Andreas, Anna, Christian, Joen, Julie, Monica, and Sofia, whom I have enjoyed supervising and spending time with in the laboratory.

I want to thank the technical staff including Christina, Lars, Lotte, Lene, Jannik, and Helene for keeping the laboratories functional so that I could do my experiments. Furthermore, thanks to Dorthe, Louise, Julie, Sanne, and Tine without whom I would not have been able to fill out all documentation and practicalities.

I was fortunate to spend two month at Division of Cellular Medicine, School of Medicine, Dundee University under Dr. Graham Rena. I want to thank Graham for letting me into his laboratory to test out my ideas and to all the member of the Division of Cellular Medicine for making me fell home at the hospital and in Dundee.

In short, all the mentioned people has made it possible for me to spend three years working and thinking on this PhD project which has been fun and challenging. I hope that is reflected in this thesis.

Abstract

Oral drug delivery is the preferred drug administration route, however, many oral drugs are rejected during *in vivo* studies. Before an oral drug reaches the systemic circulation, it is exposed to first pass metabolism which reduces the amount of active drug reaching its target. The first pass metabolism is a combination of the gastrointestinal tract which absorbs the drug into the blood vessels which transport the drug to the liver which metabolizes the drug. In drug discovery, good prediction of the first pass metabolism can help to select the best oral drugs and formulations for the subsequent *in vivo* studies.

To predict the first pass metabolism, three *in vitro* cell-based tissue models have been developed throughout this PhD project. The cells are grown on or in soft hydrogel growth-matrices in 3D-printed inserts which are compatible with commercial titer plates. To secure *in vivo*-like growth matrices, a method for measuring hydrogel stiffness has been developed and employed to characterize the hydrogel growth-matrices. The Caco-2 cell line, HUVEC cells, and the HepG2 cell line are used in this project to simulate the small intestinal tissue, the vascular tissue and the liver tissue, respectively. The 3D-printed inserts with each their tissue model can easily be connected by assembling the inserts on top of each other. This allows for investigation of interactions between the tissues.

The Caco-2 small intestinal tissue model displays drug permeabilities comparable to what is previously seen for this cell line. However, the electrical resistance is closer to that found *in vivo* then other Caco-2 based models. The HUVEC vascular endothelial tissue model only serves as a diffusional barrier. This tissue model can in the future be improved by addition of shear stress to gain *in vivo*-like flow resembling the bloodstream. The HepG2 liver tissue model grows as spheroids in 3D giving the hepatic cells gradients of nutrients resembling the *in vivo* liver tissue.

In conclusion, this PhD project covers an *in vitro* method for predicting the first pass metabolism of drugs. Potentially, this method can increase the success rate of *in vivo* studies and reduce drug development costs.

Resumé

Orale lægemidler er den foretrukne lægemiddel administrationsvej, men mange orale lægemidler bliver frasorteret ved *in vivo*-studier. Før et oral lægemiddel når det systemiske blodkredsløb, undergår det førstepassage-metabolisme, hvilket reducerer mængden af aktivt lægemiddel, der når dets mål. Førstepassage-metabolismen er en kombination af mavetarmsystemet, der absorberer lægemidlet til blodkarrerne, der transporterer lægemidlet til leveren, der nedbryder lægemidlet. I lægemiddeludvikling kan en god forudsigelse af førstepassage-metabolismen hjælpe med at udvælge de bedste lægemidler og formuleringer til efterfølgende *in vivo*-studier.

For at forudse førstepassage-metabolismen er tre *in vitro*-cellebaserede vævsmodeller blevet udviklet i dette PhD-projekt. Cellerne vokser på eller i en blød hydrogel-vækstmatrix i 3D-printede holdere, der passer i kommercielle brøndplader. For at sikre *in vivo*-lignende vækst-matricer er en metode til at karakterisere hydrogel hårdhed blevet udviklet og brugt til at måle hydrogel-vækstmatricer. Caco-2-cellelinjen, HUVEC-celler og HepG2-cellelinjen er brugt i dette projekt til at simulere tyndtarmsvæv, vaskulært væv og levervæv. De 3D-printede holdere med hver sin vævsmodel kan nemt forbindes ved at samle dem oven på hinanden. Dette giver mulighed for at undersøge interaktioner mellem vævene.

Tyndtarmsmodellen af Caco-2-celler har lægemiddel-permeabilitet tæt op ad det, der før er set for denne cellelinje. Dog er den elektriske modstand i den præsenterede model tættere på det, man ser *in vivo* end andre Caco-2-modeller. Den vaskulære endotelmodel af HUVEC-celler tjener kun som en diffusionsbarriere. Denne vævsmodel kan i fremtiden forbedres ved at tilføje shear stress for at opnå et *in vivo*-lignende flow, der minder om blodkredsløbet. Levermodellen af HepG2-celler vokser som sfæroider i 3D. Dette giver hepatocytterne gradienter af næringsstoffer som minder om det, man finder i *in vivo* levervæv.

Dette PhD-projekt præsenterer en *in vitro* metode til at forudsige førstepassage-metabolisme af lægemidler. Denne metode kan potentielt øge succesraten af *in vivo*-studier og reducere omkostningerne ved lægemiddeludvikling.

Publications

Paper I
M. L. Jepsen, A. Willumsen, C. Mazzoni, L. H. Nielsen, A. Boisen, and M. Dufva, '3D-printed stackable titer plate inserts supporting three interconnected tissue models for drug screening,'
Submitted to *Advanced Biosystems*

Paper II
M. L. Jepsen, L. H. Nielsen, A. Boisen, K. Almdal, and M. Dufva, 'Characterization of thin gelatin hydrogel membranes with balloon properties for dynamic tissue engineering,' *Biopolymers.* vol. 110, no. 1, p. e23241, 2019.

Paper III
J. R. Jørgensen, **M. L. Jepsen**, L. H. Nielsen, M. Dufva, H. M. Nielsen, T. Rades, A. Boisen, and A. Müllerts, 'Microcontainers for oral insulin delivery–In vitro studies of permeation enhancement,' *European Journal of Pharmaceutics and Biopharmaceutics* vol. 143, pp. 98-105, 2019
(Results not included or discussed in thesis)

Contribution to Papers

Paper I
I performed and planned the experimental work and data analysis with help from A. Willumsen for work with hepatocytes and from C. Mazzoni for work with valacyclovir. From interpretation of the results I wrote the scientific article.

Paper II
I performed and planned the experimental work and data analysis. From interpretation of the results I wrote the scientific article.

Paper III
I helped with confocal microscopy and planning of what to stain cells with.

Conference Contributions

1. **M. L. Jepsen**, A. Willumsen L. H. Nielsen, K. Almdal, A. Boisen, and M. Dufva, '*In vitro* triple cell model in a 3D printed platform for assessing drug absorption and metabolism,' *Controlled Release Society Meeting*, Valencia, Spain, 2019. (Oral presentation)

2. **M. L. Jepsen**, L. H. Nielsen, K. Almdal, A. Boisen, and M. Dufva, '3D printed system for based on hydrogels for drug transport,' *Northern Pharma Network Meeting*, Odense, Denmark, 2018. (Poster presentation)

3. **M. L. Jepsen**, L. H. Nielsen, K. Almdal, A. Boisen, and M. Dufva, '3D printed system for testing intestinal drug transport,' *11th World Meeting on Pharmaceutics, Biopharmaceutics and Pharmaceutical Technology*, Granada, Spain, 2018. (Poster presentation)

Contents

List of Figures

List of Tables

Glossary

2D Two Dimensional

3D Three Dimensional

ABS Acrylonitrile Butadiene Styrene

ADME Absorption Distribution Metabolism and Excretion

AM Additive Manufacturing

AMPK Adenosine Monophosphate-activated Protein Kinase

BCS Biopharmaceutics Classification System

CAD Computer-Added Design

cAMP Cyclic Adenosine Monophosphate

CYP Cytochrome P450

DFR Dry Film Resist

ECM Extracellular Matrix

FDM Fused Deposition Modeling

G6Pase Glucose-6-Phosphatase

GALT Gut-Associated Lymphoid Tissue

HBSS Hank's Balanced Salt Solution

hOCT1 human Organic Cation Transport 1

HUVEC Human Umbilical Vein Endothelial Cells

IC_{50} Half Maximal Inhibitory Concentration

IV Intravenous

K_f Fluid filtration coefficient

L_p Hydraulic conductivity

logP Partition coefficient

MCT1 Monocarboxylate Transporter 1

MDCK Madin-Darby Canine Kidney

P_{app} Apparent solute Permeability

PAMPA Parallel Artificial Membrane Permeability Assay

PDMS Polydimethylsiloxane

PEPT1 human Peptide Transport 1

PLA Polylactic Acid

RA Rheumatoid Arthritis

SLA Stereolithography

TEER Transepithelial/transendothelial Electrical Resistance

TNFα Tumor Necrosis Factor Alpha

UV Ultra Violet

VCAM-1 Vascular Cell Adhesion Molecule 1

VSMCs Vascular Smooth Muscle Cells

ZO-1 Zonula Occludens-1

Chapter 1

Introduction

This introductory chapter provides an overview of the field of oral drug administration. The chapter focuses on the oral drug route and how different tissues affect how much active drug reaches its target.

Drug development is a long and expensive process. The average cost of bringing a new drug to the market is ~$1.8-2.6 billion.[1,2] The steps of developing a new drug include drug discovery, formulation, pre-clinical testing, clinical trials, and regulatory approval (Figure 1.1).

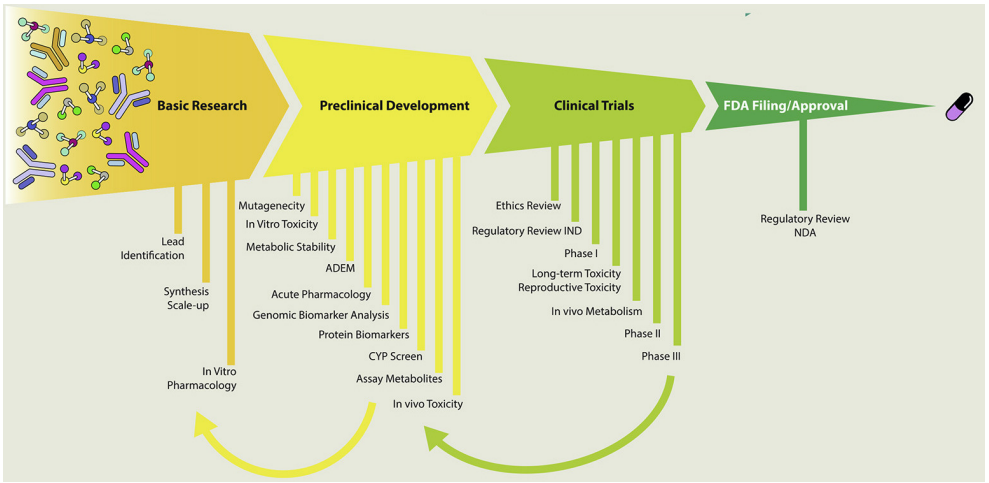

Figure 1.1: Schematic representation of the individual step in drug discovery and development processes. Reprinted with permission from.[3]

Early in drug discovery, a biological target is identified such as a receptor, protein, or gene.[3] This is followed by development and optimization of drug formulation and the drug's target specificity. Pre-clinical testing includes *in vitro* cell studies and *in vivo* animal studies. *In vitro* studies are used to obtain information about drug absorption and metabolism and drug interactions

affecting metabolism.[4] This is collected under the common abbreviation absorption, distribution, metabolism, and excretion (ADME). Absorption covers how well a drug is absorbed into the systemic circulation of the body. Distribution covers how the drug is carried to its effector site. Metabolism covers how certain mechanisms in the body change the drug such as inactivation or activation. Excretion covers how the drug and its metabolites are removed from the body.

A good *in vitro* prediction of ADME helps foresee how a drug will behave during *in vivo* studies. However, 90 % of lead drug candidates identified using *in vitro* methods fail to reach the market.[4,5] As, they are rejected in *in vivo* studies, clinical trials, and regulatory approval. Currently, ADME studies are performed with cell cultures modeling single tissues, however, *in vivo* tissues affect drugs in synergy. For instance, efficient drug distribution in systemic circulation leads to a large concentration gradient which favorizes further absorption and metabolized drugs can be excrete more efficient.

In summary, better modeling of ADME in the pre-clinical phase can help to identify the best drug candidates for *in vivo* studies thereby reducing the overall cost of drug development.

1.1 Drug Delivery

When treating a disease with a drug, the drug must reach its target in its active form to have the desired effect. There are several ways to administer drugs depending on the characteristics of the given drug and the target. The main focus of this chapter is on how drugs get from outside of the body to systemic circulation and not on how the target is reached once the drug is in systemic circulation.

The four main groups of drug delivery include enteral (i.e. oral), parenteral (e.g. intravenous (IV)), mucous membrane (e.g. lungs), and transdermal delivery (e.g. skin).[6] The tissues of the gastrointestinal tract are mucosal, however, this route is excluded from the mucous membrane drug delivery group. The oral route is excluded from the mucous membrane route because orally administered drugs go through the harsh gastrointestinal environment and can be metabolism in the liver before reaching systemic circulation.

The oral drug route is preferred due to its convenience, low costs, safety, and high patient compliance.[7,8] When patients are given a drug that has the same efficacy and side effects orally and IV administrated, they prefer the oral.[9,10] Oral administration can be perceived more convenient by the patient, since they have the possibility to stay at home during the treatment and can easily continue their jobs compared to IV treatment where they would need to go to the hospital.[11] The treatment costs can be lowered due to avoidance of hospitalization, sterile manufacturing, and assistance of trained personal.[8] This preference of oral drugs has led to that the pharmaceutical

market is composed of 60 % oral drugs.[12] However, for some drugs such as macromolecular drugs (e.g. insulin) oral drug delivery can be a challenge due to their large size.[13,14] Whereas, for the anabolic steroid testosterone the challenge is extensive metabolism in the liver.[15] Hence, there is a need to gather information to identify why drugs fail in oral delivery and to evaluate attempts to increase the amount of active drug reaching systemic circulation.

In summary, there is a large market and interest from patients in oral drug delivery, but there are still major challenges in delivering some drugs orally. It is of interest to gain information on oral drug delivery and find causes of and solutions to the challenges.

1.1.1 The Oral Drug Delivery Route

Bioavailability, for a drug administered by a given delivery route, is a measure of amount of active drug reaching systemic circulation compared to the given drug dose.[16] For orally administered drugs the first pass metabolism affects the oral bioavailability. The first pass metabolism is what orally administered drugs go through before reaching systemic circulation. It can cause some drugs to have a low bioavailability either by hindering a drug in reaching circulation or inactivating the drug before it reaches circulation.[17] Orally administered drugs are swallowed and absorbed through the gastrointestinal tract. The gastrointestinal tract consists of the mouth, esophagus, stomach, small intestine, colon, and appendix (Figure 1.2A).

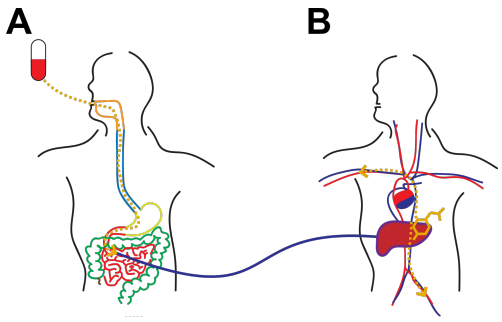

Figure 1.2: Schematic representation of the oral administration pathway: A) Orally administered drugs are swallowed and travel to the small intestine. B) The blood stream carries the drugs to the liver before reaching systemic circulation.

Depending on the drug and the absorption strategy, absorption can be through different organs. Oral drugs can be absorbed through the stomach,[18] small intestine, and colon.[19] However, 90 % of nutrient absorption takes place in the small intestine and it is the main site of drug absorption.[20] From the gastrointestinal tract drugs travel via the portal vein to the liver (Figure 1.2B)[21]. In the liver the drugs will undergo further metabolism before reaching systemic circulation.[22]

The Small Intestine

The small intestine consists of three sections duodenum, jejunum, and ileum.[19,23] The duodenum is short and has fast passage hence low absorption of drugs, whereas the jejunum is the main place of drug absorption. The jejunum is especially well-suited for absorption due to its highly active peristalsis.[24] The small intestine has a large surface area due to a unique anatomy of three types of structural projections; plicae circulares, villi, and microvilli, these increase the area three, ten, and 20 times, respectively (Figure 1.3B-D). This results in a 600 times increase in the absorptive area.

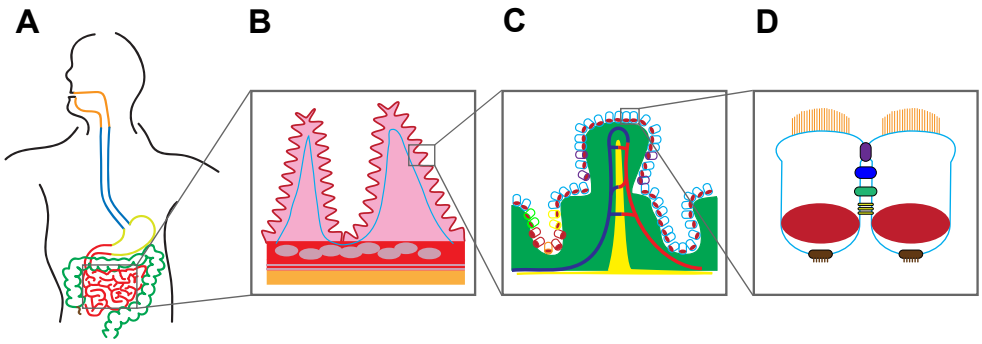

Figure 1.3: Schematic representation of the small intestine: A) The digestive system. B) Plicae circulares. C) Villi-crypt unit with various cell types. D) Enterocytes with microvilli on top and different kinds of junctions; tight junctions (purple), adherens junctions (blue), desmosomes (green), gap junctions (yellow), and anchoring junction (brown).

Enterocytes, which are polarized epithelial cells covering the villi, are the absorptive cells of the small intestine, however, other types of cells exist in the villi-crypt unit of the small intestine (Figure 1.3C).[25] Between the villi are the crypts of Lieberkühn housing enteric endocrine-cells, stem cells, Paneth cells, and undifferentiated crypt cells.[23,26] On the villi, apart from enterocytes, goblet cells reside. Goblet cells secrete high-molecular-weight glycoproteins known as mucins.[27,28] Mucins along with bound water, electrolytes, sloughed epithelial cells, and secreted immunoglobulins make up a protective barrier known as mucus. The mucus is both a physical and chemical barrier against luminal substances such as enteric bacteria and environmental and bacterial toxins.[28] Underneath the mucus are the enterocytes to secure that nothing that is not supposed to enter the body enters the body.

The enterocytes are tightly bound to each other through junctions (Figure 1.3D). Between the cells are several junction types such as tight junction (zonula occludens), adherens junction (zonula adhaerens), desmosome (macula adhaerens), and gap junction.[29,30] Of these junctions, the tight junctions secure the tight barrier of the small intestine (Figure 1.4).[30] Tight junctions consist of multiple proteins one of these is zonula occludens-1 (ZO-1) which is

used in cell cultures for assessment of membrane integrity by immunostaining and visualization by fluorescence microscopy.[31].

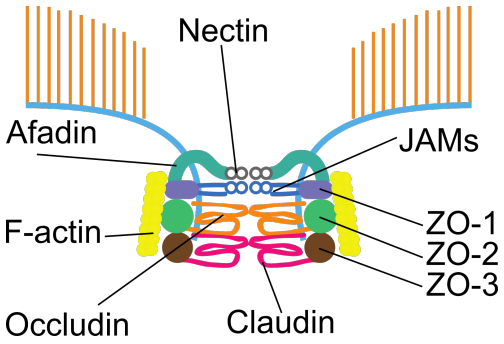

Figure 1.4: Cartoon of tight junction associated proteins between enterocytes: Including junctional adhesion molecules (JAMs) and zonula occludens proteins (ZO). Modified from.[32]

A drug can be absorbed in several ways depending on the characteristic of the drug (Figure 1.5). Drugs are absorbed across the small intestinal barrier by either passive or active transport. Lipophilic compounds can use the passive transcellular route as they can cross the lipid bilayer of the cell membrane (Figure 1.5A).[33] Whereas, hydrophilic drugs can also be passively diffuse across the cell layer but are restricted to the paracellular route (Figure 1.5B),[31] since hydrophilic molecules cannot be distributed into cell membranes. It is the tight junctions that regulate paracellular passage of ions, water, and molecules.[34]

Active transport routes include carrier mediated transport and transcytosis. In carrier mediated transport, the carriers are situated both at the apical and basolateral membrane (Figure 1.5C). Peptides, amino acids, and their drug analogs can be transported by carriers.[35] In contrast, proteins and small nucleotides are transported by transcytosis (Figure 1.5D).[33,36] The first step in transcytosis is endocytosis, where a material is taken up by the cell into intracellular vesicles. Endocytosed drugs are either exocytosed basolaterally, broken down, or recycled through efflux mechanisms (Figure 1.5D-F).

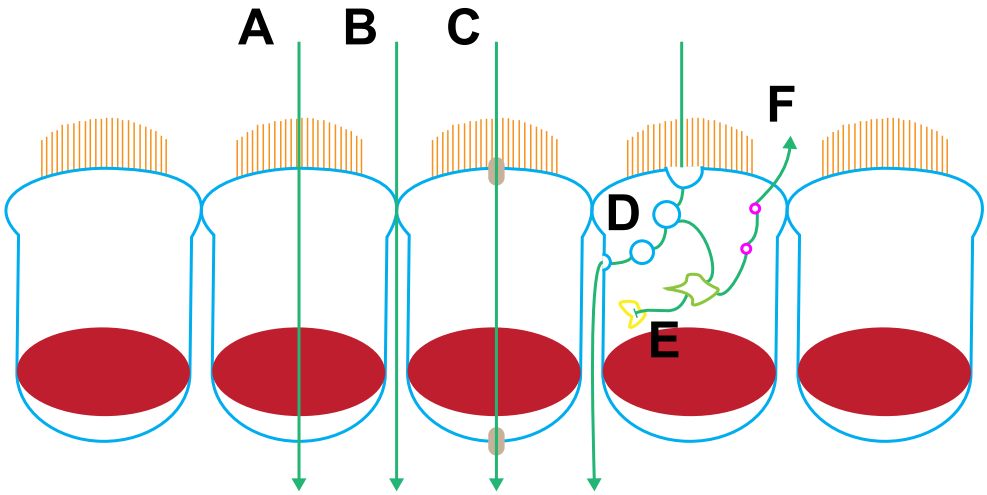

Figure 1.5: Drawing of transport ways through intestinal epithelial cell barrier: A) Passive transcellular transport. B) Passive paracellular transport. C) Active carrier mediated transport. D) Active transcytosis. E) Endocytose resulting in intestinal metabolism. F) Efflux.

Even though, drugs mainly travel to the liver via the portal vein, the villi also have lymph drainage.[37] The molecular mass and water solubility determine whether drugs go to the portal vein or the intestinal lymphatic system.[38,39] Hence, aiming for the lymphatic system in oral drug delivery can be used to circumvent the metabolism from the liver. Oral testosterone administration has been improved by targeting the lymphatic system with a lipophilic ester of testosterone.[15] Another approach is with liposomal formulations.[40]

In summary, the small intestine is divided into villi-crypt units giving rise to a small intestinal barrier consisting of a monolayer of tightly bound epithelial cells. If a drug is successful in reaching the capillaries of the small intestinal villi they are transported to the liver for further metabolism before reaching systemic circulation.

The Liver

One of the main functions of the liver is to protect the body against intoxication, by ensuring that toxic compounds are inactivated and transformed to a form in which they can be excreted by the kidneys.[22] The kidneys filter the blood from metabolic compounds and toxins while maintaining the body's fluid status, electrolyte balance, and acid-base balance by reabsorption.[41,42] However, lipid-soluble drugs are able, through back diffusion, to pass through the tubule cells of the kidneys after glomerular filtration (Figure 1.6). Thereby, lipid-soluble drugs re-enter the body, hence before lipophilic drugs can be excreted the liver needs to transform them to their water soluble counterparts. Transformation to water-soluble substrates and inactivation of

drugs can happen through various processes in the liver such as oxidation by cytochrome P450 (CYP) enzymes, reduction by flavin enzymes, hydrolyses by esterases, and conjugations by transferases (e.g. glucuronidation).[22] These processes take place in the endoplasmic reticulum of the hepatocytes and lead to either exposure or addition of polar groups. Most CYPs are found in the liver, however, small amounts are also found in kidneys, lungs, intestinal mucosa, and skin.[22,43,44] Hence, metabolism of drugs can be initiated in the small intestine before reaching the liver.[20,25] As drugs reach systemic circulation before being exposed to renal excretion, the kidneys are not included in the first pass metabolism.

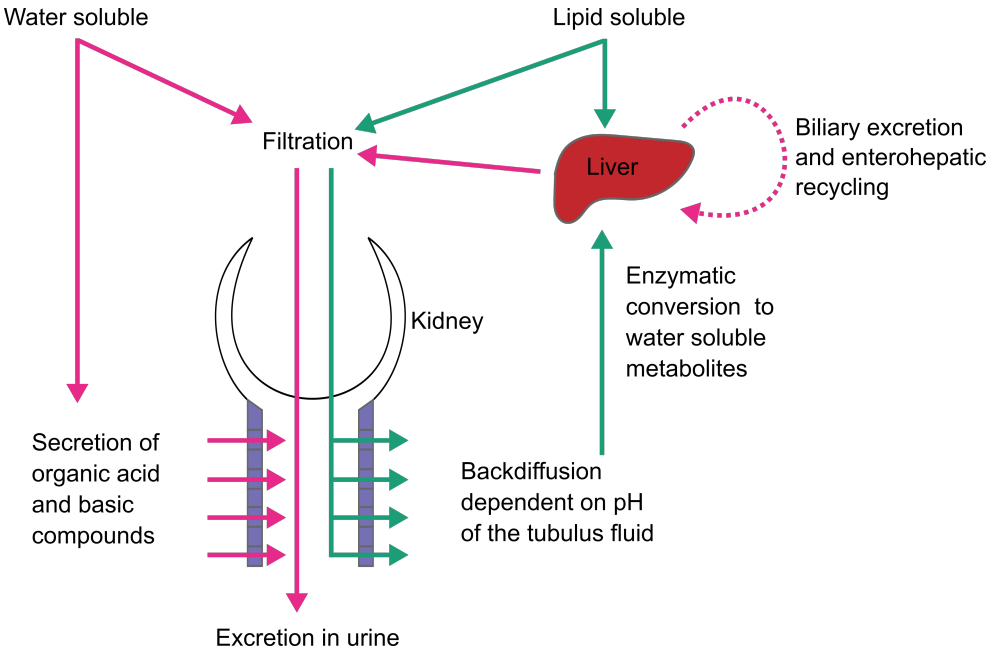

Figure 1.6: Scheme of drug excretion and hepatic transformation of lipid soluble drugs: Lipid soluble drugs (green lines) are transformed to water soluble drugs(pink lines) by the liver. Water soluble drugs are either excreted through the kidneys or through biliary excretion, the latter can result in enterohepatic recycling. Modified from.[22]

The liver is arranged in hexagonal units called lobuli, in such a way that the hepatocytes are exposed to different levels of oxygen and solutes.[45,46] The gradient comes from how the supply from the hepatic arteriole is placed and this divides each liver lobule into three zones with different oxygenation levels (Figure 1.7). In zone I, the hepatocytes closest to the hepatic arteriole receive the highest concentration of oxygen and solutes. Whereas, zone III is the least oxygenated. As a result, different enzymes are active in each zone leading to different processes taking place in each zone.[47] Processes like fatty acid oxidation and sulfation occurs mostly in zone I with high oxygenation, whereas

processes like glucuronidation, glutathione transferase, and CYP enzyme activity occurs mostly in zone III under less oxygenation. Though metabolism of drugs helps to avoid toxicity, metabolism of drugs by the liver comes with a risk of creation of more active and toxic compounds which can lead to liver injury.[22]

The liver does not only secure drug excretion by preparing drugs for renal excretion but also by biliary excretion.[48] The liver produces bile and it can excrete drugs via the bile (Figure 1.7). However, drugs that are biliary excreted often go through reabsorption to some extent this includes drugs such as mycophenolic acid,[49] warfarin,[50] and digoxin.[51] This phenomenon is known as enterohepatic recycling (Figure1.6).

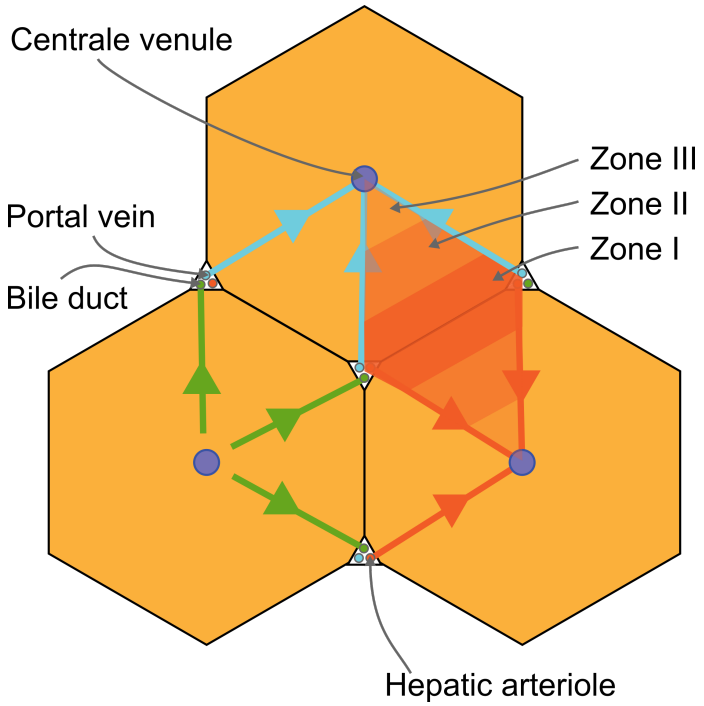

Figure 1.7: Drawing of liver lobuli with drainage of venous and arterial blood and bile: Drainage of blood from the portal vein to the hepatic central venule (blue). Drainage of blood from the hepatic artery to the hepatic central venule (red). Drainage of bile from hepatocytes to the bile duct (green).

In summary, the liver is responsible for inactivating drugs and making them water soluble so they can be excreted. The liver is organized in lobuli which gives the liver hepatocytes different profiles of metabolic enzyme expression. For a drug to successfully reach systemic circulation it must travel from the small intestine to the liver and avoid metabolism in the liver.

1.1.2 The First Pass Metabolism

The effectiveness of a drug depends on how much drug in the active form reaches its receptor. The body affects drugs thereby influencing the drugs' effectiveness in several ways such as metabolism or activation. An example of a drug which is activated by the body is the prodrug valacyclovir which is administered in its inactive, but orally absorptive, form and is activated in the body.[52] Valacyclovir is acyclovir modified to be a substrate for an active transporter.[53] Once valacyclovir has entered the body it is transformed to its active form acyclovir that can treat herpes viruses.[52,53] In contrast, a drug such as propranolol is highly metabolized and inactivated by the liver.[54] The effect the body has on the drug is called pharmacokinetic.[55] The focal point of pharmacokinetics is ADME. Pharmacodynamic is the effect the drug has on the body. The focus of this thesis is on pharmacokinetic.

A drug can be bound to proteins in blood plasma such as albumin and globulins.[56] Binding to blood plasma proteins can protect a drug from hepatic metabolism and renal excretion, however, a bound drug can be hindered in reaching the desired target site (Figure 1.8).[57] Albumin tends to bind acidic and neutral drugs, whereas globulins tend to bind basic drugs.

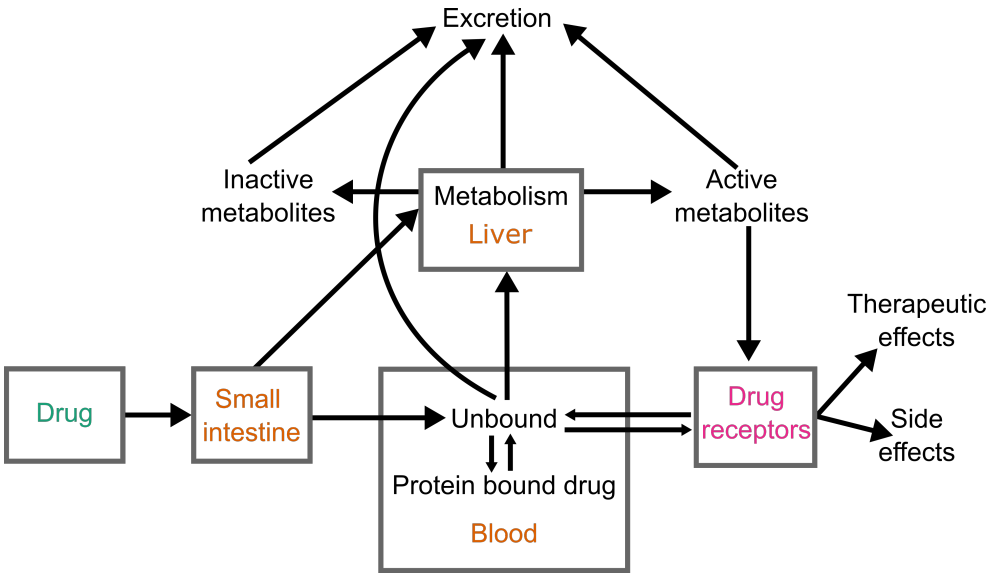

Figure 1.8: Scheme of the pharmacokinetics of orally administered drugs: Display of the influences different tissues and processes of the body have on the drug. Modified from.[57]

Depending on how a drug is metabolized, protein binding either prolongs or shortens the life time of the drug in the body. For propranolol, which is highly plasma bound, the binding to plasma proteins increases delivery to the liver and thereby its metabolism.[56,58] Thus, the propranolol metabolism is flow dependent since it depends on the flow of propranolol to the liver for

metabolism and not on how much propranolol is albumin bound. Whereas, a drug like warfarin, which is also highly bound to albumin, is only metabolized in its unbound state.[57] Therefore, the metabolism of warfarin is flow independent, since it depends on the dissociation of the drug from the protein to which it is bound. Drug-protein binding also affects the absorption by increasing the concentration gradient in the small intestine. A higher concentration gradient will help absorption in the small intestine, however, highly bound proteins are less likely to diffuse to the target tissue.[59]

In summary, the small intestine, blood vessel, and liver affect the amount of active drug reaching systemic circulation, in short, they are responsible for the first pass metabolism. Pre-clinical pharmacokinetic studies are important to achieve information on how much drug is needed to reach the therapeutic window (range of effective drug dose) and which effect each tissue has on the drug to find potential points of improvement.

Chapter 2

Hypotheses and Aims

2.1 Hypotheses

The hypotheses of this PhD project were:

i) Inserts for connected cell cultures can be fabricated with 3D printing

ii) A good prediction of the first pass metabolism can be obtained by connecting *in vitro* cell based tissue models

iii) Stiffness characterization of soft cell growth-matrices can be achieved while the growth matrices are submerged in a relevant buffer

2.2 Aim of the Project

The overall goal of the presented PhD project was to make ADME testing of new drugs more efficient by increasing the success rate of *in vivo* studies in the pre-clinical drug developmental phase. To reach this goal there was three the project aims:

i) Development of a triple cell culture based tissue model method

ii) Simulate the first pass metabolism with small intestinal cells, vascular endothelial cells, and liver hepatocytes

iii) Characterize the stiffness of the cell growth matrix

Chapter 3

Pre-clinical Pharmacokinetic Modeling

This chapter covers in vitro and in vivo models of the human body including cell based models and which cell based models were chosen for the presented PhD project. Moreover, this chapter includes a discussion of current methods of connecting cell based models and their advantages and shortcomings.

When developing new drugs, studies must be performed to find therapeutic effects and side effects. Before clinical trials, pre-clinical studies are performed with the goal of revealing therapeutic effects and side effects. Pre-clinical studies are performed with the use of models for the human body. Various models have been obtained and utilized. It was discovered over 2,400 years ago that animals could be used as a model to study the human body.[60] Animals from zebrafish and rodents to pigs and rhesus monkeys have been utilized for testing of pharmaceuticals. Even transgenic humanized rats, expressing genes specific for humans, have been explored.[61]

In *ex vivo* modeling, drug testing is performed directly on specific tissues from animals by removing the tissues from the animal before studying it. One such method is the Ussing chamber which is a side-by-side diffusion chamber. The Ussing chamber allows for testing of transport across a piece of tissue taken out from an animal.[62] This has been done with porcine and murine small-intestinal tissue to test drug absorption.[63,64] Another method of testing tissues *ex vivo* is with the Franz cell, however, this method is mainly used for testing of transdermal absorption.[65,66] By testing transport across *ex vivo* small-intestinal tissue, all cell types of the small intestine are present. Whereas, with *in vitro* it can be difficult to include multiple cell types at the same time. However, many pathogens are species specific, hence failures from toxicities not predicted with animal studies can arise in clinical trials causing a drug candidate to fail.[4] What is more, animal studies for pre-clinical drug testing whether *in vivo* or *ex vivo* come with considerable ethical concerns and

considerations.

Some models of the human body avoid the use of animals completely. *In vitro* macro models are good for understanding microbial behavior since parameters like pH and temperature can be precisely controlled by a computer.[67,68] The parallel artificial membrane permeability assay (PAMPA) utilizes an artificial membrane for evaluating passive permeation of human skin compounds.[69] *In silico* mathematical and computational models modeling of flow, absorption, distribution, and more have also been explored.[67]

A middle ground between animal studies and completely leaving out cells is *in vitro* cell culture studies with either primary cells from animals, patients or healthy individuals or immortalized cell lines.[70] Cell studies are used to predict drug behavior prior to in vivo testing. Cells are initially obtained from either humans or animals and cultured in the laboratory before drug testing.

In summary, various approaches to modeling of the human body exist. Good prediction with *in vitro* models can help select drug candidates and limit the number of animals needed for animal testing. The focus in the subsequent sections will be on *in vitro* cell based models for absorption, distribution, and metabolism.

3.1 *In Vitro* Cell Based Models of Individual Tissues

3.1.1 Cell Based Small Intestinal Models

Multiple cell based models of the small intestine *in vitro* have been explored of these the most broadly used is the Caco-2 cell line.[71,72] The Caco-2 cell line, obtained from a colorectal adenocarcinoma, displays enterocyte-like differentiation spontaneously in the absence of inducers.[73,74] Caco-2 cells grown on a permeable filter can be used to determine how and how much of a drug is transported across a cell layer. The Caco-2 cell line has shown a good correlation with oral absorption data from humans.[72] It is possible to test if a drug is transported passively if the transport rate from the apical to basolateral side is the same as the transport rate in the opposite direction, the drug transport must be passive, as the active transport is directional specific. However, the Caco-2 cell line has some limitations such as low endocytic activity compared to *in vivo* intestinal tissue.[75] Other limitations include interlaboratory variations,[76] lack of mucus,[77] and low expression of metabolic enzymes, specifically CYP3A4.[20] CYP3A4 is the main CYP enzyme in small intestinal enterocytes.[78,79]

Other intestinal cell lines include T84, which like Caco-2 originate from human colorectal adenocarcinoma. T84 cells have shorter microvilli than Caco-2 cells and a higher expression of monocarboxylate transporter 1 (MCT1), a protein primarily expressed apically in colonocytes.[80] Therefore, T84 cells

retain their colonic profile more than Caco-2 cells and are thus better suited for modelling of the colon.

The Madin-Darby Canine Kidney (MDCK) cell line is a non-intestinal cell line derived from kidney tubules.[67] MDCK cell line grow to confluent monolayers of differentiate cells with tight junctions rapidly (3 to 6 days).[81] However, a low activity of peptide transports limits the MDCK cell line's use when predicting *in vivo* drug absorption.[82] IPEC-J2 is an epithelial cell line from porcine jejunum.[83] IPEC-J2 cells spontaneously differentiate to enterocytes, however, these cells are too tight.

HT29, another colon adenocarcinoma cell line, shows enterocyte behavior but requires specific inducers and culture condition for differentiation.[84] The HT29-MTX cell line was created by methotrexate induction of HT29 cells to differentiate them to goblet-like cells with high mucin expression.[85,86] Caco-2 and HT29-MTX cells can be co-cultured to obtain the features of both cell lines.[87] Other cell lines with expression mucins include LS174T and LoVo, also derived from human colon.[88] However, LS174T cells have fewer microvilli than Caco-2 cells, hence a smaller absorptive surface area.

Choice of Small Intestinal Cells

In paper I, the Caco-2 cell line was chosen for the small intestinal model because of its broad usage (Figure 3.1). Moreover, in this PhD project one goal was to grow all cells in or on hydrogels. As, Caco-2 cells have been grown on hydrogels before,[89,90] it proved to be a good choice. Though, as mentioned above, this cell line does not express mucins to the same extend as other cell lines and metabolic enzymes to the same extend as the small intestinal villi. Possible improvements to this are discussed below (Section 4.5).

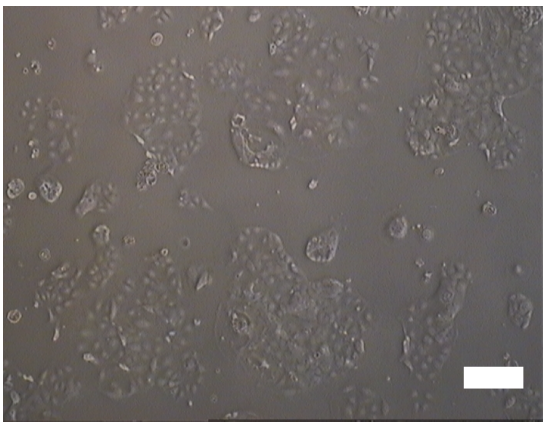

Figure 3.1: Bright-field microscopy image of Caco-2 cells. Scalebar: 100 μm.

3.1.2 Cell Based Endothelial Models

The classical model of endothelium are the human umbilical vein endothelial cells (HUVEC) which are a primary endothelial cells from the umbilical cord. HUVEC cells have a limited life span of 10 passages,[91] however, they are very well studied.[92] To work around this limited life span immortal endothelial cell lines have been created. Such as EaHy926 (CRL-2922) a hybridoma of an epithelial cells line and HUVEC cells.[93] Other immortalized cell lines include HMEC-1 and ECV304.[94,95] The immortal cell lines have some limitations such as induction of vascular cell adhesion molecule 1 (VCAM-1) and E-selectin which are very low for HMEC-1 cells and undetectable for CRL-2922 and ECV304, whereas these proteins can be induced in HUVEC cells.[96] Both are adhesion molecules activated by cytokines and play a role in inflammation.[97,98]

Choice of Endothelial Cells

In this PhD project, both HUVEC cells and the hybridoma CRL-2922 cell line were utilized for different purposes. In paper II, the CRL-2922 cells were utilized for visualizing stretching of cell on a thin hydrogel growth-matrix membrane that could be stretched by changing the water pressure. For this purpose no expression of functional proteins such as VCAM-1 and E-selectin of the endothelial cell was needed. But their elongated morphology proved useful, since stretching of the cells was easily visualized (Figure 3.2). Therefore, the CRL-2922 cell line was chosen over HUVEC cells for its ease of culturing. Caco-2 cells were also added to the thin hydrogel growth-matrix but could not be stretched, instead they moved apart from each other.

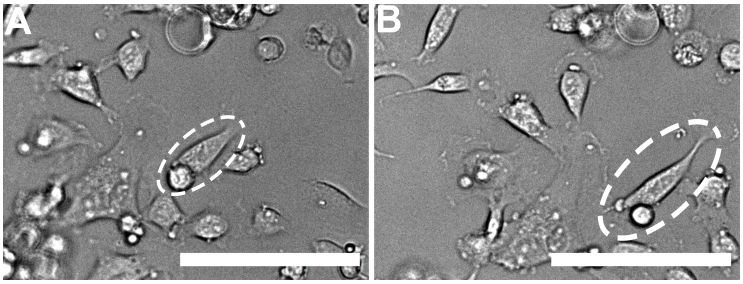

Figure 3.2: Bright-field microscopy image of stretching of CRL-2922 cells on a thin hydrogel growth matrix: A) Non-stretched CRL-2922 cell marked with the white ring. B) Stretching of the CRL-2922 cell marked with the white ring. Scalebars: 100 μm.

For paper I, HUVEC cells were used as the vascular endothelial tissue model. Though, in the paper their inducible expression of VCAM-1 and E-selectin was not utilized. However, depending on which pharmaceuticals might be tested in the future with the presented method this might become relevant. For instance, in rheumatoid arthritis (RA) it would be of interest to detect if a

drug inactivates VCAM-1, since VCAM-1 is known to be overexpressed for RA patients.[99,100] In RA treatment, several drugs on the market are inhibitors of tumor necrosis factor alpha (TNFα), which is a proinflammatory cytokine.[101] These drugs include infliximab,[102] etanercept,[103] and adalimumab.[104] The result of TNFα inhibition is a lower expression of VCAM-1. Furthermore, VCAM-1 is also relevant in diseases such as cancer and asthma.[105,106] Moreover, the culturing of HUVEC cells in the triple layered tissue model method shows that it is possible to culture primary cells and not only cell lines with the method.

In summary, both primary cells and immortal cell lines are available as cell based endothelial models. Depending on the aim either the primary HUVEC cells or the hybridoma CRL-2922 cell line was used in this PhD project.

3.1.3 Cell Based Liver Models

Both primary cells and cell lines of hepatic cells are available. Primary hepatocytes can be maintained in culture for a few days while retaining their phenotype.[107] Several immortal cell lines exist such as HepG2, Mz-Hep, Chang, Hep3B, HuFoe-15, PLC/PRF/5, and BC2, these are isolated from human hepatomas. These cell lines have different expression of various metabolic enzymes. Of these HepG2 is one of the most widely used. HepG2 for instance show many liver-specific functions and conjugating enzymes, however, lack expression of most CYP enzymes. Hepatic cell lines with non-human origin also exist such as the murine cell line AML12.[108]

Choice of Hepatic Cells

In paper I, the HepG2 cell line was utilized to grow hepatic spheroids in the hydrogel growth-matrix. The HepG2 cell lines was chosen because it is known to be able to form spheroids when cultured in a three dimensional (3D) environment (Figure 3.3).[109–112] Though, Hep3B cells aggregate faster than HepG2 cells in a hanging drop setup.[113] However, in the hanging drop setup the cells are cultured in a drop of cell medium, thus the cells grow without the mechanical support from a growth matrix. Moreover, the HepG2 cell line was chosen because it is one of the most widely used hepatic cell lines.

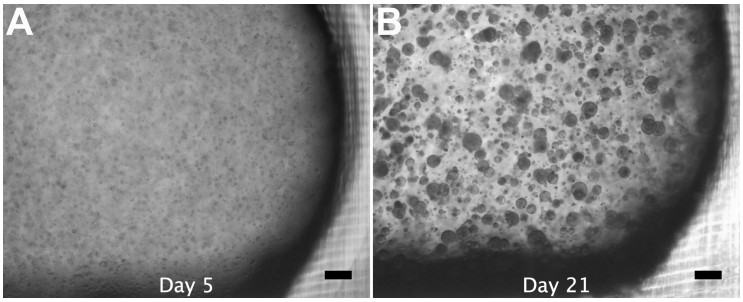

Figure 3.3: Bright-field microscopy image of growth of HepG2 spheroids in a hydrogel growth-matrix over three weeks: A) HepG2 spheroids cultured in the hydrogel growth-matrix after 5 days. B) HepG2 spheroids cultured in the hydrogel growth-matrix after 21 days. Scalebars: 500 μm.

Growth of spheroids display gradient of nutrients and gases including oxygen (Figure 3.4).[114,115] *In vivo*, the liver also has a molecular gradient of oxygen, as discussed above (Section 1.1). Hence, the consequence of the oxygen gradient could be that different metabolic enzymes were active along the oxygen gradient. Spheroids have been shown to have an increased CYP activity,[111] which also *in vivo* predominantly takes place in the least oxygenated area (zone III) of the liver lobuli.[47]

In summary, the HepG2 cell line was selected because it is well studied and has previously been grown as 3D spheroids recreating the zones of oxygenation found in the *in vivo* liver tissue.

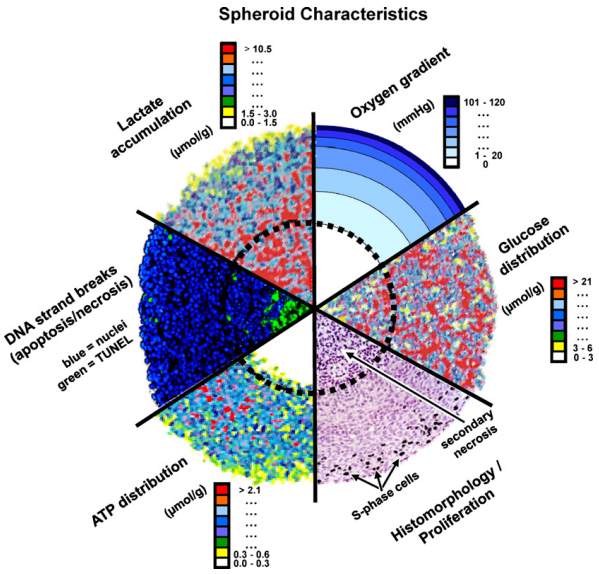

Figure 3.4: Molecular gradient characteristics of spheroid cell cultures from various assays give a concentric arrangement of cell proliferation, viability and the micromilieu in large spheroids. Reprinted with permission from.[114]

3.2 Connected *In Vitro* Cell Based Tissue Models

As, discussed above (Section 1.1), the small intestine, the vascular endothelium, and the liver are connected in the first pass metabolism, hence connected cell cultures are of interest. This section will dive into combination of multiple cell cultures. Various ways of combining cell cultures have been explored such as in titer well-plate as a batch growth and by connecting tissue models via microfluidics. One goal of combining cultures is to obtain better tissue models by utilizing the advantages of different cell lines. Another goal is to connect multiple tissue models to obtain the effect from interaction of multiple tissue models.

3.2.1 Combined Single Tissue Models

Susewind et al. have combined Caco-2 cells with macrophages and dendritic cells to achieve a better inflammatory model.[90] By induction of inflammation with pro-inflammatory cytokines, this model can be utilized to determine how microparticles from food or the environment influence inflamed tissue. Others have combined Caco-2 and HT29 cells with Raji B lymphocytes.[116] When cultured with Raji B cells Caco-2 cells express M cell phenotype. *In vivo* M cells are specialized epithelial cells which can transport antigens from the small intestinal lumen to submucosal lymphoid structures called Peyer's patches.[37,117] This along with dendritic cells, macrophages, lamina propria lymphocytes, and intraepithelial enterocytes make up the gut-associated lymphoid tissue (GALT) which is connected with the lymph drainage of the villi. Hence, this co-culture gains a better representation of the *in vivo* small intestinal villi by including GALT. Moreover, implementation of microbiota as the co-culture element have been presented.[118–121]

Other tissues further developed by multiple cell types include the liver and vascular endothelium. Nonalcoholic steatohepatitis has been modeled by co-culturing of HepG2, HUVEC, and Kupffer cells (Kupffer cells are resident macrophages in the liver).[112,122] Vascular endothelium models have been improved by co-culturing endothelial cells and smooth muscle cells to include the smooth muscle of the blood vessel.[123]

In summary, modeling of single tissue can be improved by including multiple cell types in the same model.

3.2.2 Combined Connected Tissue Models

Co-cultures can also be used for investigating tissue interactions. This has been achieved in batch by culturing multiple cell types in the same culture.[124] Microfluidic system can connect different *in vitro* tissue models by micrometer-sized channels with constant perfusion.[67] The benefit of this is a constant flow and a low number of cells. The flow can mimic the dynamic of bodily

fluid such as blood flow and shear stress. Combining flow and peristalsis-like deformation have been shown to induce mucin-2 production from Caco-2 cells.[125] Multiple combinations of tissues connected via microfluidics have been published.[126–129] The aim of these models was better *in vitro* prediction of ADME by including tissue interaction in the models.

Commercial microfluidic systems connecting multiple organs for ADME testing are available from TissUse GmbH and MatTek Corporation in collaboration. Their "MultiOrgan Chip" connects skin and liver obtaining a co-culture for testing of skin permeability.[130] There is also a version with four interconnected organs available called "Four Organs-Chip" which connects intestine, liver, skin, and kidney.[131] These microfluidic devices are, however, often made in polydimethylsiloxane (PDMS). A problem with PDMS is that small hydrophobic molecules tend to diffuse into it.[132–134] This is a drawback when for ADME studies. Moreover, PDMS is also permeable to gasses.[135]

Another commercial system, by MIMETAS B.V., is called "OrganoPlate". The OrganoPlate introduces microfluidic flow to epithelial cell cultures without tubing by a rocking system to ensure medium exchange within the microfluidic chamber.[136] The OrganoPlate microfluidic chips are fabricated using dry film resist (DFR), thereby the OrganoPlate avoids PDMS and gain complete control of gas pressure.[137] Furthermore, the OrganoPlate does not rely on artificial membranes but have a hydrogel growth-matrix incorporated for the cells to grow on. Hepatocyte and fibroblast co-cultures have been connected with the OrganoPlate technology to study interactions of these two cell types.[137]

Tissue models connected via a string have even been publish as a completely different approach from microfluidics.[138] Connected tissue models in microfluidics often share the same medium, this can be problematic as different cell can need specific culture conditions for optimal growth and differentiation.[139] This has been circumvented by connecting tissue models through membrane in between them each tissue model can have its own optimized growth medium.[140] However, cells do not necessarily need the same time for differentiation. Another problem with microfluidics is to test microparticles and drug delivery systems which can be in the size range of 400 μm,[141–143] as microfluidic channels often are in the sizes of a few hundred μm.[120,131]

In summary, connecting different tissue models *in vitro* allows us to gain insight processes and ADME testing but the current methods have certain areas that can be improved. The areas that can be improved include individual growth conditions of cells, avoidance of PDMS, and testing of larger drug delivery systems. Moreover, recyclable growth platforms and easy customization of the system would allow for cutting costs and designing platform for specific needs from cell cultures. Moreover, improved *in vitro* tissue models can potentially increases successes in animal testing.

Chapter 4

First Pass Metabolism Model

This chapter includes results of the project presented paper I '3D-printed stackable titer plate inserts supporting three interconnected tissue models for drug screening' and a discussion of these results. The HepG2 based liver model was developed in collaboration with Andreas Willumsen, whom I supervised during his special course 'Entrapment of hepatocytes in hydrogels for 3D cultures'. Results on valacyclovir transport were obtained in collaboration with Chiara Mazzoni.

4.1 Triple Layered Tissue Models

Paper I focuses on the first two aims:

i) Development of a triple cell culture based tissue model method

ii) Simulate the first pass metabolism with small intestinal cells, vascular endothelial cells, and liver hepatocytes

The method presented in this paper consists of three inserts that can be connected by assembling them on top of each other (Figure 4.1). Each insert contains 12 wells with a hydrogel growth-matrix for the cells. To fabricate the inserts, the additive manufacturing (AM) technique known as 3D printing was utilized. The 3D-printed inserts are compatible with a commercial 12 well titer plate. The Caco-2 cell line, HUVEC cells, and the HepG2 cell line were used for tissue models of the small intestine, the vascular endothelium, and the liver, respectively. All the tissue models consisted of a 3D printed insert with a hydrogel growth-matrix. Caco-2 and HUVEC cells were cultured on top of the hydrogel-growth matrix to simulate two dimensional (2D) barrier tissues. Whereas, HepG2 cells were cultured in the hydrogel growth-matrix to simulate a 3D solid tissue (Figure 4.1B,C).

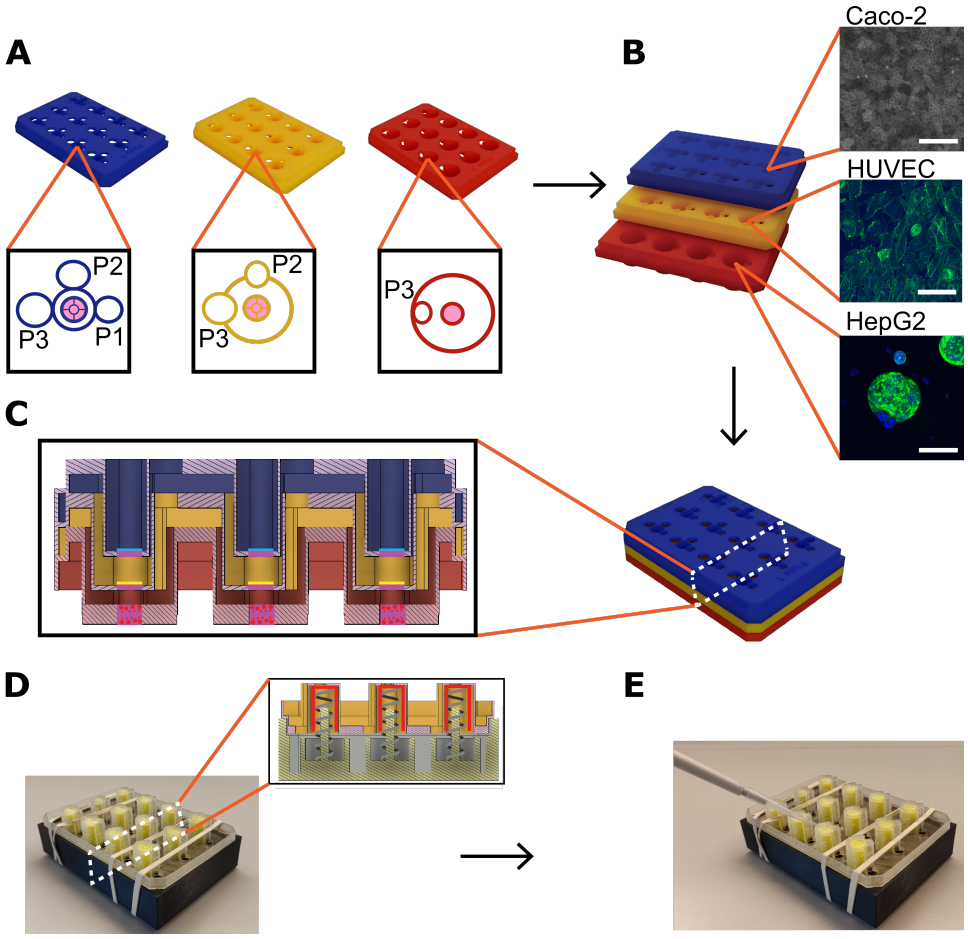

Figure 4.1: Schematic illustrations of triple layered tissue models: A) Individual tissue-model inserts of Caco-2 cells (blue), HUVEC (yellow), and HepG2 (red) with hydrogel growth-matrices (pink). The inserts have sampling holes at each level, P1 for sampling under the Caco-2 cells, P2 for sampling under the HUVEC cells, and P3 for sampling under the HepG2 cells. B) Assembly of triple layered tissue models. Scalebars: 100 µm. C) Sideview of assembled triple layered tissue models. D) 3D-printed inserts clamped with rubber bands to the casting device. E) Casting of the hydrogel growth-matrix into the holes of 3D-printed inserts.

The hydrogel growth-matrix for the HepG2 liver tissue model was 5 mm in diameter and 4 mm in thickness to resemble a solid tissue. Whereas, the hydrogel growth-matrix for Caco-2 and HUVEC cells was 5 mm in diameter but only 1 mm in thickness to allow for faster diffusion. To support this thin hydrogel, a cross was added to the hole to give the hydrogel growth-matrix mechanical support so it would not bend under water pressure from the growth medium. Cells for each tissue model were seeded and cultured individually under each their optimized conditions and assembled once each tissue model was fully differentiated. The three 3D-printed inserts were designed in such a

way that samples of medium or buffer could be taken under each tissue model while the three inserts were assembled on top of each other (Figure 4.1A). This allowed for performance of drug transport studies while the three tissue models were connected. To cast the hydrogel growth-matrix, the 3D-printed inserts were placed on a casting device with spring loaded pillars to cover the holes and the 3D-printed inserts were held down by rubber bands (Figure 4.1D). Once assembled, hydrogel solution could be pipetted into the holes (Figure 4.1E). Once polymerized the casting device and 3D-printed insert were disassembled and cells could be cultured in the insert.

This chapter focuses on the components, design, and evaluation of the triple layered tissue models for first pass metabolism modeling.

4.2 3D Printing - Additive Manufacturing

3D printing is additive manufacturing from 3D modeled data. The benefits of include design freedom, high resolution, fabrication of complex geometries, minimum use of materials, and personal customization.[144] Designs are normally done using computer-aided design (CAD). Several 3D printing techniques exist such as stereolithography (SLA), fused deposition modeling (FDM), inkjet printing, and powder bed fusion (Figure 4.2).[144] The focus for the rest of this section will be on SLA and FDM since these two techniques have been available for the PhD project.

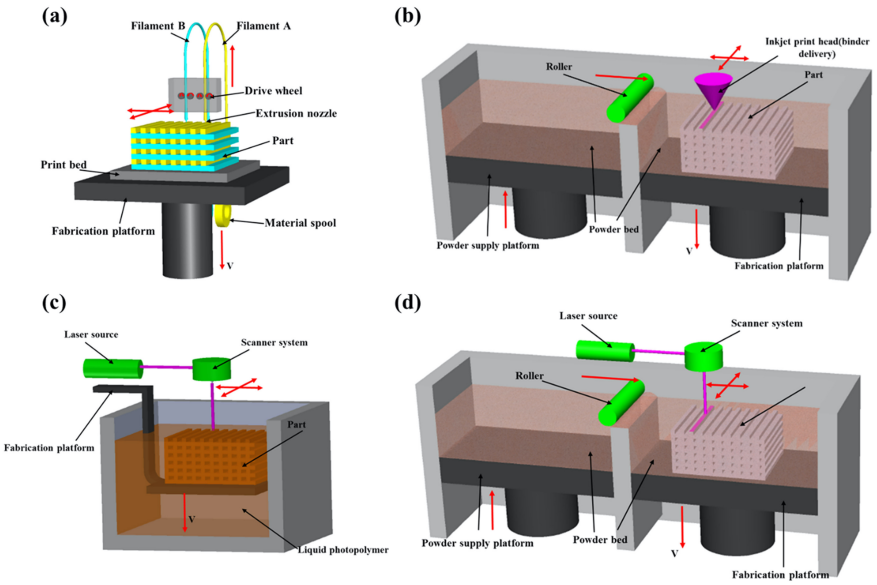

Figure 4.2: Schematic representation of 3D printing techniques: A) Fused deposition modeling, B) inkjet printing, C) Stereolithography, and D) powder bed fusion. Reprinted with permission from.[145]

4.2.1 Fused Deposition Modeling and Stereolithography

In FDM printing, a filament of, a thermoplastic polymer, is continuously pushed out through a heated nozzle to reach a semi-liquid state and the filament is extruded onto a platform with a lower temperature than the nozzle (Figure 4.2A). FDM is typically done with thermoplastic materials such as polylactic acid (PLA) and acrylonitrile butadiene styrene (ABS).[144] The benefits of FDM are low cost, high speed, and simplicity. However, FDM suffers from weak mechanical properties, a layer-by-layer appearance, a limited number of thermoplastic materials, and poor surface quality.[146] Especially, the former is a large drawback for this project since a rough surface finish would make it difficult to seal for hydrogel casting.

SLA, developed in 1986, is one of the first 3D printing techniques.[147] This technique uses an ultra violet (UV) laser to polymerize layers of a resin or monomer solution (Figure 4.2C).[144] Since printing takes place in a resin or monomer basin, the print is covered in unreacted resin/monomer solution which can be cleaned when printing is finished. The result is a print with a fine finish in high quality and resolution.

In summary, the resolution of SLA printing is down to 10 μm, whereas with FDM the resolution is 50-200 μm.[145] However, SLA printing is rather slow, expensive, and includes cleaning steps after printing.

4.2.2 Choice of 3D Printers and Printing Material

The Form 2 SLA 3D printer from Formlabs was used to print the inserts for the first pass metabolism model. The inserts were printed in Dental LT resin. Dental LT resin is formulated for printing of dental splints and surgical guides and is rated class IIa biocompatible.[148] Class IIa means that it follows the requirement given by the European Parliament and Council for this specific type of medical devices.[149] This class of medical devices are classified as medium risk and include surgically invasive products.[150] Moreover, medical devices in this class have been tested and found nontoxic to cell cultures.[151] However, the protocol for post processing presented in paper I differs from the protocol given by the manufacturer. Since the 3D-printed inserts are larger and with more corners compared to dental splints and surgical guides a more thorough post processing was needed.

With the high resolution of an SLA 3D-printer it is possible to make a tight seal and cast hydrogels into the inserts. However, fabrication of these inserts using an SLA 3D-printer and special resin is not cheap. Therefore, an FDM 3D-printer was used for components that did not need to be in contact with the cells and did not require as high a resolution. This was for things such as the casting device.

4.3 Growth Matrices

In vivo tissues have different stiffnesses from very soft such as lung and breast tissue to very stiff like bone.[152] The plastics used for cell cultures *in vitro* are comparable to bone in stiffness but are much stiffer than soft tissues such as the intestines and the liver. The softness of the growth matrix is important since *in vivo* increased stiffness can be pathological, as it is seen in diseases such as liver cirrhosis,[153,154] pulmonary fibrosis, systemic sclerosis,[155] and breast cancer.[152] One way cells can sense the softness of their growth substrate is by mechanosensing through cell-matrix adhesions such as focal adhesions.[156–158] Soft growth matrices give rise to more *in vivo*-like cell morphology such as polarization of epithelium and neuron branching.[159–161] Neuron branching and epithelial polarization are important steps during developmental phases of these types of tissues.

In vivo, the extracellular matrix (ECM) is the non-cellular component and growth matrix within all tissues.[162] It provides the essential physical scaffold and initiates biochemical and biomechanical cues for tissue morphogenesis, differentiation, and homeostasis. Cells are connected to the ECM by proteins such as integrins and syndecans.[163,164] The ECM consists of two main classes of molecules; fibrous proteins and proteoglycans.[165] Collagens are the main fibrous protein group making up 30 % of the total protein mass of multicellular animals.[166] The ECM regulates cell adhesion, provide tensile strength, support chemotaxis and migration, and direct tissue development.

In cell cultures, cells are grown on plastic dishes or filters coated with adhesion molecules to help the cells adhere. However, this limits the cultures to 2D growth, and what is more the plastic is much stiffer than most tissues *in vivo*.

Cells cultured in 3D have one more dimension of external mechanical inputs and adhesion. This affects integrin ligation, cell contraction, and associated intracellular signaling.[167,168] In addition, the 3D matrix affects diffusion of effector molecules such as growth factors and enzymes resulting in gradients.[115] For a synthetic 3D environment there is solely a need to provide an initial set of cues to achieve a relevant physiological environment, since cells are able to secrete and incorporated their own ECM into their local microenvironment.[115]

In summary, *in vivo* tissues are softer than plastic cell culture dishes and flasks. Therefore, a hydrogel was chosen as a soft growth-matrix. Below is discussed what a gel is and what a hydrogel is and which hydrogel was used as cell culture growth-matrix.

4.3.1 Gels

A gel is a polymeric solid made of a 3D network of polymer chains joined at connection sites (Figure 4.3).[169] The connection sites can be chemically

covalent-bonds or physical interactions. Rubber is a polymeric gel and is in a liquid state before gelation (i.e. cross-linking of branch points) and becomes solid once gelated. In the gelated state, its shape is maintained, however, it can be deformed by force but will return to its original shape once the force is removed. Hence, rubber behaves as an elastic solid. Gels have also been defined to consist of two or more components of which one is a liquid,[170] hence, cross-linked hydrophilic polymer chains in an aqueous microenvironment.[171] This definition will be used for hydrogels and elaborated on in the following sections.

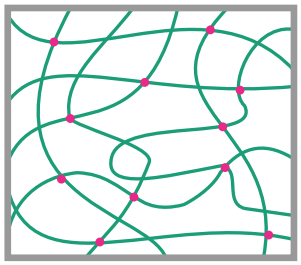

Figure 4.3: Drawing of a polymeric cross-linked gel: The gel consists of polymeric chains (green) cross-linked at specific points (pink). Modified from.[169]

4.3.2 Hydrogels

Where a gel is a polymeric solid, a hydrogel is a swelled polymeric solid, either of synthetic or natural origin.[170] The polymeric network of a hydrogel is able to absorb water from 10 % up to thousands of times its own dry weight.[172]

Hydrogels can be cross-linked in various ways such self-assembly,[173] anionic gelation,[174] chemical cross-linking,[175] and enzymatic protein cross-linking.[176] Hydrogel-forming polymers compatible with cell cultures include biopolymers, synthetic polymers, and hybrid polymers.[177]

4.3.3 Choice of Hydrogel

The biopolymer gelatin was utilized for in the presented project due to its availability, low costs, and the knowledge of this type of hydrogel in the group. Gelatin is a biopolymer of proteins obtained by denatured collagen.[178] Gelatin is solid at room temperature but liquid at 37 °C.[178,179] However, when cross-linked to a hydrogel, gelatin is a hydrogel at 37 °C as needed for cell cultures. Gelatin hydrogels have been used as the growth-matrix for human endothelial, epithelial, fibroblast, glial, and osteoblast cells.[180] These can attach, spread, and proliferate on and in a gelatin hydrogel.

Transglutaminase can enzymatically cross-link gelatin.[181] Transglutaminase catalyzes the covalent bound formation between lysine and glutamine

yielding a ε-(γ-glutamyl)lysine cross-link.[182,183] The stiffness of gelatin hydrogels is tunable by the gelatin and transglutaminase concentrations, incubation time, temperature, and pH.[109,184,185] As mentioned above, synthetic 3D environments only need to provide an initial set of cues, the gelatin hydrogels utilized in this PhD project for the tissue models were not coated with adhesion molecules.

In summary, hydrogels can be used as artificial ECMs in cell culture and for this PhD project gelatin hydrogel growth-matrices were chosen as the artificial ECM of all cell based tissue models presented. In Chapter 5, stiffness and how to measure stiffness of hydrogels will be discussed.

4.4 Permeability Testing of Cell Based Tissue Models

Several method are available for assessing a cell monolayers' confluency and barrier function including transepithelial/transendothelial electrical resistance (TEER),[186] hydraulic conductivity (L_p),[187] fluid filtration coefficient (K_f), and apparent solute permeability (P_{app}).[188]

L_p and K_f are two fluid flow parameters. L_p is a filtration parameter extensively used to study the vascular permeability.[187,189] L_p is the slope of the relationship between the volume flow and the driving pressure, thus to measure this parameter there is a need for control of a changing pressure. L_p is normalized to the surface area and is an intrinsic property of a tissue.[190] Therefore, L_p can be used to compare tissue samples. Whereas, K_f is proportional to L_p but is not an intrinsic property of tissues as it is not normalized to the area. In the method presented in paper I, there is not implemented a precise control of pressure.

As the interest in paper I was to measure the first pass metabolism, the transport of molecules was more important to gain than fluid flow parameters. The transport across a cell layer is not only determined by the fluid flow as it can be influenced solvent drag/convection, diffusion, and active carriers.[191–193] These are taken into consideration with the P_{app}, therefore P_{app} was obtained to compare permeabilities of hydrogels and cell layers. P_{app} is defined by:[31]

$$P_{\text{app}} = \frac{(dQ/dt)}{AC_0} = \frac{F}{C_0} \tag{4.1}$$

Where, dQ/dt is the rate of drug permeation, A is the absorption area, F is the flux, and C_0 is the initial donor concentration.

In addition to P_{app}, TEER measurements were performed to characterize the Caco-2 monolayers. TEER measurements are based on two electrodes on either side of a cell monolayer.[186,194] The electrodes usually come as two chopsticks inserted on each side of the monolayer or as a small cup in for individual cell inserts (Figure 4.4A). The TEER value is a measure of ionic

conductance of the paracellular pathway, thereby the resistance is obtained through Ohm's law (Figure 4.4B). The TEER value of cell monolayers is given in Ω cm^{-2}. It is used to determine the integrity of tight junctions.[194] However, a downside of TEER measurements is that different equipment tend to give different TEER values.[186] In paper I, Caco-2 monolayers with a TEER value above 300 Ω cm^{-2} were deemed tight. This is in accordance with what has previously been measured on Caco-2 monolayers of soft growth-matrices.[89,90]

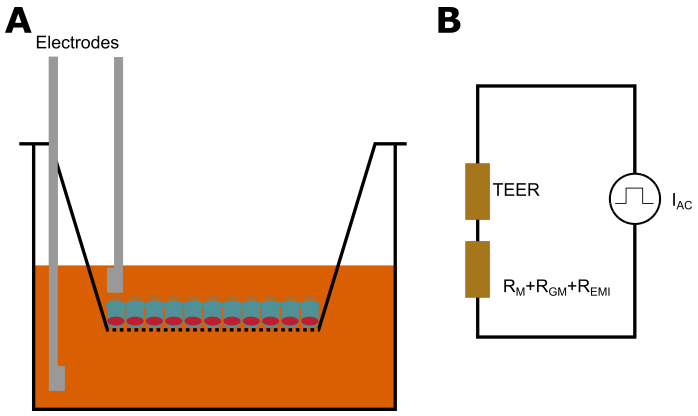

Figure 4.4: Schematic of TEER measurement with chopstick electrodes: A) Principle of chopstick based TEER measurements. B) Electrical diagram of TEER measurements. Alternating current (I_{AC}) in introduced and the total ohmic resistance arise from the cell monolayer (TEER) and the cell culture medium (R_M), growth matric (R_{GM}), and electrode medium interface (R_{EMI}). Modified from.[186]

In paper I, it is discussed that the TEER value of Caco-2 cells on the hydrogel growth-matrix is lower than Caco-2 cells grown on a polyester filter but that they both are higher than *ex vivo* small intestinal tissue. As mentioned above, the benefit of *ex vivo* tissue is that all cell types of the specific tissue are present. Since the enterocytes are the cells responsible for the tightness, the presence of multiple other cells could be the reason for the lower TEER values of *ex vivo* tissue compared to cell based *in vitro* models. As discussed above (Section 1.1), hydrophilic drugs are restricted to the paracellular route, therefore the Caco-2 small intestinal tissue model on the hydrogel growth-matrix might be more suitable for testing of paracellular transport of hydrophilic drugs than Caco-2 cells on a polyester filter.

In summary, L_p and K_f characterize the tightness of monolayers by information on fluid flow. L_p might be interesting to obtain before and after a drug transport study to evaluate if a drug influences the blood vessel. P_{app} and TEER were utilized in paper I to characterize the barrier function of the tissue models.

4.4.1 Permeability Coefficients Obtained with the Triple Layered Cell Based Models

In paper I, three different molecules were utilized as a model compounds to assess the barrier function of the different tissue models. The three molecules used to test permeability were; lucifer yellow, furosemide, and valacyclovir (Figure 4.5).

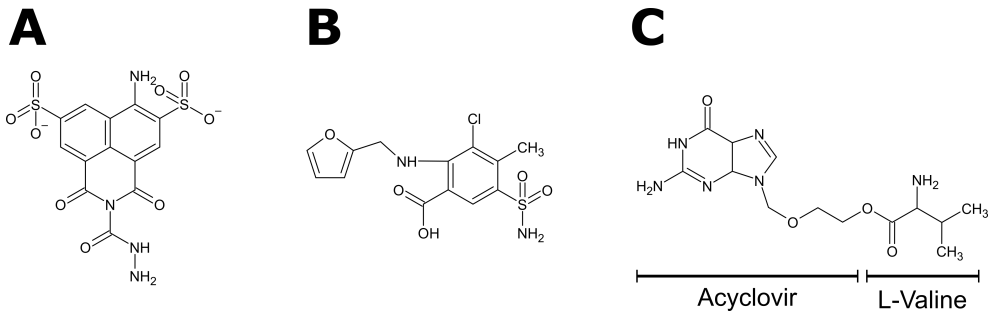

Figure 4.5: Drawing of the chemical structures of A) lucifer yellow, B) furosemide, and C) valacyclovir.

Lucifer Yellow Permeability Studies

Lucifer yellow is a small hydrophilic molecule which crosses a cell layer via the passive paracellular route (Figure 4.5A).[33] The lucifer yellow permeability was measured for all three tissue models while they were assembled on top of each other and was used to determine whether tissue models were tight monolayers. As discussed in paper I, only the Caco-2 based small intestinal model of the three tissue models could be determined as a tight monolayer. The lucifer yellow permeability showed that the Caco-2 based small intestinal model was able to act as a barrier, whereas the HUVEC based endothelial model was not. Hence, an improvement of the HUVEC based endothelial model is of interest, a possible improvement of the HUVEC endothelial model is discussed below (Section 6.2). The hydrogel growth-matrix of the HepG2 based liver model showed very limited lucifer yellow permeability with and without HepG2 spheroids presented, this point to that the hydrogel growth-matrix of 4 mm was too thick for lucifer yellow to cross in the time span which was measured.

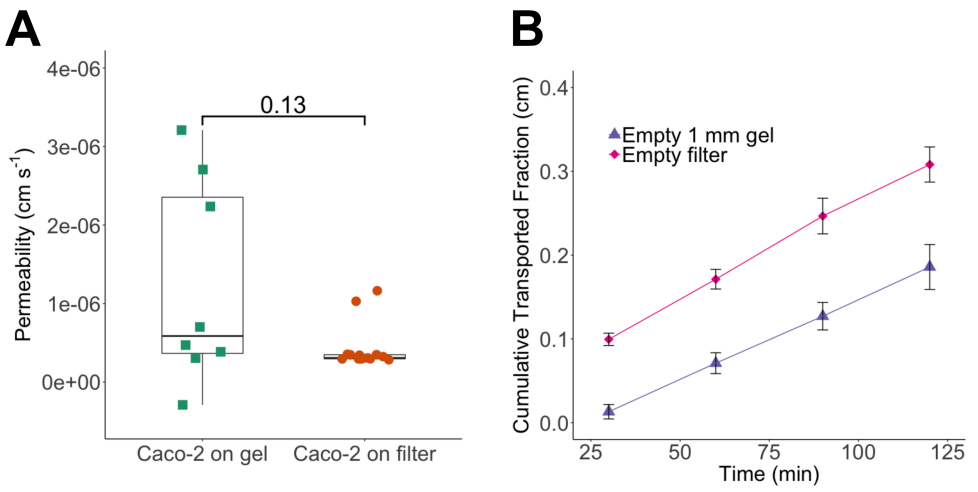

Figure 4.6: Transport of lucifer yellow across Caco-2 monolayers, the hydrogel growth-matrix, and polyester filters: A) Permeability of lucifer yellow across Caco-2 cells on the hydrogel growth-matrix (n=9) and Caco-2 cells on polyester filters (n=15). B) Cumulative transported fraction of lucifer yellow across empty hydrogel growth-matrices (mean±SD, n=8) and empty polyester filters (mean±SD, n=9).

In paper I, the permeability across Caco-2 cells on the hydrogel growth-matrix and on the polyester filters was not significantly different (p-value=0.13) (Figure 4.6A). Though, the average permeability across the hydrogel growth-matrix was 1.22×10^{-6} cm s^{-1}, whereas it was 4.19×10^{-7} cm s^{-1} across the polyester filters. On the permeability plot (Figure 4.6) it is clear that the average permeability across the Caco-2 cell monolayers on the hydrogel growth-matrix is increased by some large measurements and that is has a large standard deviation. Hence, the permeability of Caco-2 cells on the polyester filters is more reproducible than for Caco-2 cells on the hydrogel growth-matrices. The tightness of Caco-2 cells on the hydrogel growth-matrices was supported by ZO-1 stains which showed expression of ZO-1 indicating tight junctions.

The cumulative transport fraction of lucifer yellow for the 1 mm hydrogel growth-matrix and the polyester filter might be the same, however, the hydrogel growth-matrix displays a delay (Figure 4.6B). This delay of transport could be improved by either a thinner hydrogel growth-matrix or changing the material of the hydrogel growth-matrix. A thinner hydrogel growth-matrix would lead to problems with keeping the casted shape. As is seen in paper II, thin gelatin hydrogels are stretchable and stretching lead to cell detachment.[184] Hence, potential solution to this problem could be a hydrogel of a different material. A third possibility would be to incorporate polyester filter and coat them with a soft hydrogel. However, in initial test to do so it proved difficult to glue the filters without glue getting in the pores of the filters.

Furosemide Permeability Studies

Furosemide, which is a loop diuretic, is a weak acid and a biopharmaceutics classification system (BCS) class IV drug meaning that it is both poorly soluble and poorly absorbed in the small intestine (Figure 4.5B).[195,196] Since furosemide is a weak acid, it is more soluble at high pH. In paper I, the furosemide permeability across a Caco-2 monolayer on the hydrogel growth-matrices was reported as 1.53×10^{-6} cm s^{-1} in a pH 7.4 Hank's balanced salt solution (HBSS) buffer. This permeability value is in the range of what has previously been reported for furosemide permeability across Caco-2 monolayers (Table 4.1).

The TEER value of Caco-2 cells grown on the hydrogel growth-matrix was 551 Ω cm^{-2}, whereas the TEER value of Caco-2 cells grown on the polyester filters was 1585 Ω cm^{-2}. This point towards a less tight paracellular barrier of Caco-2 cells grown on the hydrogel growth-matrix, since the TEER value is tight junction characterization. As furosemide mainly crosses Caco-2 monolayers transcellularly,[196] the less tight paracellular barrier did not seem to affect the furosemide transport.

Table 4.1: Furosemide permeabilities across Caco-2 monolayers reported in literature.

Permeability (cm s^{-1})	**Buffer**	**Reference**
8.6×10^{-6}	HBSS buffer Apical pH: 6.5 Basolateral pH: 7.4	[197]
5.4×10^{-6}	Buffer not reported pH not reported	[198]
5.1×10^{-6}	Glucose containing PBS buffer pH: 5.4	[199]
1.3×10^{-6}	DMEM medium with 10 % FBS pH: 7.4	[200]
6.8×10^{-7}	HBSS buffer pH: 6.8	[201]
2.9×10^{-7}	HBSS buffer pH: 6.5	[202]
1.2×10^{-7}	PBS buffer containing glucose pH: 7.2	[199]

Table key: Dulbecco's modified Eagle media (DMEM), fetal bovine serum (FBS), Hank's balanced salt solution (HBSS), and phosphate buffered saline (PBS).

Valacyclovir Permeability Studies

In contrast to lucifer yellow and furosemide, which are transported passively across the small intestinal barrier, valacyclovir is transported actively. Valacyclovir is a modified version of the drug acyclovir with improved small intestinal absorption by incorporation of L-valine through an ester bond (Figure 4.5C).[52] This addition makes valacyclovir a substrate for the human peptide transporter 1 (PEPT1) solute carrier.[52,203] Valacyclovir was not shown to cross the Caco-2 monolayer on the hydrogel growth-matrix in paper II. This is believed to be caused by transformation of valacyclovir to acyclovir before it could be transported. Valacyclovir has been shown to be stable in buffer below pH 4,[52] and the transport study was carried out at pH 7.4. Hence, transport with valacyclovir could be performed at a lower pH for future studies. On the other hand, the physiological pH in the small intestine might be higher than 4 as it fluctuates from 4.0 to 7.5 throughout the small intestine.[20] So, a study below pH 4 is not necessary the best representation of the *in vivo* situation.

In summary, the Caco-2 cells cultured on the hydrogel growth-matrix display lucifer yellow and furosemide permeabilities in accordance with what has been reported for Caco-2 monolayers on polyester membranes. However, the TEER value is lower than on the polyester filter and the transport was delayed. The HUVEC cells on the hydrogel growth-matrix did not display any barrier function.

4.5 Possible Improvements Tissue Models

The presented Caco-2 based small intestinal model can be improved by including more cell types than enterocytes, as the small intestinal tissue includes several cell types. The lymphatic/immune function, mucus, and metabolic enzymes are the three main functionalities lacking in the presented Caco-2 based small intestinal model compared to the *in vivo* small intestinal tissue.

To incorporate mucus in the model, one could imagine adding another 3D-printed insert on top of the insert with Caco-2 cells. This insert could be with HT29-MTX, LS174T, or LoVo, thereby obtaining a mucus layer. A mucus layer on a membrane directly on top of a Caco-2 layer has been seen before though with a coating of porcine mucins instead of a layer of mucin producing cells.[121] Another approach may be to use the co-culture of Caco-2 and HT29-MTX cells. This approach might be more suited, since it avoids another layer and a further diffusional gradient. Kim et al. saw mucus on a Caco-2 layer by introduction of shear stress and peristalsis-like movements.[125] If this could be incorporated that could potentially induce mucus expression in the Caco-2 cells.

Caco-2 cells lack expression of metabolic enzymes, but this can be circumvented. CYP3A4 expression can be induced by growing Caco-2 cells on Matrigel® coated filters the presence of vitamin D.[204] Caco-2 cells in the

Caco-2 based small intestinal model also grow on a soft hydrogel growth-matrix it may be possible to induce expression of CYP3A4.

To model lymphoid tissue better, incorporation of macrophages, dendritic cells, and lymphocytes could be considered to gain better representation of the GALT. This will help in absorption modeling for lipophilic drugs, since these can target lymphatic drainage.

Another approach to improve then first pass metabolism model could be addition the nonalcoholic steatohepatitis model in the case of developing a drug for this disease. Moreover, the co-culture of endothelial cells and smooth muscle cells could be included, as smooth muscle cells are also present in the underlying the villi in the lamina propria along with capillaries.[205] Though, in terms of interaction with smooth muscle cells this might be better to model larger vessels that can be contracted and relaxed.

Chapter 5

Determination of Growth Matrix Stiffness

This chapter includes results of the project presented paper II 'Characterization of thin gelatin-hydrogel membranes with balloon properties for dynamic tissue engineering' and a discussion of these results.

Paper II focuses on the third aim:

iii) Characterize the stiffness of the cell growth matrix

The method presented in this paper consists a thin gelatin-hydrogel membrane in a 3D-printed insert (Figure 5.1A). Once submerged in a buffer, the thin gelatin-hydrogel membrane could be stretched by stepwise addition of buffer on top of the membrane (Figure 5.1B). This resulted in equibiaxial stretching of the membrane, like a balloon. From the stepwise stretching of the membrane a curve of the pressure of the water column against the stretch ratio could be obtained (Figure 5.1C). The stiffness of the gelatin-hydrogel membrane was obtained from the curve. The stretching of the gelatin-hydrogel was shown to be reversible as removal of buffer from on top of the gelatin-hydrogel membrane would let it contract (Figure 5.1D).

This chapter focuses on the theory behind stiffness determination of elastic materials and evaluates the method of equibiaxial stretching based hydrogel stiffness determination.

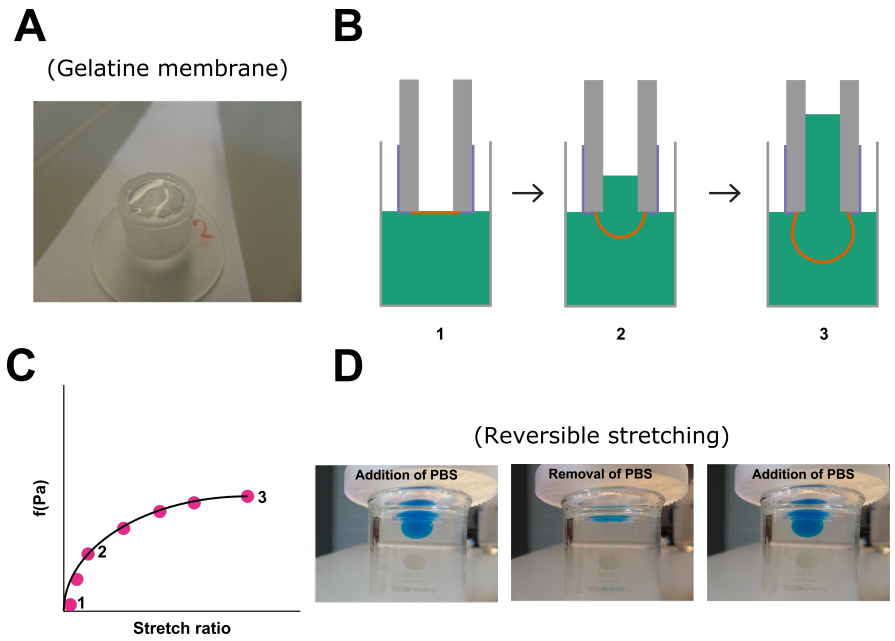

Figure 5.1: Schematic illustrations of the submerged equibiaxial gelatin-hydrogel membrane stretching method for determination of hydrogel stiffnesses: A) The gelatin-hydrogel membrane in a 3D-printed insert. B) The gelatin-hydrogel membrane (orange) is submerged in buffer (green) and stepwise stretched by an increasing water column. C) Plot of the pressure of the water column as a function of the stretch ratio. D) Images of stretching and contraction of the gelatin-hydrogel membrane. Reprinted with permission from.[184]

5.1 Stretchable Materials

5.1.1 What Makes a Material Elastic?

For a material to exhibit elasticity, three requirements must be met; the presence of long-chain molecules with freely rotating links, weak secondary forces between the molecules, and interlocking of the molecules at a few places to create a 3D network.[206]

i) Long-chain molecules, with freely rotating links, lead to a greater amplitude of vibrations perpendicular to the chain than in the direction of the chain itself, due to weaker lateral forces between the chains than the primary valence forces within the chains.[207]

ii) The variety of conformations of rubber-like elastics must not be impeded by the surrounding molecules, thus the secondary forces between the molecules must be weak.[206]

iii) The interlocking cross-links of molecular chains with permanent primary chemical bonds are what distinguishes a rubber from a liquid (Figure 4.3).[169] Few linked points along the length of the molecules produce a linked

network of all molecules, thus the molecules cannot move independently as in a liquid.

As a result, a rubber-like material will have polymer chains that are curled up, randomly oriented, and isotropic (i.e. directional independent).[206] However, when deformed, such as when stretched by a tensile force, the polymeric chains are stretched and become highly anisotropic (i.e. directional dependent) (Figure 5.2).

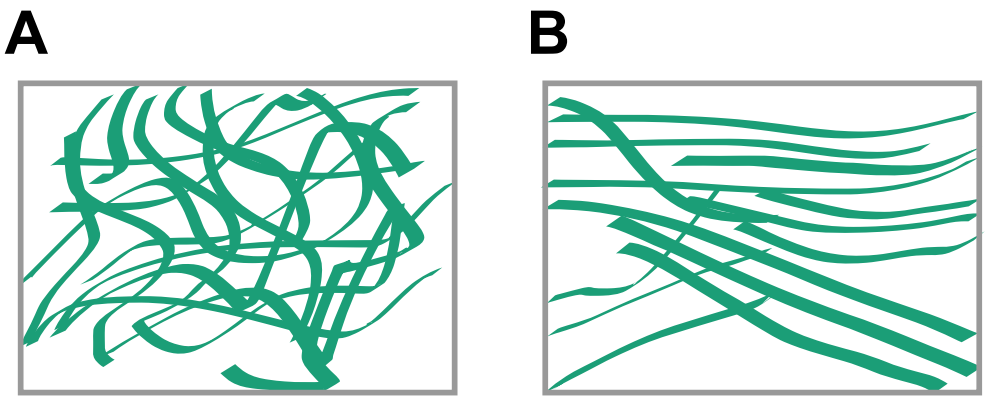

Figure 5.2: Schematic of the polymer chain organization of elastic materials in: A) Polymer chains in the natural state. B) Polymer chains in the deformed state. Modified from.[206]

5.1.2 Stretching of a Rubber

Hydrogels are rubber-like elastic,[208,209] therefore stretching of hydrogels can give information about their stiffnesses. When a rubber or rubber-like elastic is stretched, strain (i.e. deformation of the material) is introduced resulting in a reduction in entropy (i.e. a reduction in the number of allowable the polymer configurations). The internal forces of the material try to counter act the strain by increasing the entropy to let the polymer chains to curl up. Curled up polymer chains reduce the strain and let the material retract. However, the internal forces or resistance in a continuous material do not change for large strains, since the polymeric chains in this state are fully stretched.[169,206] In short, the retractive force is almost solely due to the tendency of polymer chains in rubbers to return to a less ordered curled up state. This distinguishes rubbers from ordinary solids as their elasticity is caused by intermolecular forces.[210] The stiffness of a solid material can be determined from the relationship between the stress introduced and the strain it results in, this ratio is known as the Young's modulus.[211] This value can be obtained by rheological measurements.

5.2 Rheological Stiffness Measurements

Rheology is the study of flow and deformation of materials.[211] Rheology can be used to determine viscosities of liquids and emulsions and to determine stiffness and yield stress of solid materials.[212] In rheology, two types of material deformations are in focus; tensile stress or shear stress (Figure 5.3).

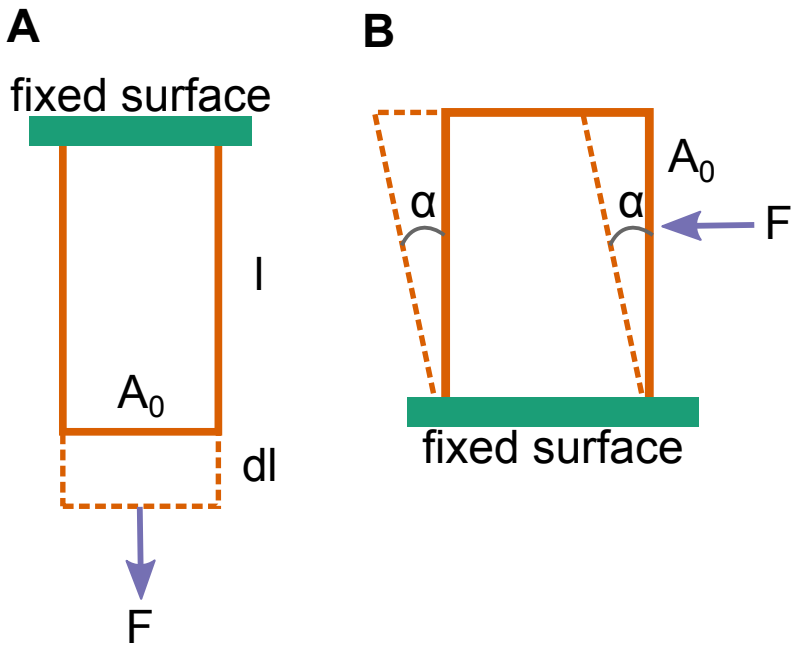

Figure 5.3: Schematic of two types of material deformation: A) Tensile deformation results from a tensile stress introduced into the material. B) Shear deformation results from a stress introduced transverse into a material fixed to a surface. Modified from.[211]

During tensile stress (σ) deformation is introduced by the force (F) acting on the surface area (A_0) resulting in a tensile strain (ε) that is dl/l, of which l is the original length and dl is the change as a result of the tensile stress. From which the Young's modulus (E) can be obtained:

$$E = \frac{\sigma}{\varepsilon} = \frac{(F/A_0)}{(dl/l)} \tag{5.1}$$

Hence, Young's modulus is a measure of a material's ability to withstand changes in length under lengthwise tension or compression and is normally given in pascal. However, tensile stress is not always a viable option strain introduction as materials rarely come as perfect cubes, hence shear stress can be utilized.

When a material is exposed to shear stress a shear modulus (G) can be obtained, as was done in paper I. Shear stress (τ) is achieved by fixating the

strained object to a surface transverse of the force. The tangent angle of the shear stress (α) gives the shear strain (γ). The shear modulus is then a measure of a material's ability to withstand transverse force:

$$G = \frac{\alpha}{\gamma} = \frac{(F/A_0)}{tan\ \alpha} \tag{5.2}$$

The shear modulus and the Yong's modulus are related to each other through the following equation:

$$E = 2G\ (1 + \nu) \tag{5.3}$$

Where, ν is Poisson's ratio (i.e. the ratio of transverse strain ($\varepsilon_{\text{transverse}}$) to the longitudinal strain ($\varepsilon_{\text{longitudinal}}$)):[213]

$$\nu = \frac{\varepsilon_{\text{transverse}}}{\varepsilon_{\text{longitudinal}}} \tag{5.4}$$

Theoretically, isotropic materials have a Poisson's ratio between -1$\leq\nu\leq$ 0.5. A Poission's ratio of ν=0.5 means that the material is incompressible and when stretched in the longitudinal axis there is a corresponding shortening of the transverse axis. Hence, incompressible materials display a volume constant deformation. A perfectly elastic material has a Poisson's ratio of ν=0.5. A fully swollen hydrogel behaves as a rubber-like material,[209] and has a Poisson's ratio close to 0.5.[177,208] Hence, the Young's modulus of a hydrogel is given by about three times the shear modulus (Equation 5.3).

In summary, the Young's modulus can be obtained by measuring the force applied and change in shape of a cube of hydrogel. However, materials rarely come as perfect cubes, hence it is necessary to have others ways to introduce stress and measure strain. One method of introducing shear stress is a rheometer with which viscoelastic materials are often characterized.

5.2.1 Rheometer

Certain materials flow, act like liquids, when observed over time these are considered viscoelastic.[214] Viscoelastic materials have three properties:

i) When exposed to a step constant strain display decreased stress (stress relaxation)

ii) When exposed to a step constant stress display increased strain (creep)

iii) Displays a stress-strain phase lag (hysteresis)

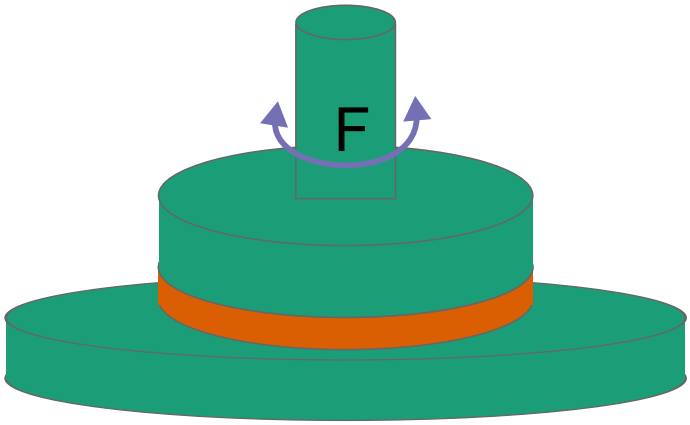

Figure 5.4: Cartoon of the principle of a rheometer: The substrate (red) is placed in between two parallel plates (green). The top plate oscillates with a given force thereby applying shear stress resulting in shear strain from which storage and loss moduli are obtained.

A rheometer introduces shear strain into a viscoelastic material between two parallel plates (Figure 5.4).[211]In a rheometer one of the two parallel plates is fixed and the other plate oscillates to introduce shear stress into the sample. The oscillating shear stress consists of an in-phase and an out-of-phase shear stress part. Resulting in a complex shear modulus (G) consisting of two components; the elastic (in-phase) shear storage modulus (G') and the viscous (out-of-phase) shear loss modulus (G'').[212] The shear storage modulus is the energy stored and recovered in cyclic deformation and the shear loss modulus is the energy dissipated as heat. The shear modulus can give the Young's modulus (Equation 5.3), and it can be obtained from the shear and loss moduli output from a rheometer:

$$G^2 = G'^2 G''^2 \tag{5.5}$$

These moduli can only be achieved under very small strains therefore a rheometer rely on very small oscillation and precise measurements, hence rheometers are expensive.[211]

5.3 Rheometer Compared to Equibiaxial Stretching

As mentioned above, paper II describes a method that was developed to determine the softness of hydrogels in an aqueous environment. Shear stress is achieved by equibiaxial stretching of the gelatin-hydrogel membrane, similar to inflating a balloon.[215] The stretch ratio is measured for specific pressures. From the stretch ratio and the corresponding pressure the shear modulus (G)

can be obtained from which the Young's modulus can be obtained (Equation 5.3). As the gelatin-hydrogel membrane is submerged in a buffer, swelling of the hydrogel is secured meaning $\nu \approx 0.5$ and precise determination of the softness given by Young's modulus.

A rheometer is expensive since it needs to do very precise measurements, whereas the presented method only relies on very few components that would usually be in a laboratory. Though, a rheometer has multiple functions, such as following the gelation, which the equibiaxial stretching method does not have.

In the equibiaxial stretching method, the gelatin-hydrogel membrane is submerged in a buffer so it is swollen. Swelling is more difficult to achieved when using a rheometer. Furthermore, evaporation is more likely to occur in the rheometer, but it can be avoided by addition of oil around the sample.

In paper II, a 5 % gelation hydrogel membrane was measured, and the Young's modulus measured with the equibiaxial stretching method was 350 Pa, whereas with a rheometer it was 780 Pa. Hence, the two methods give comparable results. The lower Young's modulus measured with the equibiaxial stretching method could be due to the swelling of the gelatin-hydrogel membrane. These measurements, however, are close to the stiffnesses of the *in vivo* tissues modeled in the first pass metabolism model. Where, epithelial tissue have a Young's modulus of close to 1,000 Pa.[152,216] Moreover, epithelial cell lines have been shown to display epithelial polarization when casted in hydrogel growth-matrices with a Young's modulus <400 Pa.[160] Hence, the gelatinhydrogel growth-matrix has a stiffness suitable for the tissues models in paper I.

One can imagine seeding cells on the hydrogel and measure the Young's modulus to determine the influence from the cells on the stiffness of the hydrogel. This can give information about the nature of the specific cells. This could be relevant for cell types such as muscle cells to determine how 'strong' they are. Another goal could be to 'train' cells such as vascular smooth muscle cells (VSMCs) which can detect mechanical stimulus from pulsatile stretch and change gene expression as a consequence thereof.[217,218] This influences cellular functions such as proliferation, apoptosis, and migration.

As mentioned above (Section 3.2), peristalsis-like deformation have led to expression of mucin-2 from Caco-2 cells.[125] One could imagine combining the thin stretchable gelatin-hydrogel membrane from paper II with the Caco-2 based small intestinal model from paper I. By moving the insert up and down to create a change in water pressure peristalsis-like movements can be introduced. This might push the Caco-2 cells to express mucus.

Chapter 6

Ongoing Research Project with the First Pass Metabolism Model

This chapter is based on preliminary data from ongoing or unfinished projects. Section 6.1 includes research performed on external stay at the School of Medicine at Dundee University, United Kingdom. Section 6.2 includes results obtained by Anna Kathrine Bach Mortensen, whom I supervised during her master project 'Rolling capture of monocytes on endothelial layers for atherosclerosis modelling'.

6.1 Transport of Phenformin Measured by Luciferase

6.1.1 Inhibition of the Gluconeogenesis from Phenformin

To show a drug absorbed through the small intestine having an effect on the liver compartment, phenformin was used to affect the liver compartment. For this study the HUVEC based endothelial model was left out to secure that a higher amount of absorbed phenformin would reach the liver compartment.

Phenformin, like metformin, is a biguanide that can inhibit the gluconeogenesis in the liver (Figure 6.1A).[219] Both drugs inhibit the respiratory chain complex I in the mitochondria leading to activation of adenosine monophosphate-activated protein kinase (AMPK) and inhibition of the gluconeogenesis (Figure 6.1B).[220,221] Phenformin has been shown to be transported by the human organic cation transport 1 (hOCT1).[222] Caco-2 cells have a low expression of this transporter.[76] It has been shown that blocking of hOCT1 can hinder the activation AMPK by metformin but not by phenformin.[220] Hence, the cellular uptake of phenformin is not completely dependent on the hOCT1 transporter as it is for metformin. Therefore, phenformin

was chosen to try and block the gluconeogenesis of hepatic cells, as it was believed to have a higher chance to cross the Caco-2 cell monolayer. Phenformin with a partition coefficient (logP) of -0.83 is more lipophilic than metformin with a logP of -1.43, as a result metformin is a specific but weak inhibitor of complex I, whereas phenformin is more potent but less specific. [221,223,224] The higher lipophilicity could also be the explanation for why the cellular uptake is not hindered by inhibition of hOCT1, since lipophilic drugs are better at crossing the lipid bilayer cell membrane than hydrophilic drugs.

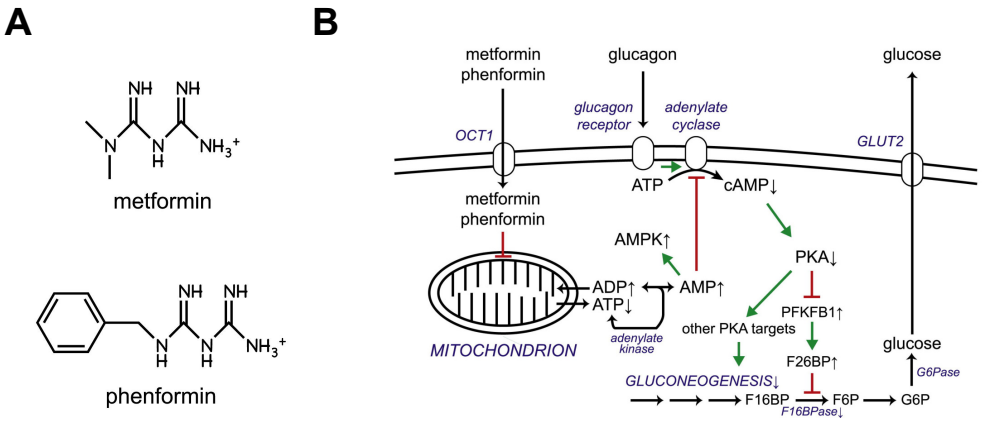

Figure 6.1: Structures of phenformin and metformin and diagram of mechanic of inhibition of hepatic gluconeogenesis: A) Chemical structure of metformin and phenformin. B) Phenformin inhibition of the gluconeogenesis.
Figure key: adenosine diphosphate (ADP), adenosine monophosphate (AMP), adenosine monophosphate-activated protein kinase (AMPK), adenosine triphosphate (ATP), cyclic adenosine monophosphate (cAMP); fructose-1,6-bisphosphate (F16BP); fructose-2,6-bisphosphate (F26BP); fructose-1,6-bisphosphatase (F16BPase); fructose-6-phosphate (F6P); glucose-6-phosphate (G6P), glucose-6-phosphatase (G6Pase); glucose transporter-2 (GLUT2); organic cation transporter 1 (OCT1); 6-phosphofructo-2-kinase/fructose-2,6-bisphosphatase 1(PFKFB1); protein kinase A (PKA). Reprinted with permission from. [225]

Glucose-6-phosphatase (G6Pase) is important for providing the body with glucose during fasting and is mainly found in the liver and the kidneys. [226] Its transcription can be inhibited by phenformin that lowers the promoter activity. [227] During fasting lactate, pyruvate, glycerol, and certain amino acids are converted to glucose through the gluconeogenic pathway of which a hydrolysis of glucose-6-phosphate to glucose by G6Pase is the last step before release of glucose from the liver to circulation (Figure 6.1B). [228] The gluconeogenesis is upregulated in the liver during fasting and diabetes.

Phenformin has been shown to reduce the G6Pase promoter activity with a half maximal inhibitory concentration (IC_{50}) value of 8.7 μM. [227] To show this effect a G6Pase promoter luciferase cell line called LLGH replaced the HepG2 based liver model. [229] To obtain LLGH cells, cells from a rat hepatoma

cell line were previously transfected with the pGL4-Human G6Pase construct using the calcium phosphate transfection methodology. By lysing the cells and mixing the lysate with a luciferase agent it was possible to obtain a relative amount of G6Pase promoter.

6.1.2 Phenformin Transport Study

The setup of the phenformin study included the Caco-2 small intestinal tissue model and LLGH cells underneath the Caco-2 cells (Figure 6.2). By changing the growth conditions, cells can be manipulated to a fasting state this switches the metabolism from glycolysis to gluconeogenesis. In this study, the growth conditions for the LLGH cells simulated a fasting state by addition of dexamethasone, which is a glucocorticoid, and cyclic adenosine monophosphate (cAMP).[227] cAMP increases G6Pase expression,[230] and glucocorticoids promote hepatic gluconeogenesis.[231] The hypothesis of this study was:

Phenformin can cross the Caco-2 monolayer and reach the LLGH cells underneath to inhibit the gluconeogenesis that would otherwise be upregulated in the fasting state.

100 μM phenformin was added apically to either a Caco-2 monolayer or an empty hydrogel growth-matrix. As a positive control the same amount of phenformin was added directly to the LLGH cells. As phenformin reduce the amount of G6Pase promoter, a reduced luciferase signal corresponds to a lowered amount of G6Pase promoter.

Hence, the aim was to see a larger drop of the luminescent signal when phenformin was added to an empty hydrogel growth-matrix than when a Caco-2 monolayer was present.

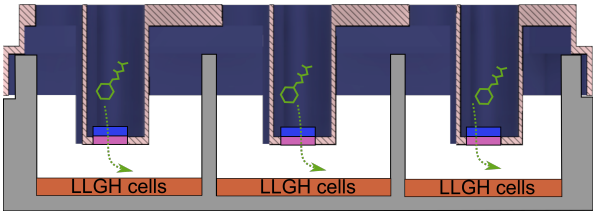

Figure 6.2: Schematic drawing of experimental setup for LLGH luciferase assay connected with the Caco-2 small intestinal tissue model.

When phenformin was not added G6Pase was expressed and there was a luminescent signal (Figure 6.3). When phenformin was added directly to the LLGH cells, basolateral for the Caco-2 cells, there was a drop in luminescence (Figure 6.3). When phenformin instead was added apically to a Caco-2 monolayer or an empty hydrogel growth-matrix there was not a drop in luminescence.

One could speculate that it would have been better to add dexamethasone and cAMP after the transport study. Thereby, fasting would not be initiated before phenformin has a chance to be transported. Since, the transcription of G6Pase promoter might already be initiated before phenformin could reach the cells. In short, initiating fasting after the transport study secures that the measured luminescence is not from G6Pase promoter transcribed before inhibition of transcription.

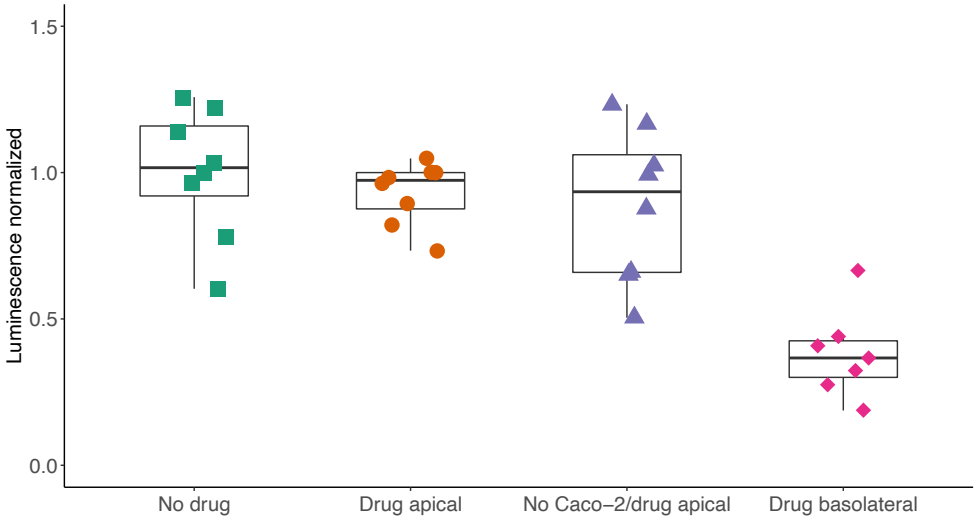

Figure 6.3: LLGH luciferase assay on transported phenformin: Luminescence shown as normalized to "no drug" sample for each individual of three independent experiments. No drug, n=8; Drug apical, n=8; No Caco-2/drug apical, n=8; Drug basolateral, n=7.

Another explanation can be the diffusional barrier of the hydrogel. The thickness of the hydrogel growth-matrix, on which the Caco-2 cells are, is 1 mm. However, *in vivo* the capillaries in the villi are right under the basal membrane of the epithelial cells.[205,232] Much thinner hydrogel growth-matrices would better resemble the connective tissue of the small intestinal villi *in vivo*. Furthermore, *in vivo* there is a larger concentration gradient as the blood vessels beneath the basal membrane transport the absorbed drug quickly via the blood stream. Whereas, in the model the transported drug passes through the hydrogel growth-matrix much slower, resulting in a smaller concentration gradient.

6.2 Shear Stress on Endothelial Cells

In paper I, the HUVEC based endothelial model did not display barrier function. It was grown in stagnant cell medium which far from the *in vivo* situation. *In vivo*, the vascular endothelial cells are subjected to flow and are able

to sense flow through a variety of receptors.[233,234] Laminar flow on vascular endothelial cells affects gene expression of multiple processes; alignment, mechanical properties, proliferation, apoptosis, migration, and permeability.[235] Moreover, it has previously been shown that shear stress can lead to alignment of endothelial cells.[236,237] Therefore, the hypothesis for this study was:

A better morphology of HUVEC cells can be obtained by implementation of an in vivo-like flow.

To apply flow to the endothelial cells a rotor system, which could fit into a titer plate, was developed with the thought of potentially being combined with the HUVEC endothelial model (Figure 6.4). The 3D-printed shear system had a Lego Mindstorms® motor attached to revolve a shaft connected to gears with rotors that would rotate in each well of a titer plate. In this study, HUVEC cells were exposed to shear for 48 h with the 3D-printed shear method.

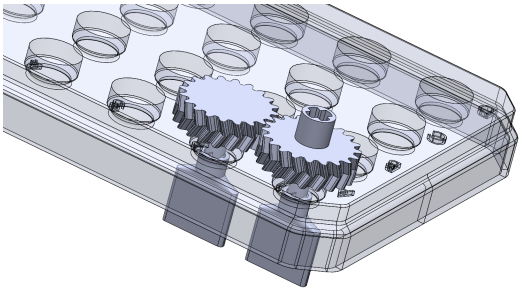

Figure 6.4: Rendering 3D-printed insert a long with gears connected to rotors that fit in a 24 well titer plate.

As expected, the HUVEC cells displayed dense peripheral bands of F-actin when not exposed to shear stress (Figure 6.5A).[238] When the endothelial cells were exposed to shear stress, the F-actin fibers orient parallel to the long axis of the cell (Figure 6.5B). TNFα induced morphological changes to endothelial cells such as elongation and F-actin reorganization (Figure 6.5C).[239,240] Thus, what was seen with both TNFα and shear stress was a synergistic effect (Figure 6.5D).

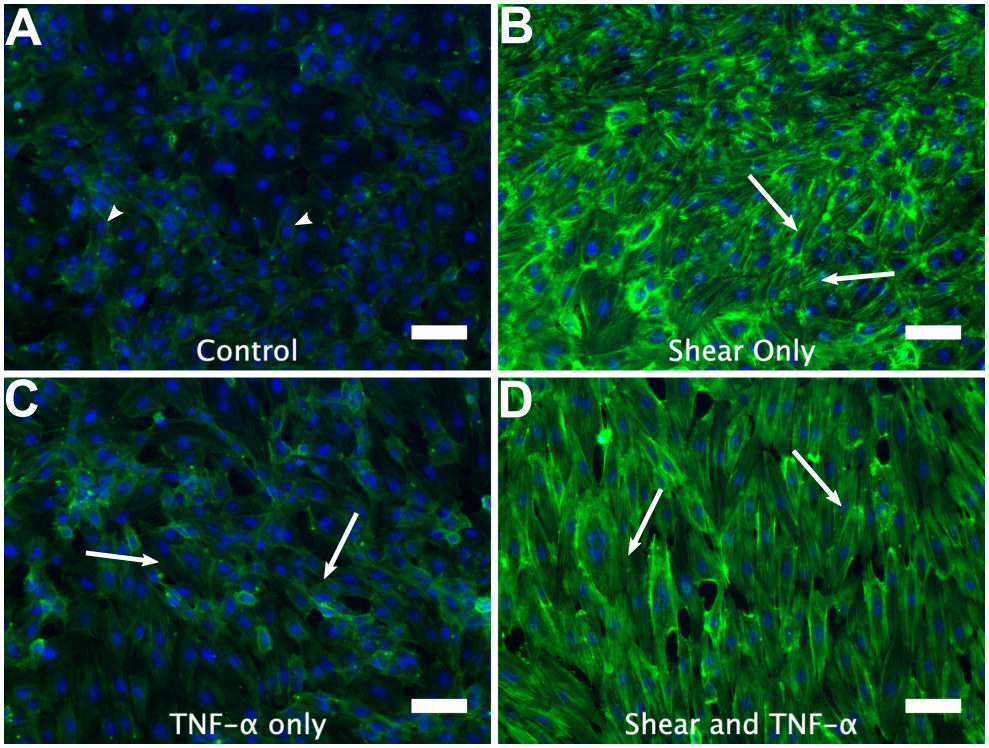

Figure 6.5: Images obtained by confocal microscopy representing of HUVEC cells exposed to shear and TNFα: A) Control HUVEC cells without shear stress and TNFα stained for F-actin (green) and nucleus (blue) showing dense peripheral bands (arrowheads). B) HUVEC cells exposed to shear stress displaying stress fibers (arrows). C) HUVEC cells exposed to TNFα displaying stress fibers (arrows). D) HUVEC cells exposed to shear stress and TNFα displaying stress fibers (arrows). Scalebars: 100 μm.

The shear stress of the shear system was estimated to $\sim$0.5 dyn cm^{-2} (data not shown), which is substantially lower than the 12-40 dyn cm^{-2} which previously have been used to introduce shear stress to F-actin reorganization.[236–238,241,242] Though, the estimate of $\sim$0.5 dyn cm^{-2} might not be precise as it was calculated from difference of movement speed of floating cells in two different planes under flow. Even though, it is not necessary in this case to increase the shear stress, it would be possible to change the rotor of the system. If the rotor is designed as a flat disc, as in a rheometer (Section 5.2), the shear stress would increase. Another way could be by increasing the viscosity of the cell culture medium.

Chapter 7

Conclusion

In this PhD project, a first pass metabolism method consisting of three cell based tissue models was presented. Evaluations of cell permeability and morphology of the tissue models were presented in paper I. A method to evaluate the stiffness of the growth matrices was presented in paper II.

The first hypothesis for this PhD project was:

i) Inserts for connected cell cultures can be fabricated with 3D printing

The tissue models for the first pass metabolism method were based on 3D-printed inserts with hydrogel growth-matrices. With the 3D-printed inserts it proved easy to culture multiple cell types individually and to connect them once fully differentiated. The cultures can grow as either 2D or 3D cultures under each their optimized growth conditions. The hydrogel growth-matrices can be dissolved and the 3D-printed inserts can be reused, however, the hydrogel growth-matrices need to be re-casted each time. Due to the casting of the hydrogel growth-matrices, the method is more time consuming than commercial titer plate inserts with polyester filters. Nonetheless, the hydrogel growth-matrix allows for following the growth of cell cultures as it is transparent.

The method is not based on PDMS, and thus there is not a risk of small hydrophobic molecules diffusing into it. The material of the 3D-printed inserts is laborious to get biocompatible and the fabrication is slow. If the method was to be standardized, it would be of interest to injection mold the 3D-printed inserts. Injection molding will speed up the production and give the possibility of selecting well characterized biocompatible materials.

The second hypothesis for this PhD project was:

ii) A good prediction of the first pass metabolism can be obtained by connecting *in vitro* cell based tissue models

The design of the connected tissue models allowed for sampling underneath each tissue model. As a result, it was possible to mimic and follow a drug's way from the small intestine to the liver. Thereby, the model displays the connection of the small intestine, the vascular endothelium, and the liver. However, the single cell-type based tissue models presented are simple and lack some functionality. The Caco-2 small intestinal model lacks metabolic enzymes, mucus, and immune activity. The HUVEC endothelial model did not display a barrier function. Functional tests of the metabolic activity of the HepG2 liver model are yet to be performed. However, the method can be used as a base for more complex tissue models.

The Caco-2 small intestinal tissue model displayed permeabilities both paracellularly and transcellularly comparable with Caco-2 cells cultured on polyester filters, even if the electrical resistance was lower. Though, the lower electrical resistance is closer to the *in vivo* resistance than the high resistance of Caco-2 cells on polyester filters. However, the thickness of the hydrogel growth-matrix acts as a diffusional barrier slowing transport. Hence, the method would benefit from replacing the gelatin hydrogel growth-matrix with a hydrogel of a material with a higher permeability.

The third hypothesis for this PhD project was:

iii) Stiffness characterization of soft cell growth-matrices can be achieved while the growth matrices are submerged in a relevant buffer

The stiffnesses of thin gelatin-hydrogel membranes measured with the equibiaxial stretching method was close to but slightly lower than that observed with a rheometer. Hence, the method could be used to determine stiffnesses of soft hydrogel growth-matrices while submerged in a buffer. Moreover, the method does not rely on expensive equipment, and thus can be a cheap way to measure stiffnesses of soft hydrogel growth-matrices. However, the method relies on laborious analysis of stretching images with image-analysis software and plotting of graphs where data processing is more automatic with a rheometer. In addition to stiffness characterization of soft hydrogels, it was possible to stretch cells with the thin gelatin-hydrogel membrane.

Bibliography

[1] S. M. Paul, D. S. Mytelka, C. T. Dunwiddie, C. C. Persinger, B. H. Munos, S. R. Lindborg, and A. L. Schacht, "How to improve RD productivity: The pharmaceutical industry's grand challenge," *Nature Reviews Drug Discovery*, vol. 9, no. 3, pp. 203–214, 2010.

[2] J. A. DiMasi, H. G. Grabowski, and R. W. Hansen, "Innovation in the pharmaceutical industry: New estimates of R&D costs," *Journal of Health Economics*, vol. 47, pp. 20–33, 2016.

[3] R. C. Mohs and N. H. Greig, "Drug discovery and development: Role of basic biological research," *Alzheimer's & Dementia: Translational Research & Clinical Interventions*, vol. 3, no. 4, pp. 651–657, 2017.

[4] A. Sivaraman, J. Leach, S. Townsend, T. Iida, B. Hogan, D. Stolz, R. Fry, L. Samson, S. Tannenbaum, and L. Griffith, "A Microscale In Vitro Physiological Model of the Liver: Predictive Screens for Drug Metabolism and Enzyme Induction," *Current Drug Metabolism*, vol. 6, no. 6, pp. 569–591, 2005.

[5] J. Törnell and M. Snaith, "Transgenic systems in drug discovery: from target identification to humanized mice," *Drug Discovery Today*, vol. 7, no. 8, pp. 461–470, 2002.

[6] Q. J. Baca and D. E. Golan, "Principles of Pharmacology," in *Principles of Pharmacology*, ch. 3, pp. 27–42, Baltimore: Lippincott Williams & Wilkins, 3 ed., 2012.

[7] P. V. Balimane, S. Chong, and R. A. Morrison, "Current methodologies used for evaluation of intestinal permeability and absorption," *Journal of Pharmacological and Toxicological Methods*, vol. 44, no. 1, pp. 301–312, 2000.

[8] K. Thanki, R. P. Gangwal, A. T. Sangamwar, and S. Jain, "Oral delivery of anticancer drugs: Challenges and opportunities," *Journal of Controlled Release*, vol. 170, no. 1, pp. 15–40, 2013.

[9] D. Eek, M. Krohe, I. Mazar, A. Horsfield, F. Pompilus, R. Friebe, and A. L. Shields, "Patient-reported preferences for oral versus intravenous administration for the treatment of cancer: A review of the literature," *Patient Preference and Adherence*, vol. 10, pp. 1609–1621, 2016.

[10] G. Liu, E. Franssen, M. I. Fitch, and E. Warner, "Patient preferences for oral versus intravenous palliative chemotherapy," *Journal of Clinical Oncology*, vol. 15, no. 1, pp. 110–115, 1997.

[11] M. Górnaś and C. Szczylik, "Oral treatment of metastatic breast cancer with capecitabine: What influences the decision-making process?," *European Journal of Cancer Care*, vol. 19, no. 1, pp. 131–136, 2010.

[12] P. Colombo, F. Sonvico, G. Colombo, and R. Bettini, "Novel platforms for oral drug delivery," *Pharmaceutical Research*, vol. 26, no. 3, pp. 601–611, 2009.

[13] J. R. Jørgensen, M. L. Jepsen, L. H. Nielsen, M. Dufva, H. M. Nielsen, T. Rades, A. Boisen, and A. Müllertz, "Microcontainers for oral insulin delivery – In vitro studies of permeation enhancement," *European Journal of Pharmaceutics and Biopharmaceutics*, vol. 143, pp. 98–105, 2019.

[14] E. Moroz, S. Matoori, and J. C. Leroux, "Oral delivery of macromolecular drugs: Where we are after almost 100 years of attempts," *Advanced Drug Delivery Reviews*, vol. 101, pp. 108–121, 2016.

[15] D. M. Shackleford, W. A. Faassen, N. Houwing, H. Lass, G. A. Edwards, C. J. Porter, and W. N. Charman, "Contribution of lymphatically transported testosterone undecanoate to the systemic exposure of testosterone after oral administration of two andriol formulations in conscious lymph duct-cannulated dogs," *Journal of Pharmacology and Experimental Therapeutics*, vol. 306, no. 3, pp. 925–933, 2003.

[16] T. Hetal, P. Bindesh, and T. Sneha, "A review on techniques for oral bioavailability enhancement of drugs," *International Journal of Pharmaceutical Sciences Review and Research*, vol. 4, no. 3, pp. 203–223, 2010.

[17] S. M. Pond and T. N. Tozer, "First-Pass Elimination Basic Concepts and Clinical Consequences," *Clinical Pharmacokinetics*, vol. 9, pp. 1–25, 1984.

[18] R. Pratley, A. Amod, S. T. Hoff, T. Kadowaki, I. Lingvay, M. Nauck, K. B. Pedersen, T. Saugstrup, and J. J. Meier, "Oral semaglutide versus subcutaneous liraglutide and placebo in type 2 diabetes (PIONEER 4): a randomised, double-blind, phase 3a trial," *The Lancet*, vol. 394, no. 10192, pp. 39–50, 2019.

[19] A. L. Daugherty and R. J. Mrsny, "Transcellular uptake mechanisms of the intestinal epithelial barrier - Part one," *Pharmaceutical Science and Technology Today*, vol. 2, no. 4, pp. 144–151, 1999.

[20] P. Balimane and S. Chong, "Cell culture-based models for intestinal permeability: a critique," *Drug discovery today*, vol. 10, no. 5, pp. 335–343, 2005.

[21] K. E. Andersson, B. Bergdahl, H. Dencker, and G. Wettrell, "Proscillaridin activity in portal and peripheral venous blood after oral administration to man," *European Journal of Clinical Pharmacology*, vol. 11, no. 4, pp. 277–281, 1977.

[22] H. Remmer, "The role of the liver in drug metabolism," *The American Journal of Medicine*, vol. 49, no. 5, pp. 617–629, 1970.

[23] H. J. Binder, "Intestinal Fluid and Electrolyte Movement," in *Medical Physiology*, ch. 44, pp. 933–948, Philadelphia: Elsevier, 2012.

[24] P. A. Billat, E. Roger, S. Faure, and F. Lagarce, "Models for drug absorption from the small intestine: where are we and where are we going?," *Drug Discovery Today*, vol. 22, no. 5, pp. 761–775, 2017.

[25] K. C. Kwan, "Oral Bioavailability and First Pass Effects," *Drug Metabolism and Disposition*, vol. 25, no. 12, pp. 1329–1336, 1997.

[26] F. Delie and W. Rubas, "A Human Colonic Cell Line Sharing Similarities With Enterocytes as a Model to Examine Oral Absorption: Advantages and limitations of the Caco-2 model," *Critical Reviews in Therapeutic Drug Carrier System*, vol. 14, no. 3, pp. 221–286, 1997.

[27] J. Forstner, "Intestinal Mucins in Health and Disease," *Digestion*, vol. 17, no. 3, pp. 234–263, 1978.

[28] R. D. Specian and M. G. Oliver, "Functional biology of intestinal goblet cells," *American Journal of Physiology - Cell Physiology*, vol. 260, no. 2 29-2, pp. 83–93, 1991.

[29] D. A. Goodenough and P. D. L., "Gap junctions," *Cold Spring Harbor Perspectives in Biology*, vol. 1, no. 1, p. a002576, 2009.

[30] M. G. Farquhar and G. E. Palade, "Junctional complexes in various epithelia," *The Journal of cell biology*, vol. 17, pp. 375–412, 1963.

[31] S. Tavelin, J. Gråsjö, J. Taipalensuu, G. Ocklind, and P. Artursson, "Applications of Epithelial Cell culture in Studies of Drug Transport," in *Epithelial Cell Culture Protocols*, ch. 21, pp. 233–272, Totowa, NJ: Humana Press, 2002.

[32] A. L. Kierszenbaum and L. L. Tres, "Epithelium," in *Histology and Cell Biology An Introduction to Pathology*, ch. 1, pp. 1–55, Philadelphia: Elsevier Saunders, 2012.

[33] T. Lea, "Epithelial Cell Models; General Introduction," in *The Impact of Food Bio-Actives on Gut Health: In Vitro and Ex Vivo Models*, ch. 9, pp. 95–111, Springer, 2015.

[34] L. González-Mariscal, A. Betanzos, P. Nava, and B. E. Jaramillo, "Tight junction proteins," *Progress in Biophysics and Molecular Biology*, vol. 81, no. 1, pp. 1–44, 2003.

[35] P. J. Sinko, Ming Hu, and G. L. Amidon, "Carrier mediated transport of amino acids, small peptides, and their drug analogs," *Journal of Controlled Release*, vol. 6, no. 1, pp. 115–121, 1987.

[36] P. Lundquist and P. Artursson, "Oral absorption of peptides and nanoparticles across the human intestine: Opportunities, limitations and studies in human tissues," *Advanced Drug Delivery Reviews*, vol. 106, pp. 256–276, 2016.

[37] T. W. Spahn and T. Kucharzik, "Modulating the intestinal immune system: The role of lymphotoxin and GALT organs," *Gut*, vol. 53, no. 3, pp. 456–465, 2004.

[38] W. N. A. Charman and V. J. Stella, "Estimating the maximal potential for intestinal lymphatic transport of lipophilic drug molecules," *International Journal of Pharmaceutics*, vol. 34, no. 1-2, pp. 175–178, 1986.

[39] C. J. Porter, N. L. Trevaskis, and W. N. Charman, "Lipids and lipid-based formulations: Optimizing the oral delivery of lipophilic drugs," *Nature Reviews Drug Discovery*, vol. 6, no. 3, pp. 231–248, 2007.

[40] H. Ahn and J. H. Park, "Liposomal delivery systems for intestinal lymphatic drug transport," *Biomaterials Research*, vol. 20, no. 1, pp. 16–21, 2016.

[41] J. L. Zhuo and C. L. Xiao, "Proximal Nephron," *Comprehensive physiology*, vol. 3, no. 3, pp. 1079–1123, 2013.

[42] R. Bendayan, "Renal drug transport: A review," *Pharmacotherapy*, vol. 16, no. 6, pp. 971–985, 1996.

[43] H. Uehleke, "Cytochrome and Microsomal Drug Metabolism in Extra-Hepatic Tissues," *Deutsche Apotheker Zeitung*, vol. 108, no. 33, p. 1204, 1968.

[44] M. Gertz, A. Harrison, J. B. Houston, and A. Galetin, "Prediction of Human Intestinal First-Pass Metabolism of 25 CYP3A Substrates from In Vitro Clearance and Permeability Data," *The American Society for Pharmacology and Experimental Therapeutics*, vol. 38, no. 7, pp. 1147–1158, 2010.

[45] A. M. Rappaport, Z. J. Borowy, W. M. Lougheed, and W. N. Lotto, "Subdivision of hexagonal liver lobules into a structural and functional unit. Role in hepatic physiology and pathology," *The Anatomical Record*, vol. 119, no. 1, pp. 11–33, 1954.

[46] A. M. Rappaport and W. D. Wilson, "The stuctural and functional unit in the human liver (liver acinus)," *The Anatomical Record*, vol. 130, no. 4, pp. 673–689, 1958.

[47] T. Kietzmann, "Metabolic zonation of the liver: The oxygen gradient revisited," *Redox Biology*, vol. 11, no. December 2016, pp. 622–630, 2017.

[48] G. Ghibellini, E. M. Leslie, and K. L. Brouwer, "Methods to evaluate biliary excretion of drugs in humans: An updated review," *Molecular Pharmaceutics*, vol. 3, no. 3, pp. 198–211, 2006.

[49] R. E. S. Bullingham, A. J. Nicholls, and B. R. Kamm, "Clinical pharmacokinetics of mycophenolate mofetil," *Clinical Pharmacokinetics*, vol. 34, no. 6, pp. 429–455, 1998.

[50] E. Jahnchen, T. Meinertz, H. Gilfrich, F. Kersting, and U. Groth, "Enhanced elimination of warfarin during treatment with cholestyramine," *British Journal of Clinical Pharmacology*, vol. 5, no. 5, pp. 437–440, 1978.

[51] M. S. Roberts, B. M. Magnusson, F. J. Burczynski, and M. Weiss, "Enterohepatic circulation: Physiological, pharmacokinetic and clinical implications," *Clinical Pharmacokinetics*, vol. 41, no. 10, pp. 751–790, 2002.

[52] G. E. Granero and G. L. Amidon, "Stability of valacyclovir: Implications for its oral bioavailability," *International Journal of Pharmaceutics*, vol. 317, no. 1, pp. 14–18, 2006.

[53] C. MacDougall and B. J. Guglielmo, "Pharmacokinetics of valaciclovir," *Journal of Antimicrobial Chemotherapy*, vol. 53, no. 6, pp. 899–901, 2004.

[54] Y. Weiss, M. Safar, J. Lehner, J. Levenson, A. Simon, and J. Alexandre, "(+)-Propranolol clearance, an estimation of hepatic blood flow in man," *British Journal of Clinical Pharmacology*, vol. 5, no. 5, pp. 457–460, 1978.

[55] R. Urso, P. Blardi, and G. Giorgi, "A short introduction to pharmacokinetics," *European Review for Medical and Pharmacological Sciences*, vol. 6, no. 2, pp. 33–44, 2002.

[56] W. J. Jusko and M. Gretch, "Plasma and tissue protein binding of drugs in pharmacokinetics," *Drug Metabolism Reviews*, vol. 5, no. 1, pp. 43–140, 1976.

[57] W. E. Lindup and M. C. L'e Orme, "Clinical pharmacology: Plasma protein binding of drugs," *British Medical Journal (Clinical research ed.)*, vol. 282, no. 6259, pp. 212–214, 1981.

[58] G. H. Evans, A. S. Nies, and D. G. Shand, "The disposition of propranolol. 3. Decreased half-life and volume of distribution as a result of plasma binding in man, monkey, dog and rat," *Journal of Pharmacology and Experimental Therapeutics*, vol. 186, no. 1, pp. 114–122, 1973.

[59] W. E. Lindup, "Drug-Albmin Binding," *Biochemical society Transactions*, vol. 3, no. 5, pp. 635–640, 1975.

[60] A. C. Ericsson, M. J. Crim, and C. L. Franklin, "A brief history of animal modeling.," *Missouri medicine*, vol. 110, no. 3, pp. 201–205, 2013.

[61] J. D. Taurog, S. D. Maika, N. Satumtira, M. L. Dorris, I. L. McLean, H. Yanagisawa, A. Sayad, A. J. Stagg, G. M. Fox, A. L. O'Brien, M. Rehman, M. Zhou, A. L. Weiner, J. B. Splawski, J. A. Richardson, and R. E. Hammer, "Inflammatory disease in HLA-B27 transgenic rats," *Immunological Reviews*, vol. 169, pp. 209–223, 1999.

[62] H. H. Ussing and K. Zerahn, "Active Transport of Sodium as the Source of Electric Current in the Short-Circuited Isolated Frog Skin," *Acta physiologica Scandinavica*, vol. 23, pp. 110–127, 1951.

[63] C. Mazzoni, R. D. Jacobsen, J. Mortensen, J. R. Jørgensen, L. Vaut, J. Jacobsen, C. Gundlach, A. Müllertz, L. H. Nielsen, and A. Boisen, "Polymeric Lids for Microcontainers for Oral Protein Delivery," *Macromolecular Bioscience*, vol. 19, p. 1900004, 2019.

[64] L. L. Clarke, "A guide to Ussing chamber studies of mouse intestine," *American Journal of Physiology - Gastrointestinal and Liver Physiology*, vol. 296, no. 6, pp. 1151–1166, 2009.

[65] T. J. Franz, P. A. Lehman, and S. G. Raney, "Use of excised human skin to assess the bioequivalence of topical products," *Skin Pharmacology and Physiology*, vol. 22, no. 5, pp. 276–286, 2009.

[66] A. Simon, M. I. Amaro, A. M. Healy, L. M. Cabral, and V. P. de Sousa, "Comparative evaluation of rivastigmine permeation from a transdermal system in the Franz cell using synthetic membranes and pig ear skin with in vivo-in vitro correlation," *International Journal of Pharmaceutics*, vol. 512, no. 1, pp. 234–241, 2016.

[67] C. A. M. Fois, T. Y. L. Le, A. Schindeler, S. Naficy, D. D. McClure, M. N. Read, P. Valtchev, A. Khademhosseini, and F. Dehghani, "Models of the Gut for Analyzing the Impact of Food and Drugs," *Advanced Healthcare Materials*, vol. 8, p. 1900968, 2019.

[68] K. Molly, M. Vande Woestyne, and W. Verstraete, "Development of a 5-step multi-chamber reactor as a simulation of the human intestinal microbial ecosystem," *Applied Microbiology and Biotechnology*, vol. 39, no. 2, pp. 254–258, 1993.

[69] G. Ottaviani, S. Martel, and P. A. Carrupt, "Parallel artificial membrane permeability assay: A new membrane for the fast prediction of passive human skin permeability," *Journal of Medicinal Chemistry*, vol. 49, no. 13, pp. 3948–3954, 2006.

[70] G. Kaur and J. M. Dufour, "Cell lines: Valuable tools or useless artifacts," *Spermatogenesis*, vol. 2, no. 1, pp. 1–5, 2012.

[71] A. R. Hilgers, R. A. Conradi, and P. S. Burton, "Caco-2 cell monolayers as a model for drug transport across the intestinal mucosa," *Pharmaceutical research*, vol. 7, no. 9, pp. 902–910, 1990.

[72] P. Artursson and J. Karlsson, "Correlation between oral drug absorption in humans and apparent drug permeability coefficients in human intestinal epithelial (Caco-2) cells," *Biochemical and Biophysical Research Communications*, vol. 175, no. 3, pp. 880–885, 1991.

[73] I. J. Hidalgo, T. J. Raub, and R. T. Borchardt, "Characterization of the Human Colon Carcinoma Cell Line (Caco-2) as a Model System for Intestinal Epithelial Permeability," *Gastroenterology*, vol. 96, no. 2, pp. 736–749, 1989.

[74] M. Pinto, S. R. Leon, and M. Appay, "Enterocyte-like differentiation and polarization of the human colon carcinoma cell line Caco-2 in culture," *Biology of the Cell*, vol. 47, no. 3, pp. 323–330, 1983.

[75] M. Ölander, J. Wiśniewski, P. Matsson, P. Lundquist, and P. Artursson, "The Proteome of Filter-Grown Caco-2 Cells With a Focus on Proteins Involved in Drug Disposition," *Journal of Pharmaceutical Sciencesa*, vol. 105, no. 2, pp. 817–827, 2016.

[76] R. Hayeshi, C. Hilgendorf, P. Artursson, P. Augustijns, B. Brodin, P. Dehertogh, K. Fisher, L. Fossati, E. Hovenkamp, T. Korjamo, C. Masungi, N. Maubon, R. Mols, A. Müllertz, J. Mönkkönen, C. O'Driscoll, H. M. Oppers-Tiemissen, E. G. Ragnarsson, M. Rooseboom, and A. L. Ungell, "Comparison of drug transporter gene expression and functionality in Caco-2 cells from 10 different laboratories," *European Journal of Pharmaceutical Sciences*, vol. 35, no. 5, pp. 383–396, 2008.

[77] C. Atuma, V. Strugala, A. Allen, and L. Holm, "The adherent gastrointestinal mucus gel layer: thickness and physical state in vivo," *American Journal of Physiology-Gastrointestinal and Liver Physiology*, vol. 280, no. 5, pp. G922–G929, 2001.

[78] P. B. Watkins, S. A. Wrighton, E. G. Schuetz, D. T. Molowa, and P. S. Guzelian, "Identification of glucocorticoid-inducible cytochromes P-450 in the intestinal mucosa of rats and man," *Journal of Clinical Investigation*, vol. 80, no. 4, pp. 1029–1036, 1987.

[79] J. C. Kolars, P. Schmiedlin-Ren, J. D. Schuetz, C. Fang, and P. B. Watkins, "Identification of rifampin-inducible P450IIIA4 (CYP3A4) in human small bowel enterocytes," *Journal of Clinical Investigation*, vol. 90, no. 5, pp. 1871–1878, 1992.

[80] S. Devriese, L. Van den Bossche, S. Van Welden, T. Holvoet, I. Pinheiro, P. Hindryckx, M. De Vos, and D. Laukens, "T84 monolayers are superior to Caco-2 as a model system of colonocytes," *Histochemistry and Cell Biology*, vol. 148, no. 1, pp. 85–93, 2017.

[81] M. J. Cho, D. P. Thompson, C. T. Cramer, T. J. Vidmar, and J. F. Scieszka, "The Madin Darby Canine Kidney (MDCK) Epithelial Cell Monolayer as a Model Cellular Transport Barrier," *Pharmaceutical Research: An Official Journal of the American Association of Pharmaceutical Scientists*, vol. 6, no. 1, pp. 71–77, 1989.

[82] W. S. Putnam, L. Pan, K. Tsutsui, L. Takahashi, and L. Z. Benet, "Comparison of bidirectional cephalexin transport across MDCK and Caco-2 cell monolayers: Interactions with peptide transporters," *Pharmaceutical Research*, vol. 19, no. 1, pp. 27–33, 2002.

[83] M. M. Geens and T. A. Niewold, "Optimizing culture conditions of a porcine epithelial cell line IPEC-J2 through a histological and physiological characterization," *Cytotechnology*, vol. 63, no. 4, pp. 415–423, 2011.

[84] E. Cohen, I. Ophir, and Y. B. Shaul, "Induced differentiation in HT29, a human colon adenocarcinoma cell line," *Journal of Cell Science*, vol. 112, no. 16, pp. 2657–2666, 1999.

[85] T. Lesuffleur, A. Barbat, E. Dussaulx, and A. Zweibaum, "Growth Adaptation to Methotrexate of HT-29 Human Colon Carcinoma Cells Is Associated with Their Ability to Differentiate into Columnar Absorptive and Mucus-secreting Cells," *Cancer Research*, vol. 50, no. 19, pp. 6334–6343, 1990.

[86] T. Lesuffleur, A. Barbat, C. Luccioni, J. Beaumatin, M. Clair, A. Kornowski, E. Dussaulx, B. Dutrillaux, and A. Zweibaum, "Dihydrofolate reductase gene amplification-associated shift of differentiation in methotrexate-adapted HT-29 cells," *Journal of Cell Biology*, vol. 115, no. 5, pp. 1409–1418, 1991.

[87] G. J. Mahler, M. L. Shuler, and R. P. Glahn, "Characterization of Caco-2 and HT29-MTX cocultures in an in vitro digestion/cell culture model used to predict iron bioavailability," *Journal of Nutritional Biochemistry*, vol. 20, no. 7, pp. 494–502, 2009.

[88] X. D. Bu, N. Li, X. Q. Tian, and P. L. Huang, "Caco-2 and LS174T cell lines provide different models for studying mucin expression in colon cancer," *Tissue and Cell*, vol. 43, no. 3, pp. 201–206, 2011.

[89] F. Leonard, E. M. Collnot, and C. M. Lehr, "A three-dimensional coculture of enterocytes, monocytes and dendritic cells to model inflamed intestinal mucosa in vitro," *Molecular Pharmaceutics*, vol. 7, no. 6, pp. 2103–2119, 2010.

[90] J. Susewind, C. De Souza Carvalho-Wodarz, U. Repnik, E. M. Collnot, N. Schneider-Daum, G. W. Griffiths, and C. M. Lehr, "A 3D co-culture of three human cell lines to model the inflamed intestinal mucosa for safety testing of nanomaterials," *Nanotoxicology*, vol. 10, no. 1, pp. 53–62, 2016.

[91] E. A. Jaffe, R. L. Nachman, C. G. Becker, and C. R. Minick, "Culture of human endothelial cells derived from umbilical veins. Identification by morphologic and immunologic criteria," *Journal of Clinical Investigation*, vol. 52, no. 11, pp. 2745–2756, 1973.

[92] D. Bouïs, G. A. Hospers, C. Meijer, G. Molema, and N. H. Mulder, "Endothelium in vitro: A review of human vascular endothelial cell lines for blood vessel-related research," *Angiogenesis*, vol. 4, no. 2, pp. 91–102, 2001.

[93] C. J. Edgell, C. C. McDonald, and J. B. Graham, "Permanent cell line expressing human factor VIII-related antigen established by hybridization," *Proceedings of the National Academy of Sciences of the United States of America*, vol. 80, no. 12 I, pp. 3734–3737, 1983.

[94] E. W. Ades, F. J. Candal, R. A. Swerlick, V. G. George, S. Summers, D. C. Bosse, and T. J. Lawley, "HMEC-1: Establisment of an Immortalized Human Microvascular Endothelial Cell Line," *The Journal of investigative dermatology*, vol. 99, no. 6, pp. 683–690, 1992.

[95] S. E. Hughes, "Functional characterization of the spontaneously transformed human umbilical vein endothelial cell line ECV304: Use in an in vitro model of angiogenesis," *Experimental Cell Research*, vol. 225, no. 1, pp. 171–185, 1996.

[96] E. A. Lidington, D. L. Moyes, A. M. McCormack, and M. L. Rose, "A comparison of primary endothelial cells and endothelial cell lines for studies of immune interactions," *Transplant Immunology*, vol. 7, no. 4, pp. 239–246, 1999.

[97] L. Osborn, C. Hession, R. Tizard, C. Vassallo, S. Luhowskyj, G. Chi-Rosso, and R. Lobb, "Direct expression cloning of vascular cell adhesion molecule 1, a cytokine-induced endothelial protein that binds to lymphocytes," *Cell*, vol. 59, no. 6, pp. 1203–1211, 1989.

[98] A. Hidalgo, A. J. Peired, M. Wild, D. Vestweber, and P. S. Frenette, "Complete identification of E-selectin ligand activity on neutrophils reveals a dynamic interplay and distinct functions of PSGL-1, ESL-1 and CD44," *Immunity*, vol. 26, no. 4, pp. 477–489, 2007.

[99] D. H. Kong, Y. K. Kim, M. R. Kim, J. H. Jang, and S. Lee, "Emerging roles of vascular cell adhesion molecule-1 (VCAM-1) in immunological disorders and cancer," *International Journal of Molecular Sciences*, vol. 19, no. 4, pp. 13–17, 2018.

[100] L. Wang, Y. Ding, X. Guo, and Q. Zhao, "Role and mechanism of vascular cell adhesion molecule-1 in the development of rheumatoid arthritis," *Experimental and Therapeutic Medicine*, vol. 10, no. 3, pp. 1229–1233, 2015.

[101] S. Kodama, M. Davis, and D. L. Faustman, "The therapeutic potential of tumor necrosis factor for autoimmune disease: A mechanistically based hypothesis," *Cellular and Molecular Life Sciences*, vol. 62, no. 16, pp. 1850–1862, 2005.

[102] F. J. Baert, G. R. D'Haens, M. Peeters, M. I. Hiele, T. F. Schaible, D. Shealy, K. Geboes, and P. J. Rutgeerts, "Tumor necrosis factor α antibody (infliximab) therapy profoundly down- regulates the inflammation in Crohn's ileocolitis," *Gastroenterology*, vol. 116, no. 1, pp. 22–28, 1999.

[103] J. Agnholt, J. F. Dahlerup, and K. Kaltoft, "The effect of etanercept and infliximab on the production of tumour necrosis factor α, interferon-γ and GM-CSF in in vivo activated intestinal T lymphocyte cultures," *Cytokine*, vol. 23, no. 3, pp. 76–85, 2003.

[104] B. Bain and M. Brazil, "Fresh from the pipeline: Adalimumab," *Nature Reviews Drug Discovery*, vol. 2, no. 9, pp. 693–694, 2003.

[105] G. J. Byrne, A. Ghellal, J. Iddon, A. D. Blann, V. Venizelos, S. Kumar, A. Howell, and N. J. Bundred, "Serum soluble vascular cell adhesion molecule-1: Role as a surrogate marker of angiogenesis," *Journal of the National Cancer Institute*, vol. 92, no. 16, pp. 1329–1336, 2000.

[106] Y. Ohkawara, K. Yamauchi, N. Maruyama, H. Hoshi, I. Ohno, M. Honma, Y. Tanno, G. Tamura, K. Shirato, and H. Ohtani, "In situ expression of the cell adhesion molecules in bronchial tissues from asthmatics with air flow limitation: in vivo evidence of VCAM-1/VLA-4 interaction in selective eosinophil infiltration.," *American journal of respiratory cell and molecular biology*, vol. 12, no. 1, pp. 4–12, 1995.

[107] J. V. Castell, R. Jover, C. P. Martínez-Jiménez, and M. J. Gómez-Lechón, "Hepatocyte cell lines: Their use, scope and limitations in drug metabolism studies," *Expert Opinion on Drug Metabolism and Toxicology*, vol. 2, no. 2, pp. 183–212, 2006.

[108] S. Sefried, H. U. Häring, C. Weigert, and S. S. Eckstein, "Suitability of hepatocyte cell lines HepG2, AML12 and THLE-2 for investigation of insulin signalling and hepatokine gene expression," *Open Biology*, vol. 8, no. 10, 2018.

[109] R. Pimentel C., S. K. Ko, C. Caviglia, A. Wolff, J. Emnéus, S. S. Keller, and M. Dufva, "Three-dimensional fabrication of thick and densely populated soft constructs with complex and actively perfused channel network," *Acta Biomaterialia*, vol. 65, pp. 174–184, 2017.

[110] D. Wang, D. Cheng, Y. Guan, and Y. Zhang, "Thermoreversible hydrogel for in situ generation and release of HepG2 spheroids," *Biomacromolecules*, vol. 12, no. 3, pp. 578–584, 2011.

[111] S. C. Ramaiahgari, M. W. Den Braver, B. Herpers, V. Terpstra, J. N. M. Commandeur, B. Van De Water, and L. S. Price, "A 3D in vitro model of differentiated HepG2 cell spheroids with improved liver-like properties for repeated dose high-throughput toxicity studies," *Archives of Toxicology*, vol. 88, no. 5, pp. 1083–1095, 2014.

[112] C. E. Suurmond, S. Lasli, F. W. Dolder, A. Ung, H. Kim, P. Bandaru, K. Lee, H. Cho, S. Ahadian, N. Ashammakhi, M. R. Dokmeci,

J. Lee, and A. Khademhosseini, "In Vitro Human Liver Model of Non-alcoholic Steatohepatitis by Coculturing Hepatocytes, Endothelial Cells, and Kupffer Cells," *Advanced Healthcare Materials*, p. 1901379, 2019.

[113] R. Z. Lin, L. F. Chou, C. C. M. Chien, and H. Y. Chang, "Dynamic analysis of hepatoma spheroid formation: Roles of E-cadherin and β1-integrin," *Cell and Tissue Research*, vol. 324, no. 3, pp. 411–422, 2006.

[114] F. Hirschhaeuser, H. Menne, C. Dittfeld, J. West, W. Mueller-Klieser, and L. a. Kunz-Schughart, "Multicellular tumor spheroids: An underestimated tool is catching up again," *Journal of Biotechnology*, vol. 148, no. 1, pp. 3–15, 2010.

[115] L. G. Griffith and M. A. Swartz, "Capturing complex 3D tissue physiology in vitro.," *Nature Reviews Molecular Cell Biology*, vol. 7, no. 3, pp. 211–224, 2006.

[116] F. Antunes, F. Andrade, F. Araújo, D. Ferreira, and B. Sarmento, "Establishment of a triple co-culture in vitro cell models to study intestinal absorption of peptide drugs," *European Journal of Pharmaceutics and Biopharmaceutics*, vol. 83, no. 3, pp. 427–435, 2013.

[117] A. Gebert, H. J. Rothkötter, and R. Pabst, "M cells in payer's patches of the intestine," *International Review of Cytology*, vol. 167, pp. 91–159, 1996.

[118] H. Kimura, T. Yamamoto, H. Sakai, Y. Sakai, and T. Fujii, "An integrated microfluidic system for long-term perfusion culture and on-line monitoring of intestinal tissue models," *Lab on a Chip*, vol. 8, no. 5, pp. 741–746, 2008.

[119] Q. Ramadan, H. Jafarpoorchekab, C. Huang, P. Silacci, S. Carrara, G. Koklü, J. Ghaye, J. Ramsden, C. Ruffert, G. Vergeres, and M. A. Gijs, "NutriChip: Nutrition analysis meets microfluidics," *Lab on a Chip*, vol. 13, no. 2, pp. 196–203, 2013.

[120] H. J. Kim, D. Huh, G. Hamilton, and D. E. Ingber, "Human gut-on-a-chip inhabited by microbial flora that experiences intestinal peristalsis-like motions and flow," *Lab on a Chip*, vol. 12, no. 12, pp. 2165–2174, 2012.

[121] P. Shah, J. V. Fritz, E. Glaab, M. S. Desai, K. Greenhalgh, A. Frachet, M. Niegowska, M. Estes, C. Jäger, C. Seguin-Devaux, F. Zenhausern, and P. Wilmes, "A microfluidics-based in vitro model of the gastrointestinal human-microbe interface," *Nature Communications*, vol. 7, p. 11535, 2016.

[122] L. J. Dixon, M. Barnes, H. Tang, M. T. Pritchard, and L. E. Nagy, "Kupffer cells in the liver," *Comprehensive Physiology*, vol. 3, no. 2, pp. 785–797, 2013.

[123] S. Heydarkhan-Hagvall, G. Helenius, B. R. Johansson, J. Y. Li, E. Mattsson, and B. Risberg, "Co-culture of endothelial cells and smooth muscle cells affects gene expression of angiogenic factors," *Journal of Cellular Biochemistry*, vol. 89, no. 6, pp. 1250–1259, 2003.

[124] Y. R. Álvarez-García, K. P. Ramos-Cruz, R. J. Agostini-Infanzón, L. E. Stallcop, D. J. Beebe, J. W. Warrick, and M. Domenech, "Open multi-culture platform for simple and flexible study of multi-cell type interactions," *Lab on a Chip*, vol. 18, no. 20, pp. 3184–3195, 2018.

[125] H. J. Kim and D. E. Ingber, "Gut-on-a-Chip microenvironment induces human intestinal cells to undergo villus differentiation," *Integrative Biology*, vol. 5, no. 9, pp. 1130–1140, 2013.

[126] J. H. Sung and M. L. Shuler, "A micro cell culture analog (CCA) with 3-D hydrogel culture of multiple cell lines to assess metabolism-dependent cytotoxicity of anti-cancer drugs," *Lab on a Chip*, vol. 9, no. 10, pp. 1385–1394, 2009.

[127] J. H. Sung, C. Kam, and M. L. Shuler, "A microfluidic device for a pharmacokinetic-pharmacodynamic (PK-PD) model on a chip," *Lab on a Chip*, vol. 10, no. 4, pp. 446–455, 2010.

[128] Y. Imura, K. Sato, and E. Yoshimura, "Micro total bioassay system for ingested substances: Assessment of intestinal absorption, hepatic metabolism, and bioactivity," *Analytical Chemistry*, vol. 82, no. 24, pp. 9983–9988, 2010.

[129] B. M. Maoz, A. Herland, E. A. Fitzgerald, T. Grevesse, C. Vidoudez, A. R. Pacheco, S. P. Sheehy, T. E. Park, S. Dauth, R. Mannix, N. Budnik, K. Shores, A. Cho, J. C. Nawroth, D. Segrè, B. Budnik, D. E. Ingber, and K. K. Parker, "A linked organ-on-chip model of the human neurovascular unit reveals the metabolic coupling of endothelial and neuronal cells," *Nature Biotechnology*, vol. 36, no. 9, pp. 865–877, 2018.

[130] I. Maschmeyer, T. Hasenberg, A. Jaenicke, M. Lindner, A. K. Lorenz, J. Zech, L. A. Garbe, F. Sonntag, P. Hayden, S. Ayehunie, R. Lauster, U. Marx, and E. M. Materne, "Chip-based human liver-intestine and liver-skin co-cultures - A first step toward systemic repeated dose substance testing in vitro," *European Journal of Pharmaceutics and Biopharmaceutics*, vol. 95, pp. 77–87, 2015.

[131] I. Maschmeyer, A. K. Lorenz, K. Schimek, T. Hasenberg, A. P. Ramme, J. Hübner, M. Lindner, C. Drewell, S. Bauer, A. Thomas, N. S. Sambo, F. Sonntag, R. Lauster, and U. Marx, "A four-organ-chip for interconnected long-term co-culture of human intestine, liver, skin and kidney equivalents," *Lab on a Chip*, vol. 15, no. 12, pp. 2688–2699, 2015.

[132] J. D. Wang, N. J. Douville, S. Takayama, and M. Elsayed, "Quantitative analysis of molecular absorption into PDMS microfluidic channels," *Annals of Biomedical Engineering*, vol. 40, no. 9, pp. 1862–1873, 2012.

[133] K. Y. Chumbimuni-Torres, R. E. Coronado, A. M. Mfuh, C. Castro-Guerrero, M. F. Silva, G. R. Negrete, R. Bizios, and C. D. Garcia, "Adsorption of proteins to thin-films of PDMS and its effect on the adhesion of human endothelial cells," *RSC Advances*, vol. 1, no. 4, pp. 706–714, 2011.

[134] D. Huh, H. J. Kim, J. P. Fraser, D. E. Shea, M. Khan, A. Bahinski, G. A. Hamilton, and D. E. Ingber, "Microfabrication of human organs-on-chips," *Nature Protocols*, vol. 8, no. 11, pp. 2135–2157, 2013.

[135] G. Firpo, E. Angeli, L. Repetto, and U. Valbusa, "Permeability thickness dependence of polydimethylsiloxane (PDMS) membranes," *Journal of Membrane Science*, vol. 481, pp. 1–8, 2015.

[136] S. J. Trietsch, E. Naumovska, D. Kurek, M. C. Setyawati, M. K. Vormann, K. J. Wilschut, H. L. Lanz, A. Nicolas, C. P. Ng, J. Joore, S. Kustermann, A. Roth, T. Hankemeier, A. Moisan, and P. Vulto, "Membrane-free culture and real-time barrier integrity assessment of perfused intestinal epithelium tubes," *Nature Communications*, vol. 8, no. 1, pp. 1–7, 2017.

[137] S. J. Trietsch, G. D. Israëls, J. Joore, T. Hankemeier, and P. Vulto, "Microfluidic titer plate for stratified 3D cell culture," *Lab on a Chip*, vol. 13, no. 18, pp. 3548–3554, 2013.

[138] A. Nilghaz, S. Hoo, W. Shen, X. Lu, and P. P. Chan, "Multilayer cell culture system supported by thread," *Sensors and Actuators, B: Chemical*, vol. 257, pp. 650–657, 2018.

[139] Z. Wei, S. Kale, R. El Fatimy, R. Rabinovsky, and A. M. Krichevsky, "Co-cultures of Glioma Stem Cells and Primary Neurons, Astrocytes, Microglia, and Endothelial Cells for Investigation of Intercellular Communication in the Brain," *Frontiers in Neuroscience*, vol. 13, no. April, pp. 1–8, 2019.

[140] F. An, Y. Qu, Y. Luo, N. Fang, Y. Liu, Z. Gao, W. Zhao, and B. Lin, "A Laminated Microfluidic Device for Comprehensive Preclinical Testing in the Drug ADME Process," *Scientific Reports*, vol. 6, p. 25022, 2016.

[141] Z. Abid, S. Strindberg, M. M. Javed, C. Mazzoni, L. Vaut, L. H. Nielsen, C. Gundlach, R. S. Petersen, A. Müllertz, A. Boisen, and S. S. Keller, "Biodegradable microcontainers – towards real life applications of microfabricated systems for oral drug delivery," *Lab on a Chip*, vol. 19, no. 17, pp. 2905–2914, 2019.

[142] H. D. Chirra, L. Shao, N. Ciaccio, C. B. Fox, J. M. Wade, A. Ma, and T. A. Desai, "Planar Microdevices for Enhanced In Vivo Retention and Oral Bioavailability of Poorly Permeable Drugs," *Advanced Healthcare Materials*, vol. 3, no. 10, pp. 1648–1654, 2014.

[143] K. J. McHugh, T. D. Nguyen, A. R. Linehan, D. Yang, A. M. Behrens, S. Rose, Z. L. Tochka, S. Y. Tzeng, J. J. Norman, A. C. Anselmo, X. Xu, S. Tomasic, M. A. Taylor, J. Lu, R. Guarecuco, R. Langer, and A. Jaklenec, "Fabrication of fillable microparticles and other complex 3D microstructures," *Science (New York, N.Y.)*, vol. 357, no. 6356, pp. 1138–1142, 2017.

[144] T. D. Ngo, A. Kashani, G. Imbalzano, K. T. Nguyen, and D. Hui, "Additive manufacturing (3D printing): A review of materials, methods, applications and challenges," *Composites Part B: Engineering*, vol. 143, pp. 172–196, 2018.

[145] X. Wang, M. Jiang, Z. Zhou, J. Gou, and D. Hui, "3D printing of polymer matrix composites: A review and prospective," *Composites Part B: Engineering*, vol. 110, pp. 442–458, 2017.

[146] P. Parandoush and D. Lin, "A review on additive manufacturing of polymer-fiber composites," *Composite Structures*, vol. 182, pp. 36–53, 2017.

[147] F. P. Melchels, J. Feijen, and D. W. Grijpma, "A review on stereolithography and its applications in biomedical engineering," *Biomaterials*, vol. 31, no. 24, pp. 6121–6130, 2010.

[148] Www.formlabs.com, "Formlabs Application Guide: 3D Printing Splints with the Form 2," 2017.

[149] European Parliament and Council, "Council Directive 93/42/EEC," Tech. Rep. June 1993, European Parliament and Council, 2007.

[150] M. Yaneva-Deliverska, J. Deliversky, and M. Lyapina, "Biocompatibility of medical devices - legal regulations in the european union," *Journal of IMAB - Annual Proceeding (Scientific Papers)*, vol. 21, no. 1, pp. 705–708, 2015.

[151] C. H. Hauman and R. M. Love, "Biocompatibility of dental materials used in contemporary endodontic therapy: A review. Part 1. Intracanal drugs and substances," *International Endodontic Journal*, vol. 36, no. 2, pp. 75–85, 2003.

[152] D. T. Butcher, T. Alliston, and V. M. Weaver, "A tense situation: Forcing tumour progression," *Nature Reviews Cancer*, vol. 9, no. 2, pp. 108–122, 2009.

[153] P. C. Georges, J.-J. Hui, Z. Gombos, M. E. McCormick, A. Y. Wang, M. Uemura, R. Mick, P. A. Janmey, E. E. Furth, and R. G. Wells, "Increased stiffness of the rat liver precedes matrix deposition: implications for fibrosis," *AJP: Gastrointestinal and Liver Physiology*, vol. 293, no. 6, pp. G1147–G1154, 2007.

[154] M. Yin, J. A. Talwalkar, K. J. Glaser, A. Manduca, R. C. Grimm, P. J. Rossman, J. L. Fidler, and R. L. Ehman, "Assessment of Hepatic Fibrosis With Magnetic Resonance Elastography," *Clinical Gastroenterology and Hepatology*, vol. 5, no. 10, pp. 1207–1213, 2007.

[155] T. R. Cox and J. T. Erler, "Remodeling and homeostasis of the extracellular matrix: Implications for fibrotic diseases and cancer," *DMM Disease Models and Mechanisms*, vol. 4, no. 2, pp. 165–178, 2011.

[156] B. Geiger and A. Bershadsky, "Assembly and mechanosensory function of focal contacts," *Current Opinion in Cell Biology*, vol. 13, pp. 584–592, 2001.

[157] A. D. Bershadsky, N. Q. Balaban, and B. Geiger, "Adhesion-Dependent Cell Mechanosensitivity," *Annual Review of Cell and Developmental Biology*, vol. 19, no. 1, pp. 677–695, 2003.

[158] Y. Chen, L. Ju, M. Rushdi, C. Ge, and C. Zhu, "Receptor-mediated cell mechanosensing," *Molecular Biology of the Cell*, vol. 28, no. 23, pp. 3134–3155, 2017.

[159] L. A. Flanagan, Y. E. Ju, B. Marg, M. Osterfield, and P. A. Janmey, "Neurite branching on deformable substrates," *NeuroReport*, vol. 13, no. 18, pp. 2411–2415, 2002.

[160] M. J. Paszek, N. Zahir, K. R. Johnson, J. N. Lakins, G. I. Rozenberg, A. Gefen, C. A. Reinhart-King, S. S. Margulies, M. Dembo, D. Boettiger, D. A. Hammer, and V. M. Weaver, "Tensional homeostasis and the malignant phenotype," *Cancer Cell*, vol. 8, no. 3, pp. 241–254, 2005.

[161] I. Levental, P. C. Georges, and P. A. Janmey, "Soft biological materials and their impact on cell function," *Soft Matter*, vol. 3, no. 3, pp. 299–306, 2007.

[162] C. Frantz, K. M. Stewart, and V. M. Weaver, "The extracellular matrix at a glance," *Journal of Cell Science*, vol. 123, no. 24, pp. 4195–4200, 2010.

[163] B. Yue, "Biology of the extracellular matrix: An overview," *Journal of Glaucoma*, vol. 23, no. 8 Suppl 1, pp. S20–S23, 2014.

[164] M. Barczyk, S. Carracedo, and D. Gullberg, "Integrins," *Cell and Tissue Research*, vol. 339, pp. 269–280, 2010.

[165] H. Järveläinen, A. Sainio, M. Koulu, T. N. Wight, and R. Penttinen, "Extracellular Matrix Molecules: Potential Targets in Pharmacotherapy," *Pharmacological Reviews*, vol. 61, no. 2, pp. 198–223, 2009.

[166] T. Rozario and D. W. DeSimone, "The extracellular matrix in development and morphogenesis: A dynamic view," *Developmental Biology*, vol. 341, pp. 126–140, 2010.

[167] B. Knight, C. Laukaitis, N. Akhtar, N. A. Hotchin, M. Edlund, and A. R. Horwitz, "Visualizing muscle cell migration in situ," *Current Biology*, vol. 10, pp. 576–585, 2000.

[168] C. D. Roskelley, P. Y. Desprez, and M. J. Bissell, "Extracellular matrix-dependent tissue-specific gene expression in mammary epithelial cells requires both physical and biochemical signal transduction," *Proceedings of the National Academy of Sciences of the United States of America*, vol. 91, no. 26, pp. 12378–12382, 1994.

[169] M. Doi, *Introduction to Polymer Physics*. Oxford University Press, 1996.

[170] K. Almdal, J. Dyre, S. Hvidt, and O. Kramer, "Towards a phenomenological definition of the term 'gel'," *Polymer Gels and Networks*, vol. 1, pp. 5–17, 1993.

[171] Y. S. Zhang and A. Khademhosseini, "Advances in engineering hydrogels," *Science (New York, N.Y.)*, vol. 356, p. eaaf3627, 2017.

[172] J. M. Rosiak and F. Yoshii, "Hydrogels and their medical applications," *Nuclear Instruments and Methods in Physics Research, Section B: Beam Interactions with Materials and Atoms*, vol. 151, pp. 56–64, 1999.

[173] L. E. R. O'Leary, J. A. Fallas, E. L. Bakota, M. K. Kang, and J. D. Hartgerink, "Multi-hierarchical self-assembly of a collagen mimetic peptide from triple helix to nanofibre and hydrogel," *Nature Chemistry*, vol. 3, no. 10, pp. 821–828, 2011.

[174] W. R. Gombotz and S. Wee, "Protein release from alginate matrixes," *Advanced Drug Delivery Reviews*, vol. 31, pp. 267–285, 1998.

[175] W. E. Hennink and C. F. van Nostrum, "Novel crosslinking methods to design hydrogels," *Advanced Drug Delivery Reviews*, vol. 54, pp. 13–36, 2012.

[176] T. Heck, G. Faccio, M. Richter, and L. Thöny-Meyer, "Enzyme-catalyzed protein crosslinking," *Applied Microbiology and Biotechnology*, vol. 97, no. 2, pp. 461–475, 2013.

[177] S. R. Caliari and J. A. Burdick, "A practical guide to hydrogels for cell culture," *Nature Methods*, vol. 13, no. 5, pp. 405–414, 2016.

[178] M. Djabourov, J. Leblond, and P. Papon, "Gelation of aqueous gelatin solutions. II. Rheology of the sol-gel transition," *Journal de Physique*, vol. 49, no. 2, pp. 319–332, 1988.

[179] H. Boedtker and P. Doty, "A study of gelatin molecules, aggregates and gels," *Journal of Physical Chemistry*, vol. 58, no. 11, pp. 968–983, 1954.

[180] P. Dubruel, R. Unger, S. Van Vlierberghe, V. Cnudde, P. J. S. Jacobs, E. Schacht, and C. J. Kirkpatrick, "Porous Gelatin Hydrogels: 2. In Vitro Cell Interaction Study," *Biomacromolecules*, vol. 8, no. 2, pp. 338–344, 2007.

[181] H. Long, K. Ma, Z. Xiao, X. Ren, and G. Yang, "Preparation and characteristics of gelatin sponges crosslinked by microbial transglutaminase," *PeerJ*, vol. 5, p. e3665, 2017.

[182] J. E. Folk and J. S. Finlayson, "The e-(γ-Glutamyl)Lysine Crosslink and the Catalytic Role of Transglutaminases," *Advances in Protein Chemistry*, vol. 31, pp. 1–133, 1977.

[183] T. Kanaji, H. Ozaki, T. Takao, H. Kawajiri, H. Ide, M. Motoki, and Y. Shimonishi, "Primary Structure of Microbial Transglutaminase from Streptoverticillium sp. Strain s-8112," *The Journal of Biological Chemistry*, vol. 268, pp. 11565–11572, 1993.

[184] M. L. Jepsen, L. H. Nielsen, A. Boisen, K. Almdal, and M. Dufva, "Characterization of thin gelatin hydrogel membranes with balloon properties for dynamic tissue engineering," *Biopolymers*, vol. 110, p. e23241, 2019.

[185] H. Sakamoto, Y. Kumazawa, and M. Motoki, "Strength of Protein Gels Prepared with Microbial Transglutaminase as Related to Reaction Conditions," *Journal of Food Science*, vol. 59, no. 4, pp. 866–871, 1994.

[186] B. Srinivasan, A. R. Kolli, M. B. Esch, H. E. Abaci, M. L. Shuler, and J. J. Hickman, "TEER Measurement Techniques for In Vitro Barrier Model Systems," *Journal of Laboratory Automation*, vol. 20, no. 2, pp. 107–126, 2015.

[187] P. M. Luckett, J. Fischbarg, J. Bhattacharya, and S. C. Silverstein, "Hydraulic conductivity of endothelial cell monolayers cultured on human amnion," *American Journal of Physiology - Heart and Circulatory Physiology*, vol. 256, no. 6, pp. H1675–H1683, 1989.

[188] R. L. DiMarco, D. R. Hunt, R. E. Dewi, and S. C. Heilshorn, "Improvement of paracellular transport in the Caco-2 drug screening model using protein-engineered substrates," *Biomaterials*, vol. 129, pp. 152–162, 2017.

[189] J. R. Levick and C. C. Michel, "Microvascular fluid exchange and the revised Starling principle," *Cardiovascular Research*, vol. 87, no. 2, pp. 198–210, 2010.

[190] S. Yuan and R. Rigor, "Methods for Measuring Permeability," in *Regulation of Endothelial Barrier Function*, ch. 3, Morgan & Claypool Life Sciences, 2010.

[191] V. H. Huxley, F. E. Curry, and R. H. Adamson, "Quantitative fluorescence microscopy on single capillaries: α-lactalbumin transport," *American Journal of Physiology - Heart and Circulatory Physiology*, vol. 252, no. 1, pp. H188–H197, 1987.

[192] Y. Yuan, W. M. Chilian, H. J. Granger, and D. C. Zawieja, "Permeability to albumin in isolated coronary venules," *American Journal of Physiology - Heart and Circulatory Physiology*, vol. 265, no. 2 34-2, pp. H543–H552, 1993.

[193] Z. Liu and K. Liu, "The transporters of intestinal tract and techniques applied to evaluate interactions between drugs and transporters," *Asian Journal of Pharmaceutical Sciences*, vol. 8, no. 3, pp. 151–158, 2013.

[194] K. Benson, S. Cramer, and H. J. Galla, "Impedance-based cell monitoring: Barrier properties and beyond," *Fluids and Barriers of the CNS*, vol. 10, no. 1, p. 5, 2013.

[195] S. Berkó, G. Regdon, E. Ducza, G. Falkay, and I. Eros, "In vitro and in vivo study in rats of rectal suppositories containing furosemide," *European Journal of Pharmaceutics and Biopharmaceutics*, vol. 53, no. 3, pp. 311–315, 2002.

[196] A. M. Al-Mohizea, "Influence of intestinal efflux pumps on the absorption and transport of furosemide," *Saudi Pharmaceutical Journal*, vol. 18, no. 2, pp. 97–101, 2010.

[197] L. H. Nielsen, A. Melero, S. S. Keller, J. Jacobsen, T. Garrigues, T. Rades, A. Müllertz, and A. Boisen, "Polymeric microcontainers improve oral bioavailability of furosemide," *International Journal of Pharmaceutics*, vol. 504, no. 1-2, pp. 98–109, 2016.

[198] S. R. Patil, L. Kumar, G. Kohli, and A. K. Bansal, "Validated HPLC method for concurrent determination of antipyrine, carbamazepine, furosemide and phenytoin and its application in assessment of drug permeability through Caco-2 cell monolayers," *Scientia Pharmaceutica*, vol. 80, no. 1, pp. 89–100, 2012.

[199] V. Pade and S. Stavchansky, "Estimation of the relative contribution of the transcellular and paracellular pathway to the transport of passively absorbed drugs in the Caco-2 cell culture model," *Pharmaceutical Research*, vol. 14, no. 9, pp. 1210–1215, 1997.

[200] C. Li, T. Liu, X. Cui, A. S. Uss, and K. C. Cheng, "Development of in vitro pharmacokinetic screens using Caco-2, human hepatocyte, and Caco-2/human hepatocyte hybrid systems for the prediction of oral bioavailability in humans," *Journal of Biomolecular Screening*, vol. 12, no. 8, pp. 1084–1091, 2007.

[201] B. D. Rege, X. Yu Lawrence, A. S. Hussain, and J. E. Polli, "Effect of common excipients on Caco-2 transport of low-permeability drugs," *Journal of Pharmaceutical Sciences*, vol. 90, no. 11, pp. 1776–1786, 2001.

[202] C. Hilgendorf, H. Spahn-Langguth, C. G. Regårdh, E. Lipka, G. L. Amidon, and P. Langguth, "Caco-2 versus Caco-2/HT29-MTX co-cultured cell lines: Permeabilities via diffusion, inside- and outside-directed carrier-mediated transport," *Journal of Pharmaceutical Sciences*, vol. 89, no. 1, pp. 63–75, 2000.

[203] B. Steffansen, C. U. Nielsen, B. Brodin, A. H. Eriksson, R. Andersen, and S. Frokjaer, "Intestinal solute carriers: An overview of trends and strategies for improving oral drug absorption," *European Journal of Pharmaceutical Sciences*, vol. 21, no. 1, pp. 3–16, 2004.

[204] P. Schmiedlin-Ren, K. E. Thummel, J. M. Fisher, M. F. Paine, K. S. Lown, and P. B. Watkins, "Expression of enzymatically active CYP3A4 by Caco-2 cells grown on extracellular matrix-coated permeable supports in the presence of 1alpha,25-dihydroxyvitamin D3.," *Molecular pharmacology*, vol. 51, no. 5, pp. 741–754, 1997.

[205] S. L. Palay and L. J. Karlin, "An electron microscopic study of the intestinal villus. I. The fasting animal.," *The Journal of biophysical and biochemical cytology*, vol. 5, no. 3, pp. 363–372, 1959.

[206] L. R. G. Treloar, *The physics of rubber elastics.* Oxford: Clarendon Press, third ed., 1975.

[207] E. Karrer, "Kinetic theory of the mechanism of muscular contration," *Protoplasma*, vol. 18, pp. 475–489, 1933.

[208] M. Ahearne, Y. Yang, A. J. El Haj, K. Y. Then, and K.-K. Liu, "Characterizing the viscoelastic properties of thin hydrogel-based constructs for tissue engineering applications," *Journal of The Royal Society Interface*, vol. 2, no. 5, pp. 455–463, 2005.

[209] K. S. Anseth, C. N. Bowman, and L. Brannon-Peppas, "Mechanical properties of hydrogels and their experimental determination," *Biomaterials*, vol. 17, pp. 1647–1657, 1996.

[210] R. L. Anthony, R. H. Caston, and E. Guth, "Equations of State for Natural and Synthetic Rubber-Like Materials. I Unaccelerated Natural Soft Rubber," *Rubber Chemistry and Technology*, vol. 46, no. 8, pp. 826–840, 1942.

[211] G. M. Kavanagh and S. B. Ross-Murphy, "Rheological characterisation of polymer gels," *Progress in Polymer Science*, vol. 23, no. 3, pp. 533–562, 1998.

[212] S. Hvidt, "An Introduction to Rheology," 1992.

[213] G. N. Greaves, A. L. Greer, R. S. Lakes, and T. Rouxel, "Poisson's ratio and modern materials," *Nature Materials*, vol. 10, no. 11, pp. 823–837, 2011.

[214] H. T. Banks, S. Hu, and Z. R. Kenz, "A brief review of elasticity and viscoelasticity for solids," *Advances in Applied Mathematics and Mechanics*, vol. 3, no. 1, pp. 1–51, 2011.

[215] R. W. Ogden, "Large Deformation Isotropic Elasticity - On the Correlation of Theory and Experiment for Incompressible Rubberlike Solids," *Proceedings of the Royal Society A: Mathematical, Physical and Engineering Sciences*, vol. 326, no. 1567, pp. 565–584, 1972.

[216] W. C. Yeh, P. C. Li, Y. M. Jeng, H. C. Hsu, P. L. Kuo, M. L. Li, P. M. Yang, and H. L. Po, "Elastic modulus measurements of human liver and correlation with pathology," *Ultrasound in Medicine and Biology*, vol. 28, no. 4, pp. 467–474, 2002.

[217] J. H. Haga, Y.-S. J. S. J. Li, and S. Chien, "Molecular basis of the effects of mechanical stretch on vascular smooth muscle cells," *Journal of Biomechanics*, vol. 40, no. 5, pp. 947–960, 2007.

[218] M. N. Richard, J. F. Deniset, A. L. Kneesh, D. Blackwood, and A. N. Pierce, "Mechanical stretching stimulates smooth muscle cell growth, nuclear protein import, and nuclear pore expression through mitogen-activated protein kinase activation," *Journal of Biological Chemistry*, vol. 282, no. 32, pp. 23081–23088, 2007.

[219] D. G. Hardie, "AMPK: A target for drugs and natural products with effects on both diabetes and cancer," *Diabetes*, vol. 62, no. 7, pp. 2164–2172, 2013.

[220] S. A. Hawley, F. A. Ross, C. Chevtzoff, K. A. Green, A. Evans, S. Fogarty, M. C. Towler, L. J. Brown, O. A. Ogunbayo, A. M. Evans, and D. G. Hardie, "Use of cells expressing γ subunit variants to identify diverse mechanisms of AMPK activation," *Cell Metabolism*, vol. 11, no. 6, pp. 554–565, 2010.

[221] M. Foretz, B. Guigas, L. Bertrand, M. Pollak, and B. Viollet, "Metformin: From mechanisms of action to therapies," *Cell Metabolism*, vol. 20, no. 6, pp. 953–966, 2014.

[222] Y. Sogame, A. Kitamura, M. Yabuki, and S. Komuro, "A comparison of uptake of metformin and phenformin mediated by hOCT1 in human hepatocytes," *Biopharmaceutics and Drug Disposition*, vol. 30, no. 8, pp. 476–484, 2009.

[223] C. J. Bailey, "Metformin: historical overview," *Diabetologia*, vol. 60, no. 9, pp. 1566–1576, 2017.

[224] Z. Drahota, E. Palenickova, R. Endlicher, M. Milerova, J. Brejchova, M. Vosahlikova, P. Svoboda, L. Kazdova, M. Kalous, Z. Cervinkova, and M. Cahova, "Biguanides inhibit complex I, II and IV of rat liver mitochondria and modify their functional properties," *Physiological Research*, vol. 63, no. 1, pp. 1–11, 2014.

[225] D. G. Hardie, "Metformin - Acting through cyclic AMP as well as AMP?," *Cell Metabolism*, vol. 17, no. 3, pp. 313–314, 2013.

[226] E. V. Schaftingen and I. Gerin, "The glucose-6-phosphatase system," *Biochemical Journal*, vol. 362, pp. 513–532, 2002.

[227] A. R. Cameron, L. Logie, K. Patel, S. Erhardt, S. Bacon, P. Middleton, J. Harthill, C. Forteath, J. T. Coats, C. Kerr, H. Curry, D. Stewart, K. Sakamoto, P. Repiščák, M. J. Paterson, I. Hassinen, G. McDougall, and G. Rena, "Metformin selectively targets redox control of complex I energy transduction," *Redox Biology*, vol. 14, pp. 187–197, 2018.

[228] J. Simon, Pukis, E.-M. Raafat, and T. H. Claus, "Hormonal regulation of hepatic gluconeogenesis and glycolysis," *Ann. Rev. Biochem*, vol. 57, pp. 755–773, 1988.

[229] A. R. Cameron, L. Logie, K. Patel, S. Bacon, C. Forteath, J. Harthill, A. Roberts, C. Sutherland, D. Stewart, B. Viollet, K. Sakamoto, G. McDougall, M. Foretz, and G. Rena, "Investigation of salicylate hepatic responses in comparison with chemical analogues of the drug," *Biochimica et Biophysica Acta - Molecular Basis of Disease*, vol. 1862, no. 8, pp. 1412–1422, 2016.

[230] F. Chatelain, J. P. Pégorier, C. Minassian, N. Bruni, S. Tarpin, J. Girard, and G. Mithieux, "Development and regulation of glucose-6-phosphatase gene expression in rat liver, intestine, and kidney: In vivo and in vitro studies in cultured fetal hepatocytes," *Diabetes*, vol. 47, no. 6, pp. 882–889, 1998.

[231] N. Kraus-Friedmann, "Hormonal regulation of hepatic gluconeogenesis," *Physiological Reviews*, vol. 64, no. 1, pp. 170–259, 1984.

[232] J. R. Pappenheimer and C. C. Michel, "Role of villus microcirculation in intestinal absorption of glucose: Coupling of epithelial with endothelial transport," *Journal of Physiology*, vol. 553, no. 2, pp. 561–574, 2003.

[233] P. F. Davies, "Flow-mediated endothelial mechanotransduction," *Physiological Reviews*, vol. 75, no. 3, pp. 519–560, 1995.

[234] D. A. Chistiakov, A. N. Orekhov, and Y. V. Bobryshev, "Effects of shear stress on endothelial cells: go with the flow," *Acta Physiologica*, vol. 219, no. 2, pp. 382–408, 2017.

[235] Y.-S. J. Li, J. H. Haga, and S. Chien, "Molecular basis of the effects of shear stress on vascular endothelial cells," *Journal of Biomechanics*, vol. 38, no. 10, pp. 1949–1971, 2005.

[236] A. M. Malek and S. Izumo, "Mechanism of endothelial cell shape change and cytoskeletal remodeling in response to fluid shear stress," *Journal of Cell Science*, vol. 109, no. 4, pp. 713–726, 1996.

[237] G. G. Galbraith, R. Skalak, and S. Chien, "Shear stress induces spatial reorganization of the endothelial cell cytoskeleton," *Cell Motility and the Cytoskeleton*, vol. 40, no. 4, pp. 317–330, 1998.

[238] S. Noria, D. B. Cowan, A. I. Gotlieb, and B. L. Langille, "Transient and steady-state effects of shear stress on endothelial cell adherens junctions," *Circulation Research*, vol. 85, no. 6, pp. 504–514, 1999.

[239] S. E. Goldblum, B. Hennig, M. Jay, K. Yoneda, and C. J. McClain, "Tumor necrosis factor α-induced pulmonary vascular endothelial injury," *Infection and Immunity*, vol. 57, no. 4, pp. 1218–1226, 1989.

[240] A. H. Stolpen, E. C. Guinan, W. Fiers, and J. S. Pober, "Recombinant tumor necrosis factor and immune interferon act singly and in combination to reorganize human vascular endothelial cell monolayers," *The American journal of pathology*, vol. 123, no. 1, pp. 16–24, 1986.

[241] S. Li, B. P. Chen, N. Azuma, Y. L. Hu, S. Z. Wu, B. E. Sumpio, J. Y. Shyy, and S. Chien, "Distinct roles for the small GTPases Cdc42 and Rho in endothelial responses to shear stress," *Journal of Clinical Investigation*, vol. 103, no. 8, pp. 1141–1150, 1999.

[242] G. Helmlinger, R. V. Geiger, S. Schreck, and R. M. Nerem, "Effects of pulsatile flow on cultured vascular endothelial cell morphology," *Journal of Biomechanical Engineering*, vol. 113, no. 2, pp. 123–131, 1991.

Appendix A

Paper I

3D-Printed Stackable Titer Plate Inserts Supporting Three Interconnected Tissue Models for Drug Screening

M. L. Jepsen, A. Willumsen, C. Mazzoni, A. Boisen, L. H. Nielsen, and M. Dufva

Submitted to Advanced Biosystems

WILEY-VCH

Article type: Full Paper

3D-Printed Stackable Titer Plate Inserts Supporting Three Interconnected Tissue Models for Drug Screening

Morten Leth Jepsen, Andreas Willumsen, Chiara Mazzoni , Anja Boisen, Line Hagner Nielsen and Martin Dufva

MSc M. L. J., BSc A. W., Dr. C. M., Prof. A. B., Dr. L. H. N., Dr. M. D.,

The Danish National Research Foundation and Villum Foundation's Center for Intelligent Drug Delivery and Sensing Using Microcontainers and Nanomechanics (IDUN), Department of Health Technology, Technical University of Denmark, Ørsteds Plads 345C, 2800 Kgs. Lyngby, Denmark.

Keywords: tissue engineering, Caco-2 cells, HUVEC cells, HepG2 cells, first pass metabolism

Current *in vitro* drug screening methods often rely on single cell-models and are therefore imprecise in predicting drug absorption, distribution, metabolism, excretion, and toxicity. This study presents a method to fabricate 3D printed inserts that are compatible with commercially available titer plates. Hydrogels can be casted into the inserts and cells can be cultured either in or on the hydrogels. Once individual cell cultures are fully differentiated, the three different cell cultures are stacked on top of each other for biological experiments. To show the possibilities of this approach, three tissue models representing the first pass metabolism was used. The three tissue models are based on gelatin hydrogels and Caco-2, HUVEC, and HepG2 cells to simulate the small intestine, vascular endothelium, and liver, respectively. The device is simple to fabricate, user friendly and is, an alternative to microfluidic-based organ on a chip system. The presented first pass metabolism study allows for gaining information on drug absorption, distribution, metabolism, and, in the future, excretion in one compact device complying the micro titer plate format.

1. Introduction

Oral drug administration is preferred due to low cost and high patient compliance.[1] 60 % of all drugs are administered orally emphasizing the importance of this administration route.[2] Drug development usually takes 10-15 years and costs up to $1.8 billion in total, [3,4] and improving the research and the development phases will have the biggest cost reducing effect.[4] Nearly, 90 % of drugs identified as lead candidates using current *in vitro* methods, such as immortalized cell lines and purified tissue sections, fail to reach the market. Furthermore, 50 % of the drug candidates and/or drug formulations fail due to too low oral bioavailability and/or hepatic toxicity issues during phase I clinical trials.[5–7] Pre-clinical *in vitro* testing of absorption, distribution, metabolism, and excretion (ADME) may reduce the number of failures in phase I clinical trials. Currently, each step of ADME is investigated individually using specialized cell lines. However, multicellular co-cultures have been developed for preclinical drug screening. [8] Typically, oral absorption studies are performed in transwell systems with single cell lines which are designed to model a biological barrier such as the small intestine.[9–12]

Microfluidic devices can connect multiple cells types for ADME testing.[13,14] However, microfluidic devices are difficult to up-scale because they have a tendency to be rather complex as they require tubes and pumps. While commercial systems are available, these are also not necessarily trivial to use.[14,15] Previously, a microfluidic system with multiple connected cell layers of colon adenocarcinoma cells (Caco-2), human umbilical vein endothelial cells (HUVEC), and Michigan Cancer Foundation-7 (MCF-7) cells, and hepatocytes on polycarbonate membranes has been presented.[13] However, when aiming for ADME testing of microparticles or drug delivery systems up to 400 µm in size,[16–19] there is a need for ADME test systems larger than those supported by microfluidics where channels are normally a few hundred µm in height.[13,14,20] Furthermore, most reported microfluidics systems are made of

the polymer polydimethylsiloxane (PDMS). PDMS has many properties suitable for this application, but small hydrophobic molecules have a tendency to diffuse into PDMS which can be problematic.[21–24]

In vivo, tissues are very soft.[25] Culturing of cells in a softer matrix gives a more *in vivo*-like environment for the cell cultures than on hard plastic surfaces, because cells sense the stiffness of their growth matrix.[26] Epithelial cells grown on a soft matrix display organization and polarity which resembled the phenotype found *in vivo*.[27] To obtain soft growth matrices, hydrogels have been utilized to replace the hard polycarbonate or polyester filters used in microfluidics and transwells. Cells have been cultured both inside and on top of hydrogel growth-matrices.[28–33] Transwell inserts contain a rigid membrane, but it can be functionalized with collagen or other hydrogels to obtain the softer mechanical properties or provide a true 3D environment.[32–34] Caco-2 cells grown on hydrogel growth-matrices have been shown to have higher paracellular permeability than when grown on polyester filters.[32] This is closer to the *in vivo* situation. Gelatin is denatured collagen and when cross-linked by microbial transglutaminase (mTG), a heat resistant hydrogel can be obtained. [35,36] This has been done with cell cultures such as HepG2 hepatocytes,[30,37] mesenchymal stem cells,[38] and adipose tissue-derived stromal cells.[39]

The aim of the presented study was to design and test a set of simple-to-use and easy to fabricate 12 well plate stackable inserts that addresses most of the current limitations of transwells and microfluidics technology for connected *in vitro* cell models.

2. Results and Discussion

2.1 Triple Layered Tissue Models

The design of the triple layered tissue models was inspired by commercially available inserts for cell culture titer plates. The three layers were designed so that the tissue layers could be cultured independently of each other and easily assembled before use, e.g. for drug transport studies.

2.1.1. Principle of the Triple Layered Tissue Models

A completely assembled layered system had in total 36 tissue models (three layers of 12-well titer plates inserts) organized in 12 independent test sites (Figure 1A). Each well of the three inserts had a hole where a hydrogel was casted into, resulting in suspended hydrogel growth-matrices. The suspended hydrogels were utilized as growth matrices for the cell cultures. Cells grew on the apical side of the hydrogel to model a 2D barrier or inside the gel to achieve a 3D spheroid culture. The holes for 3D spheroid tissue models were 5 mm in diameter and 4 mm in depth to support a thick hydrogel resembling a solid tissue. The holes for 2D barrier tissue-models in each well were 5 mm in diameter and 1 mm in depth to gain a thinner hydrogel. To support the thin hydrogel, a small cross was lowered 0.5 mm from the edge of the hole to ensure that the membrane did not bend. This was necessary, since soft and thin gelatin hydrogels have a tendency to bend which can result in cells detachment.[40] Critical for drug-transport studies the inserts were designed to allow for sampling of the medium between each layer (Figure 1C). This way the drug could be followed all the way through the three tissue models without disturbing the cell layers. The was also intended to be used for TEER measurements.

3D-printed inserts compatible with cell growth were achieved by 3D printing with Dental LT resin on a Form 2 3D printer. To obtain compatibility with cell growth, the 3D-printed inserts were thoroughly cleaned (Experimental Section). The cleaning protocol differed from the manufacturer's instructions but ensured good biocompatibility at least for the three

tested cell lines (Caco-2, HUVEC, and HepG2). It was found that if the 3D printed inserts were not cleaned probably, biocompatibility issues arose, resulting in cell detachment (Figure S1).

The basic design allowed for cells to be matured and cultured before stacking them together (Figure 1B). Growing each cell line individually would avoid incompatibilities of mediums.[41] Stacking tissue models after maturation (Figure 1B-C) in neutral buffer such as HBSS would minimize impact of different mediums but only sustain shorter tests (hours). Many organizations of the three insets are possible. Below, we investigate usage of epithelial- and endothelial-cells and hepatocytes to mimic the first path metabolism of oral drug delivery. Oher combinations could be endothelial cells, hepatocytes, cancer cells to models drugs injected in the blood stream, metabolized in the hepatocytes and killing cancer cells.[42]

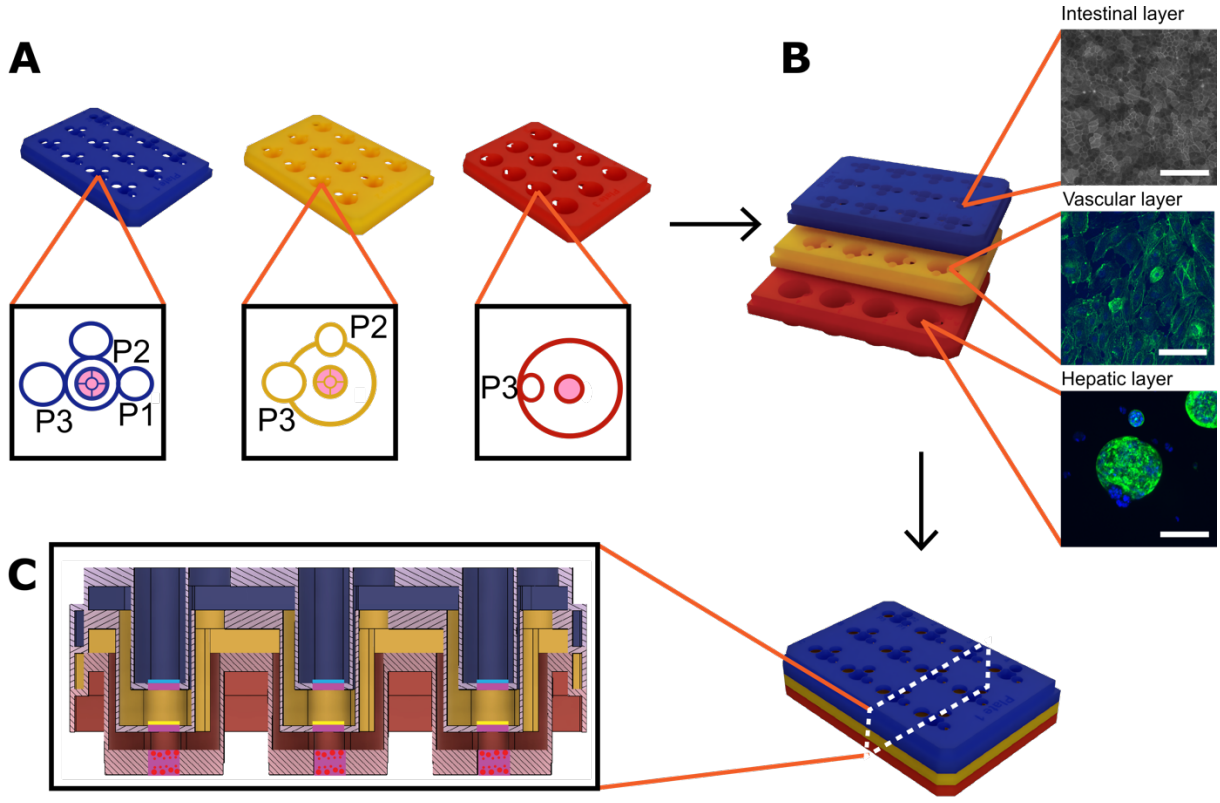

Figure 1: Schematic illustrations of tissue-model inserts. A) Individual tissue-model inserts with Caco-2 cells in blue, HUVEC in yellow, and HepG2 in red. Hydrogels are shown in pink. Sampling holes at each level, P1 for sampling under the blue insert,

P2 for sampling under the yellow insert, and P3 for sampling under the red insert. B) Assembly of tissue-model inserts. Scalebar: 100 µm. C) Sideview of assembled tissue-model inserts.

Previously, *in vitro* microfluidics systems combining cellular barriers and underlying tissues have been published.[13,14,43] However, it is difficult to scale microfluidic devices for high throughput screening applications, whereas a system based on titer plates is scalable. A microfluidic system with eight parallel intestinal barrier-models has previously been developed in our laboratory.[44] In contrast, the presented method of three 3D-printed inserts allowed for 12 parallel repetitions with three different tissue models in each. Furthermore, the presented method meets the demand for the possibility of testing microparticles and microfabricated devices for oral drug delivery that are typically 400 µm or larger. [16–18] This is not possible with the microfluidic system as these typically have channels in the range of few hundreds µm. [13,14,20] Since, the radius of the smallest well of the presented method was 5 mm, microparticles and microfabricated devices can be tested with this method (Figure S2A).

2.1.2. Casting of Gelatin Hydrogels into the 3D Printed Compartments

Gelatin hydrogels casted into the 3D-printed inserts were used as growth matrixes for the cells. We have previously functionalized hanging inserts by dipping the inserts into gelatin/mTG solution.[40] However, that resulted in thin and flexible gel which was not desired. Instead, a casting procedure was developed. The holes were closed by 3D-printed pillars covered by parafilm (Figure S3A). To ensure a tight seal from the pillars, they were placed upon springs and the inserts were held down by rubber bands (Figure S3B). Afterwards, hydrogel solution was pipetted into the holes (Figure S3C). After cross-linking and disassembly of the casting device, the inserts were placed in a standard twelve well-plate with medium (Figure S3D).

The gelatin hydrogel did not need coating since cells can secrete their own extracellular matrix to provide structural support. Therefore, the biopolymeric matrix only needed to provide an initial support and set of cues for cell adhesion and growth.[45]

2.2. Establishment of an *in vitro* first pass metabolism model

To demonstrate the principle of the triple layered transport system, the first pass metabolism was recreated with three different cell lines. The Caco-2 cell line was used to model the small intestinal barrier. This cell line differentiates spontaneously to polarized enterocyte-like cells expressing tight junctions, microvilli, and brush border enzymes.[46] The HUVEC cell line, a primary non-immortalized cell line of human origin,[47,48] was used to model the vascular endothelium. HepG2 cells, the most widely used human hepatoma cell line for studying pharmaco-toxicology,[49] was used to model the liver. These cell lines requires different medium and time in order to develop. Caco-2 developed for three weeks in Dulbecco's modified Eagle's medium (DMEM), HUVECs for two days in endothelial cell growth medium (ECGM), whereas HepG2 cells were grown for three weeks in Roswell Park Memorial Institute (RPMI 1640) medium.

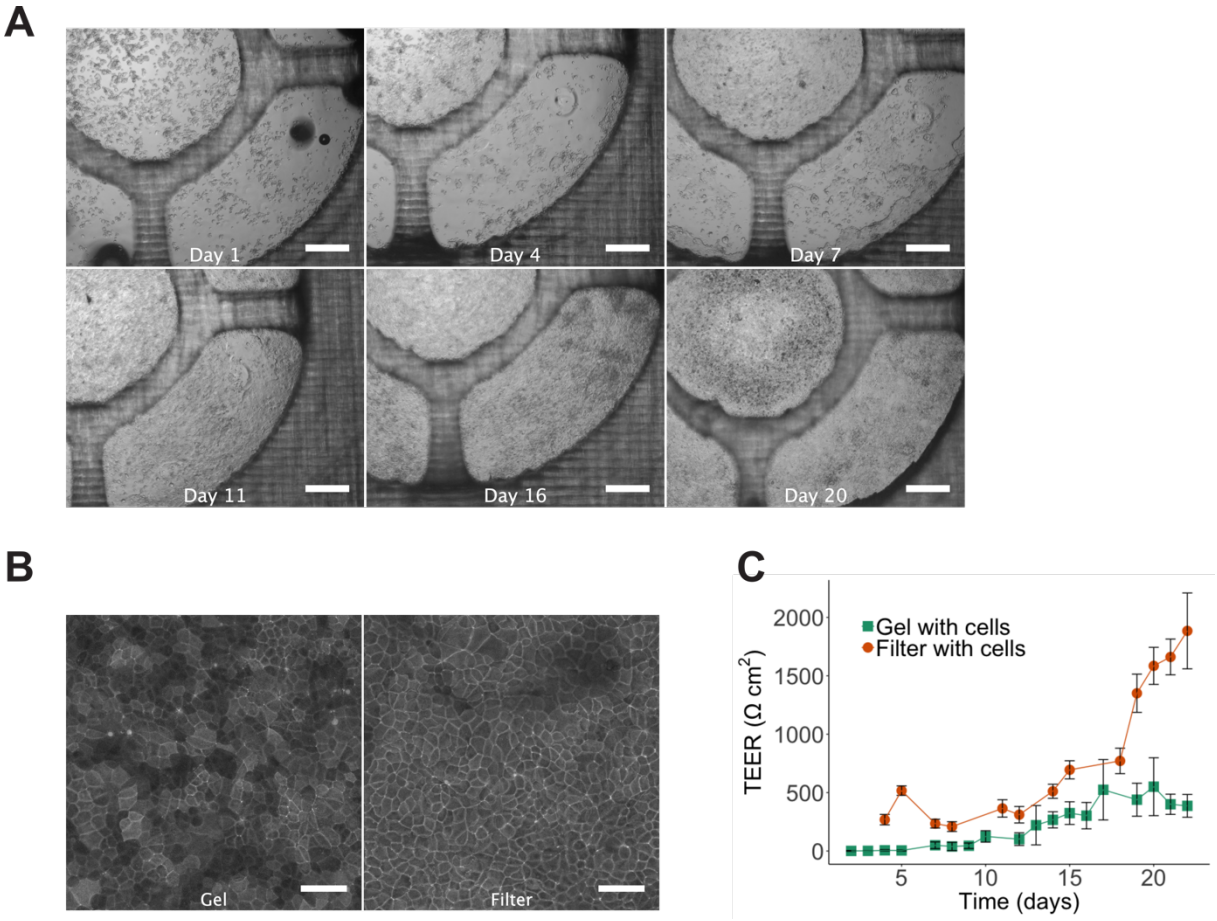

Figure 2: A) Growth of Caco-2 cells on the hydrogel growth-matrix over 20 days. Scalebars: 1000 µm. B) Tight junction (ZO-1) stain of Caco-2 cells on the hydrogel growth-matrix and polyester filters after 20 days. Scalebars: 50 µm. C) TEER value measurements for Caco-2 cells on the hydrogel growth-matrix (mean±SD, n=16) and on polyester filter (mean±SD, n=8) over three weeks.

2.2.1. Characterization of the Intestinal Layer of Caco-2 cells

Caco-2 cells grown on the hydrogel growth-matrices became a tight and evenly distributed monolayer after three weeks of growth (Figure 2A). Caco-2 cells on the hydrogel growth-matrices, as well as on the polyester filters (transwells), expressed the tight-junction protein zonula occludens-1 (ZO-1) at the cell-cell borders (Figure 2B). The Caco-2 cells grown on the hydrogel exhibited a slightly bumpy monolayer, and therefore appeared to have small holes in the layer, where cells were out of focus. The transepithelial electrical resistance (TEER) value of Caco-2 cells grown on hydrogel growth-matrices increased over three weeks to a final value

of 551±248 Ω cm^{-2} (mean±SD, n=16). By contrast, Caco-2 cells grown on polyester filters reached 1585±159 Ω cm^{-2} (mean±SD, n=8) (Figure 2C). TEER values for Caco-2 cells grown on soft growth-matrices such as collagen hydrogels have previously been reported in the range of 400-600 Ω cm^{-2}.[34,50] Hence, the value reported here of 551 Ω cm^{-2} is in accordance with what has previously been reported for Caco-2 cells on soft growth-matrices. Caco-2 cells grown directly on filters, and these are known to have higher TEER values than corresponding cultures on soft growth-matrices.[51,52] TEER values of Caco-2 cells on filters have been shown to be from ~3 times to ~12 times higher than *in vivo* small intestinal resistance that has been reported to be from 35 - 60 Ω cm^{-2}.[52,53] However, the TEER value is highly dependent on the measuring equipment used and consequently it is difficult to make a comparison.[54]

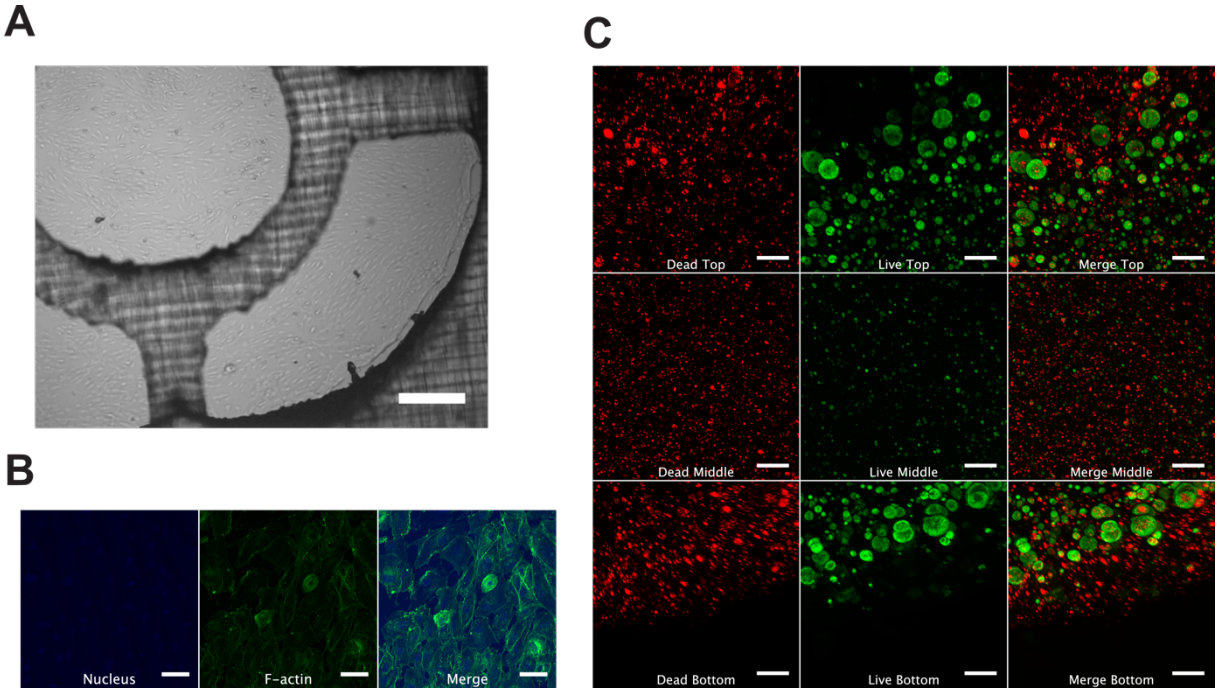

Figure 3. A) Bright-field microscopy of HUVEC cells on the hydrogel growth-matrix two days after seeding. Scalebar: 1000 µm. B) F-actin (green) and nucleus (blue) stain of HUVEC cells on the hydrogel growth-matrix. Scalebars 50 µm. C) Stain of HepG2 cells grown for 20 days in the hydrogel growth-matrix. The live (green) and dead (red) distributions in the top, middle, and bottom of the hydrogel. Scalebars: 200 µm.

2.2.2. Characterization of the Endothelial Layer of HUVEC and the Hepatic Layer of HepG2 cells

HUVEC cells have previously been grown in soft growth-matrices to obtain *in vitro* vascular networks.[55,56] In the presented study, HUVEC cells were grown on top of a hydrogel growth-matrix to gain a vascular barrier. HUVEC cells were evenly distributed two days after seeding on the gelatin hydrogel (Figure 4A). Furthermore, HUVEC cells showed elongated profiles with clearly visible actin fibers (Figure 4B), which are the characteristics of blood vessel *in vivo*. However, the HUVEC cells did not display elongation to the same extent as what was seen previously under flow.[56]

HepG2 cells grown in 3D as spheroids has been shown to have a higher drug sensitivity than HepG2 cells grown as 2D cell-cultures.[57] Hence, a 3D cell-culture would be better to detect adverse drug effects than a 2D culture. Therefore, the HepG2 cells were grown in 3D in the hydrogel growth-matrix in the presented system. Single entrapped HepG2 cells grew to large hepatic spheroids in the hydrogel growth-matrix over three weeks (Figure S4). The spheroids were largest close to the top and the bottom surfaces of the hydrogel growth-matrix, whereas in the middle of the hydrogel growth-matrix single dead hepatocytes were visible (Figure 3C). The stiffness of the hydrogel growth-matrix utilized for growth of the HepG2 cells was comparable to an *in vivo* liver,[40] which has a Young's modulus (E) of approximately 300-600 Pa.[58,59] HepG2 spheroids of <200 µm took 20 days of culture while spheroids ≥200 µm took 27 days (Figure S4). Hepatocytes grown for 20 days were thought to be more suitable for metabolic and toxic studies, since spheroids >200 µm have been shown to have a hypoxic core due to insufficient oxygen diffusion.[45,60,61]

3D cultures have molecular gradients of nutrients and effector molecules, leading to different phenotypes of the cells located centrally and peripherally in the tissue.[30,45] In the center of the hydrogel growth-matrix the hepatocytes did not grow most likely caused by lack of oxygen, since oxygen has a relatively low solubility in cell medium whereas gradients of glucose and amino acids are almost negligible.[45] However, dead HepG2 cells were also seen close to the surface, where they were able to access oxygen and nutrients. This phenomenon was also observed with HepG2 cells entrapped in gelatin hydrogels with nutrient and oxygen coming from microfluidic channels through the hydrogel.[30] While Pimentel et al.[30] could not exclude artefacts from the sacrificial molding process, the data presented here suggest that cells could have died from competition with the large nearby spheroids for nutrients.

2.3. Drug Transport Across the Triple Layered System

2.3.1. Permeability of the Triple Layered Transport System

To assess the barrier function of the different tissue models lucifer yellow was utilized as a model compound. Cumulative transport fractions and permeability of lucifer yellow were measured across cell and hydrogel growth-matrices. The empty hydrogel growth-matrix and the empty polyester filters displayed similar lucifer yellow transport slopes (Figure 4A). However, the transport across the hydrogel growth-matrix displayed a delay compared to the polyester filter indicating that the hydrogel growth-matrix acted as a diffusion barrier. This was probably due to that the hydrogel growth-matrix was 1 mm thick whereas the polyester filter was 10 µm thick. Confluent monolayers of Caco-2 cells both the hydrogel growth-matrices and polyester filters displayed a flat cumulative transported fraction slope (Figure 4A). From the cumulative transported fraction, the permeability of lucifer yellow across the different cell barriers was calculated. The barrier function of Caco-2 monolayers on the hydrogel growth-

matrix was assessed by TEER measurements and compared to the lucifer yellow permeability. A TEER value above 300 Ω cm^{-2} was determined as a tight layer because the permeability dropped approximately 14 times with TEER >300 Ω cm^{-2} (Figure 4B). Presumably, because at this TEER value, the Caco-2 cells became a tight monolayer covering the whole hydrogel growth-matrix. Empty gelatin hydrogels and polyester filters displayed similar high permeabilities of $3.18\times10^{-5}\pm4.74\times10^{-6}$ cm s^{-1} (mean±SD, n=8) and $3.90\times10^{-5}\pm3.03\times10^{-6}$ cm s^{-1} (mean±SD, n=9), respectively (Figure 4C). The permeability of the polyester filter was significantly more permeable to lucifer yellow (p-value=0.34×10^{-2}), as mentioned above due to the thickness of the hydrogel growth-matrix. Caco-2 cells on hydrogel growth-matrices and polyester filters showed comparable low permeabilities of $1.22\times10^{-6}\pm1.30\times10^{-6}$ cm s^{-1} (mean±SD, n=8) (for TEER values >300 Ω cm^{-2}) and $4.19\times10^{-7}\pm2.77\times10^{-7}$ cm s^{-1} (mean±SD, n=15), respectively. The permeability of lucifer yellow across Caco-2 monolayers on hydrogel growth-matrices and polyester filers was not found to significant (p-value=0.13).

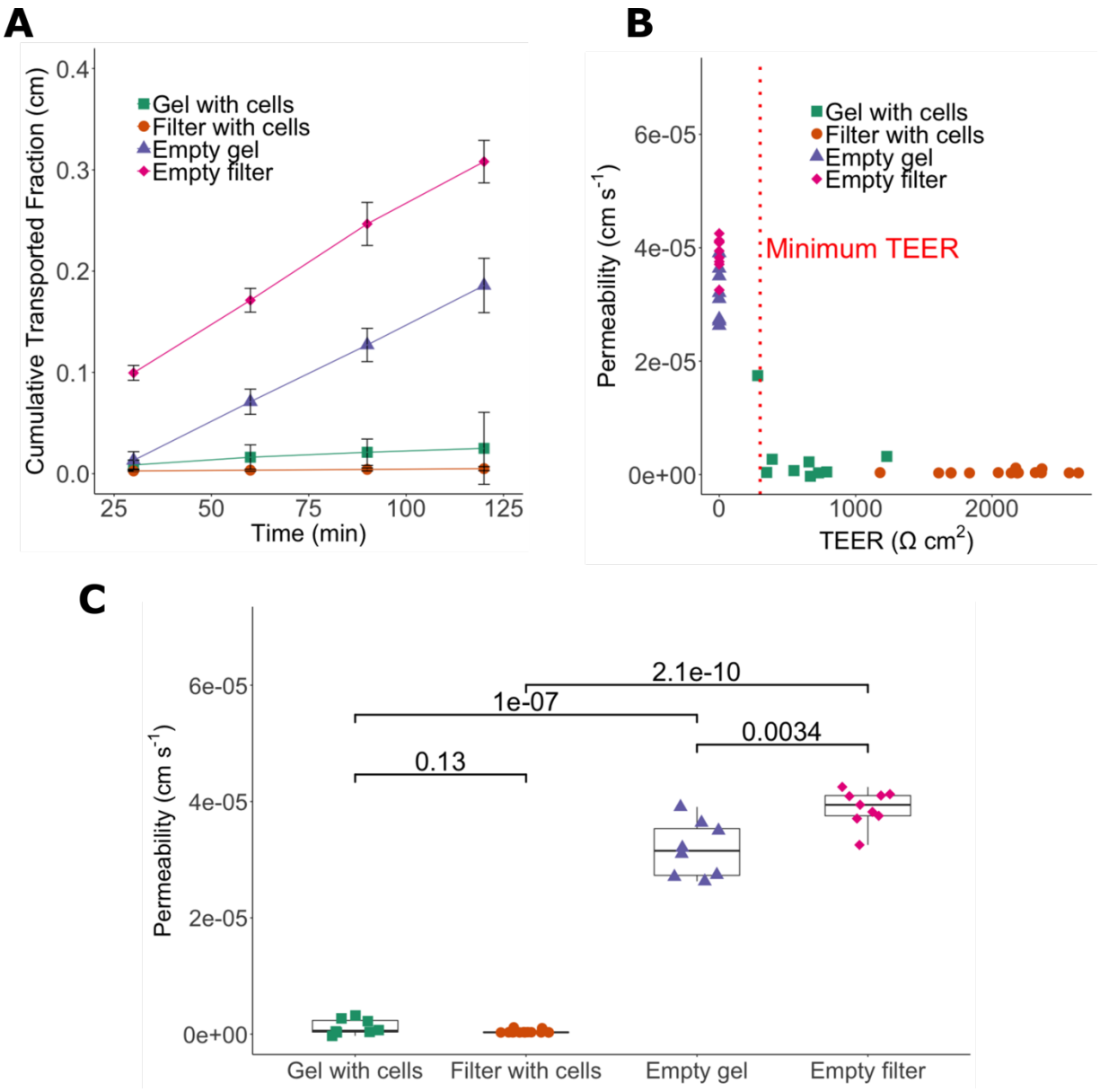

Figure 4: A) Cumulative transported fraction of lucifer yellow across Caco-2 cells on the hydrogel growth-matrix (mean±SD, n=9), empty hydrogel growth-matrices (mean±SD, n=8), Caco-2 cells on polyester filters (mean±SD, n=15), and empty polyester filters (mean±SD, n=9). B) Permeability of lucifer yellow versus TEER . C) Permeability of lucifer yellow.

A Confluent HUVEC cell layer did not inhibit the transport of lucifer yellow across the hydrogel growth-matrix (Figure 5A). The permeability of HUVEC cells on the hydrogel growth-matrix was $2.09\times10^{-5}\pm6.20\times10^{-6}$ cm s^{-1} (mean±SD, n=7) and the permeability for the empty gel was also $2.09\times10^{-5}\pm9.52\times10^{-6}$ cm s^{-1} (mean±SD, n=4) (Figure 5B). This observation

correlated with the non-measurable TEER value over the HUVEC layer. Both observations showed that the layer was leaky. This may, to some extent, model the fenestrated endothelial cells in liver sinusoids that ensure rapid transport of toxic compounds in the blood to the hepatocytes.[62]

The thicker gelatin hydrogel with entrapped HepG2 cells was a large diffusion barrier and no transport was observed with or without cells (Figure 5C). The thicker gelatin hydrogel with entrapped HepG2 cells showed a low lucifer yellow permeability of $1.40\times10^{-6}\pm1.12\times10^{-6}$ cm s^{-1} (mean±SD, n=9) with cells and $1.15\times10^{-6}\pm1.08\times10^{-6}$ cm s^{-1} (mean±SD, n=8) without cells (Figure 5D). Hence, the liver compartment acted as a sponge for drugs that crossed the two other compartments. The spheroids did not act as a barrier as the difference between empty hydrogel growth-matrices and hydrogel growth-matrices containing HepG2 spheroids was not found to be significantly different (p-value=0.65).

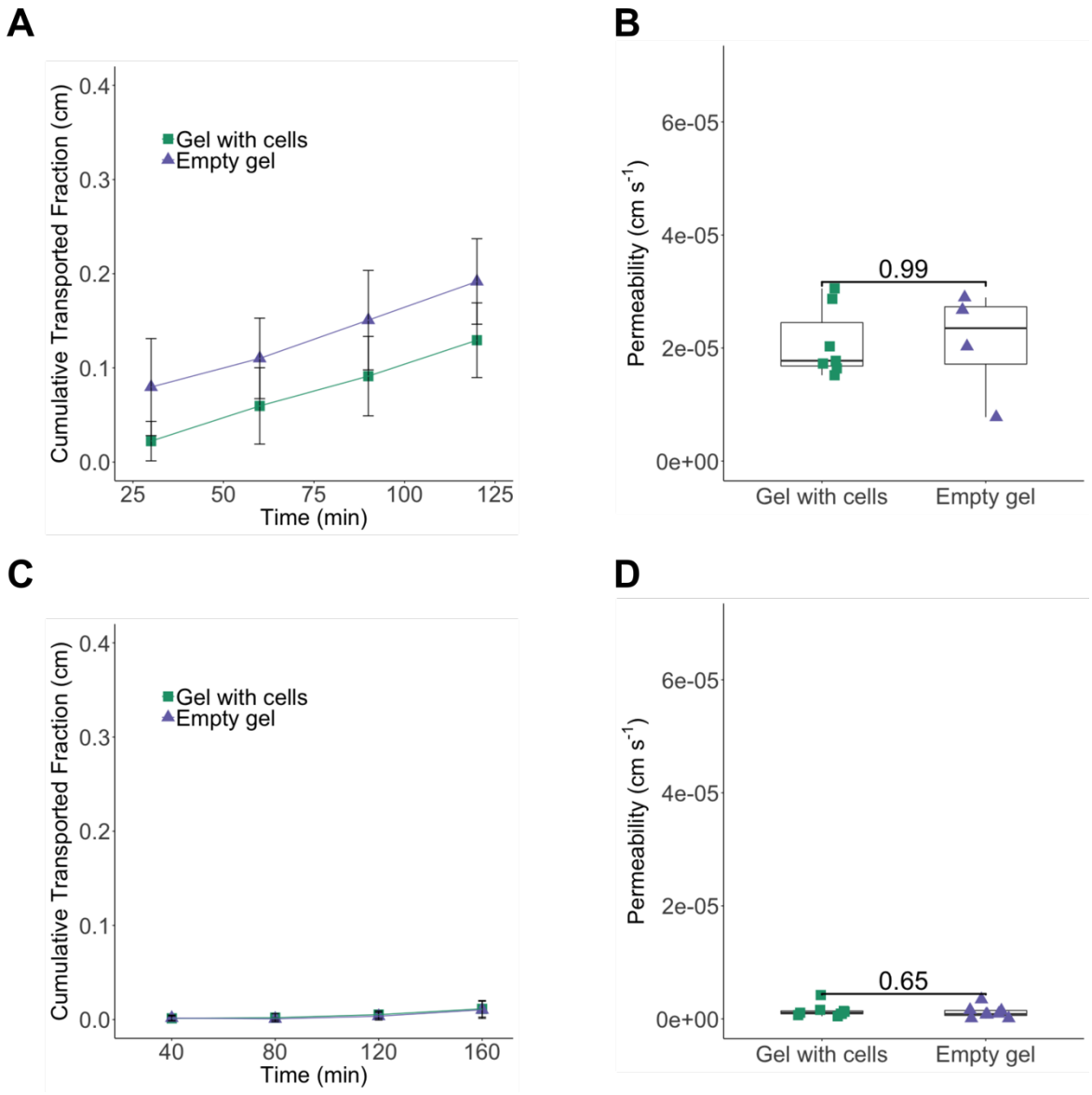

Figure 5: A) Cumulative transported fraction of lucifer yellow across HUVEC cells on the hydrogel growth-matrix (mean±SD, n=7) and empty hydrogel growth-matrices (mean±SD, n=4). B) Permeability of lucifer yellow across HUVEC cells on the hydrogel growth-matrix and empty hydrogel growth-matrices. C) Cumulative transported fraction of lucifer yellow across HepG2 cells on the hydrogel growth-matrix (mean±SD, n=9) and empty hydrogel growth-matrices (mean±SD, n=8). D) Permeability of lucifer yellow across HepG2 cells on the hydrogel growth-matrix and empty hydrogel growth-matrices.

The presented method also allowed for investigation of drug transport in the opposite direction (from basolateral to apical). For Caco-2 cells, the permeability of lucifer yellow from the basolateral to apical side was shown to be $2.12\times10^{-5}\pm5.45\times10^{-6}$ cm s^{-1} (mean±SD, n=11) for

a not fully confluent Caco-2 layer. Whereas, for HUVEC cells, the permeability of lucifer yellow from the basolateral to apical side was shown to be $2.00\times10^{-5}\pm4.35\times10^{-6}$ cm s^{-1} (mean±SD, n=17). This allows for, in the future, to simulate an intravenous injection and thereby to follow the distribution of a drug in the different tissues.

2.3.2. Transport of Furosemide and Valacyclovir Across Intestinal Caco-2 Tissue Model

Furosemide was used as a model drug to show the Caco-2 monolayer as a barrier on the hydrogel (Figure 6A). Furosemide is a poorly absorbed drug and can be used to compare the barrier function of the presented method with the *in vivo* situation. [63]

The permeability of furosemide across the Caco-2 cells on the hydrogel growth-matrix was $1.53\times10^{-6}\pm3.34\times10^{-7}$ cm s^{-1} (mean±SD, n=6), whereas the permeability across the empty hydrogel growth-matrix was $2.06\times10^{-5}\pm1.62\times10^{-6}$ cm s^{-1} (mean±SD, n=5) (p-value=5.7×10^{-6}) (Figure 6B). This is in accordance with what Li et al. observed, as they reported a furosemide permeability of 1.3×10^{-6} cm s^{-1} across a Caco-2 layer.[64] Pade et al. showed a furosemide permeability of 1.2×10^{-7} cm s^{-1} at pH 7.2 across Caco-2 cells on filters,[65] and Hilgendorf et al. showed a furosemide permeability of 2.9×10^{-7} cm s^{-1} at pH 6.5 across Caco-2 cells on filters.[66] Nielsen et al. showed a permeability of 8.63×10^{-6} cm s^{-1} with an apical pH of 7.4 and basolateral pH of 6.5,[67] and Rege et al. reported 6.8×10^{-7} cm s^{-1} with pH 6.8 both apically and basolaterally.[68]

The higher permeability of furosemide over the Caco-2 cell layer on the hydrogel growth-matrix compared to filters reported in literature was consistent with higher lucifer yellow permeability of cells on gels compared to cell on filter (see above). Another explanation could be that the Caco-2 cells on the hydrogel growth-matrices do not to express the efflux pump P-glycoprotein, of which furosemide is a substrate,[69] to the same extent as Caco-2 cells

on the polyester filter. The lower TEER values (Figure 2C) indicated that the increased permeability of the Caco-2 cells on the hydrogel growth-matrix was caused by a less tight cell layer compared to Caco-2 cells on a filter. On the other hand, the permeability of furosemide across the small intestine rat intestine *ex vivo* was shown to be 6.36×10^{-7} cm s^{-1},[69] or little more than two fold lower compared to the Caco-2 on the hydrogel growth-matrix. Hence, the presented setup might be closer to the *in vivo* situation than Caco-2 cells grown on polyester filters.

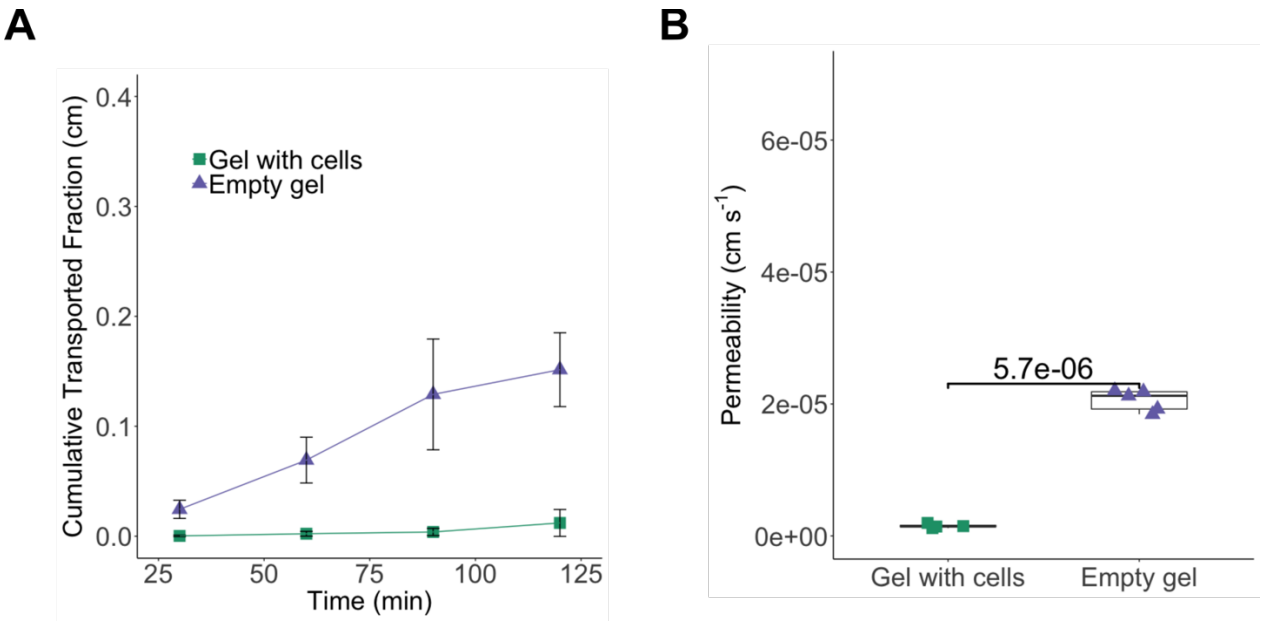

Figure 6: A: Cumulative transported fraction of furosemide across Caco-2 cells on the hydrogel growth-matrix (mean±SD, n=4) and empty hydrogel growth-matrices (mean±SD, n=5). B: cells on the hydrogel growth-matrix and empty hydrogel growth-matrices.

To show that the Caco-2 cell model was tight paracellularly, prodrugs were utilized to investigate another type of drug transport. Prodrugs are drugs given in inactive forms that can be activated in the body often with the purpose of improving absorption.[70] Valacyclovir is a prodrug derived from acyclovir with incorporation of a valine group making it a substrate for the hPepT1 transporter of enterocytes in the small intestine.[71] Transport of valacyclovir and

acyclovir across an empty hydrogel growth-matrix was 9.80±1.23 % , (mean±SD, n=4) and 11.55±0.70 % (mean±SD, n=4) over 4 h, respectively. On the hydrogel growth-matrix with a confluent Caco-2 monolayer, no transport of valacyclovir was detectable due to a fast conversion to acyclovir resulting in it no longer being a substrate for hPepT1. 83.99±2.39% (mean±SD, n=4) of valacyclovir was degraded to acyclovir in the presence of Caco-2 cells on the gel over 4 h, whereas only 40.27±2.70% (mean±SD, n=4) was converted on top of an empty gel. Since, Caco-2 cells are known to express carboxylesterases which convert valacyclovir to acyclovir,[72] this indicates that the Caco-2 cells differentiate to tight monolayers with expression of metabolic enzymes.

3. Conclusion

We report on a 3D-printed triple interconnected *in vitro* tissue method, which is cheap and easy to produce and does not rely on tubes and pumps used in microfluidic systems. The presented method can support various cell types of both hollow and solid tissues. Each individual cell culture can mature independently, and subsequently be connected for a transport study. In this way, medium incompatibility is avoided and each cell line can grow optimally. The method allows for both observing the cell culture growth with bright-field microscopy and end point staining and confocal microscopic characterization.

We present a method for simulating the first pass metabolism *in vitro*. This was done by observing intestinal drug transport via a blood compartment to a liver compartment with sampling in each individual compartment. Here, it was shown that the permeability of the intestinal Caco-2 layer was similar to that observed *in vivo* but different from that of Caco-2 on a polystyrene filter. The system is compact and flexible and can be scaled to connect different

tissue models. The system can be adjusted to the need of lower or higher cells amount, drug, and signal molecule.

4. Experimental Section

4.1. Materials

Dental LT resin (Dental LT FLDCL01) was obtained from Formlabs, Inc. (Somerville, Massachusetts, USA). High-glucose DMEM, trypsin-ethylenediaminetetraacetic acid (EDTA) solution (0.5 g L^{-1} porcine trypsin and 0.2 g L^{-1} EDTA-4Na), ECGM, Penicillin-Streptomycin (P/S), phosphate-buffered saline (PBS, D8537), RPMI 1640 medium, gelatin, Hoechst 33342 trihydrocloride trihydrate, triton X-100, 4-(2-hydroxyethyl)-1-piperazineethanesulfonic acid (HEPES), sodium bicarbonate, and bovine serum albumin (BSA) were all obtained from Sigma-Aldrich (Broendby, Denmark). Non-essential amino acids (NEAA), ZO-1 Rabbit Polyclonal antibody, Goat anti-Rabbit IgG (H+L) Superclonal Secondary Antibody – Alexa Flour® 488 conjugate, Alexa Flour™ 594 Phalloidin, LIVE/DEAD™ Viability/Cytotoxicity Kit (L3224), Hank's Balanced Salt Solution (HBSS (10X), 12 well Transwell® inserts (pore size 0.4 μm) (Corning), and lucifer yellow (Invitrogen™) was purchased from Thermo Fisher Scientific (Slangerup, Denmark). Fetal bovine serum (FBS) was obtained from Biowest, SAS (Nuaillé, France), and T-75 cell culture flasks were purchased from Starstedt (Nümbrecht, Germany). Human epithelial colon carcinoma (CACO-2 (ECACC 09042001)) cells were acquired from European Collection of Authenticated Cell Cultures (Salisbury, Great Britain), whereas the HUVEC cell line was bought from Cell Applications, Inc. (San Diego, California, United States). Human hepatoma (HepG2) cells were obtained from the European Collection of Authenticated Cell Cultures (ECACC) through Sigma-Aldrich (Broendby, Denmark).

Paraformaldehyde (16 %) was purchased from Electron Microscopy Sciences (Pensylvania, United States). Activa TI tranglutaminase was obtained from Ajinomoto Food Ingredients LLC (Chicago Illinois, USA). Furosemide (>98% purity) was purchased from Fagron Nordic (Copenhagen, Denmark), whereas valacyclovir and acyclovir were obtained from TCI Europe N.V. (Zwijndrecht, Belgium).

4.2. Cell Lines and Growth

Caco-2 cells (passage 40-75) were cultured in T-75 cell culture flasks (Starstedt, Nümbrecht, Germany) in Dulbecco's DMEM medium with FBS (20 % (v/v)), NEAA (1 % (v/v)), and P/S (100 U mL^{-1} penicillin and 100 µg mL^{-1} streptomycin). HUVEC cells (passage 3-12) were cultured in endothelial culture medium FBS (10 % (v/v)), and P/S (100 U mL^{-1} penicillin and 100 µg mL^{-1} streptomycin). HepG2 cells (passage 100-130) were cultured in RMPI 1640 medium FBS (10 % (v/v)), and P/S (100 U mL^{-1} penicillin and 100 µg mL^{-1} streptomycin).
All the cells were cultured at 37˚C and 5 % CO_2 and split with trypsin-EDTA for 5-10 min upon 80-90 % confluency. Once the cells were detached, trypsin-EDTA were inhibited by addition of cell culture medium, and a sample was taken for counting the cells (counted with NucleoCounter NC-200).

4.3. Fabrication of 3D-printed inserts

3D designs were drawn using Fusion 360 (version 1.28.2, Autodesk, San Rafael, California, USA) and print files were exported in STL format and processed in PreForm (version 2.12.0, Formlabs, Somerville, Massachusetts, USA) (Figure S2). 3D designs were printed on a Formlabs Form 2 3D printer (Formlabs, Somerville, Massachusetts, USA).

3D prints for cell cultures were printed in Dental LT resin with a layer thickness of 0.1 mm, and were subsequently cleaned twice in fresh isopropyl alcohol for 1 h and air dried overnight. The 3D prints were cured in a Formlabs Form Cure UV-oven (Formlabs, Somerville, Massachusetts, USA) for 2 h at 60 °C, after which the support structures were cut off followed by submersion in sterile water for a day. Once the prints were dry, a further 15 min cure at 60 °C for sterilization was performed.

Parts for the casting device were printed using a Prusa i3 MK3 3D printed with a 0.4 mm nozzle, a layer height of 0.2 mm and 15 % infill from PLA filament. Small springs were placed on the pillars on the board and the plugs coated with parafilm were put on the springs (Figure S3A).

4.4. Casting of Hydrogels and Seeding of Cells

For casting of hydrogel growth-matrices into, the 3D-printed inserts and casting device were assembled (Figure S3). Once assembled, 30 µL (for Caco-2 and HUVEC inserts) or 100 µL (for HepG2 inserts) of a mixture of gelatin (5 % w/v) and mTG (5 U mL^{-1} for Caco-2 and HUVEC or 2.5 U mL^{-1} for HepG2) was added. The hydrogel growth-matrix was crosslinked for 1 h at 37 °C. Afterwards, the 3D-printed insert was removed from the casting device. Either 10^6 cells mL^{-1} of HepG2 cells were seeded into the hydrogel growth-matrix while casting, or Caco-2 and HUVEC cells were seeded on top of the hydrogel growth-matrix after casting. 100,000 Caco-2 cells were seeded onto each hydrogel growth-matrix in the 3D-printed inserts corresponding to ~155,000 cells cm^{-2}, whereas polyester filters were seeded with ~140,000 Caco-2 cells corresponding to ~125,000 cells cm^{-2}. Both seedings were within the recommended density.[73] The apical medium was changed between 4 and 16 h after seeding. In the HUVEC inserts, 200,000 HUVEC cells were also seeded onto each hydrogel growth-

matrix. 1 mL medium was added on top and below the hydrogel growth-matrix with HepG2 cells. 500 µL was added on top and 1 mL below hydrogel growth-matrices with Caco-2 and HUVEC cells. The Caco-2 and HepG2 cells were cultured for three weeks with the medium exchanged two times a week. The HUVEC cells were seeded two days before use.

After use, the gelatin hydrogels could be dissolved by the use of trypsin which then made it possible to reuse the 3D printed parts without decreasing the performance of the inserts.

4.5. Staining of F-actin, Live/Dead, and ZO-1 Stains

For F-actin staining, samples were washed for 15 min in PBS followed by fixation in 3 % PFA in PBS for 30 min at room temperature. PFA was aspirated from the samples and the samples were incubated with 0.05 % Saponin/1 % BSA in PBS for 30 min at room temperature. The samples were washed three times in PBS and incubated with phalloidin stain (5 µL diluted in 200 µL PBS) for 20 min at room temperature. The samples were washed three times in PBS and left in PBS.

For ZO-1 staining, cells were washed for 15 min in PBS followed by fixation in 3 % PFA in PBS for 30 min at room temperature. PFA was aspirated and the samples were incubated in 3 % BSA in PBS for 15 min at room temperature. Afterwards, the samples were washed three times in PBS and incubated with 5 µg/mL primary antibody in PBS with 0.1 % Triton X-100 for 1 h at room temperature. This was followed by three washes in PBS. The secondary antibody in PBS (1:1000) with 0.1 % Triton X-100 was added and incubated for 1 h at room temperature. The samples were then washed three times in PBS and left in PBS.

For nuclei staining, samples were washed three times with PBS and 1 µg mL^{-1} Hoechst 33342 in PBS was added and incubated for 10 min at room temperature. The samples were then washed three times in PBS and left in PBS.

For live/dead staining, the hydrogel growth-matrices were cut out of the 3D-printed inserts and cut in half length wise. Subsequently, the samples were washed three times in PBS and stain in 500 µL of a solution with ethidium homodimer-1 (8 nM) and calcein (4 mM) for 1 h at room temperature. The samples were washed in PBS two times and then kept in 200 µL PBS to keep the hydrogel growth-matrices moisturized.

4.6. Confocal Microscopy F-actin, Live/Dead, and ZO-1 Stains

Confocal micrographs were obtained using a LSM 700 scanning confocal microscope (Carl Zeiss MicroImaging GmbH, 37081 Gottingen, Germany) with the following objectives; EC Epiplan-NEOFLUAR 10x/0.25 HD, EC Epiplan-NEOFLUAR 5x/0.13 HD, and EC Epiplan-NEOFLUAR 10x/0.5 HD. 100 µL of PBS was added around the hydrogel growth-matrices when performing microscopy to keep them moisturized. The obtained confocal micrographs were fitted with scalebars and Z-stacks were processed in Fiji by Z-projections of maximum intensities.[74]

Phase contrast bright-field micrographs were obtained using a Ziess Primovert microscope (Carl Zeiss MicroImaging GmbH, 37081 Gottingen, Germany) with the following objective: Plan-Achromat 4x/0.10. The obtained micrographs were fitted with scalebars in Fiji.[74]

4.7. Transport Studies of, Lucifer Yellow, Furosemide, and Valacyclovir

4.7.1. TEER measurements

An EVOM2 epithelial Volt/Ohm meter (World Precision Instruments, Sarasota, Florida, USA) was used to assess the resistance between the apical and the basolateral surfaces on confluent

cell monolayers. The resistance of the monolayers was corrected by subtracting the resistance of an average (n=3) from blank wells without cells:

$$R_{sample} - R_{blank} = R_{cell\ layer} \quad (1)$$

To normalize the resistance to the area, the area was multiplied by the resistance to obtain resistance values in Ω cm^2. The area of the hydrogel growth-matrix was 0.2 cm^2 and the area of the commercial 12 well transwell plates was 1.13 cm^2. From the TEER study over time, an average blank was obtained to be 130 Ω cm^2 for conventional transwells and 160 Ω cm^2 for hydrogel transwells.

4.7.2. Lucifer Yellow Transport

The three 3D-printed inserts were assembled for transport studies with lucifer yellow. Each compartment had 1 mL of preheated (to 37˚C) HBSS transport buffer (HBSS (1X), Sodium bicarbonate (0.0375 % w/v), HEPES (10 mM), BSA (0.05 % w/v, pH 7.4) while the transport study was performed at 37 °C with 100 rounds per minute (rpm) shaking. 2.25 µM lucifer yellow was added apically of the tissue model which transport across was investigated. The transport study was performed for 2 h for Caco-2 and HUVEC cells and 3 h HepG2 cells. Samples of 50 µL were taken and 50 µL HBSS transport buffer was added every 30 min for Caco-2 and HUVEC cells and 40 min HepG2 cells. After the transport experiment, the samples were measured with a TECAN spark plate reader by using an excitation of 428 nm and measuring emission at 536 nm.

4.7.3. Furosemide Transport through the Caco-2 cells

The three 3D-printed inserts were assembled for transport studies with furosemide. Each compartment had 1 mL of preheated (to 37˚C) HBSS transport buffer while the transport study

was performed. 0.75 mg mL^{-1} furosemide was added to the apical compartment. The transport study was performed for 4 h at 37 °C. Samples of 50 µL were taken and 50 µL HBSS transport buffer every 30 min for the first 2 h and every 60 min for the last 2 h. HPLC analysis was performed of the samples just after the experiments following a previous established method,[75] with slight differences. The HPLC analysis was performed on a Shimadzu HPLC system consisting of a CBM-20A system controller, SIL-20AC HT auto sampler, LC-20AD pump, DGU-20A5R degassing unit, CTO-20AC column oven, RID-20A refractive index detector, and SPD-30A photodiode array detector. A Phenomenex Kinetex ® C18 column (100 × 4.6 mm, 5 µm) was used, whereas the mobile phase consisted of purified water, methanol and phosphoric acid in a ratio of 49:50:1 v/v/v. The injection volume was 10 µL with a flow rate of 0.7 mL/min and a temperature of 25 °C. The furosemide content of the samples was identified using UV detection at a wavelength of 254 nm.

4.7.4 HPLC of valacyclovir and acyclovir

The three 3D-printed inserts were assembled for transport studies with valacyclovir and acyclovir. Each compartment had 1 mL of preheated (to 37˚C) HBSS transport buffer while the transport study was performed. 0.5 mg mL^{-1} valacyclovir was added to the apical compartment. The transport study was performed for 4 h at 37 °C. Samples of 50 µL were taken and 50 µL HBSS transport buffer every 30 min for the first 2 h and every 60 min for the last 2 h. Valacyclovir and acyclovir samples were analyzed using the same HPLC protocol as for furosemide. However, the mobile phase consisted of PBS at pH 5 and methanol in a ratio of 75:25 v/v.[76] The injection volume was 10 µL with a flow rate of 0.7 mL min^{-1} and a temperature of 40 °C. The valacyclovir/acyclovir content of samples was identified using UV detection at a wavelength of 254 nm.

4.7.5 Calculation of Transport Rates

From transport studies with the triple layered tissue models the cumulative transported fraction and the permeability were calculated by the following equations. Where, "a" refers to the compartment above the Caco-2 layer, "b" to the compartment above the HUVEC layer, "c" is the compart above the HepG2 layer, and "d" is the compartment below the HepG2 layer.

Transport Across the Intestinal layer

The donor concentration for drug transport a to b was calculated by:

$$C_D(t) = C_D(t_{i-1}) - \frac{[C_R(t) - f \times C_R(t_{i-1})] \times V_R}{V_D} \quad (2)$$

Where, V_R is the receiver volume, V_D is the donor volume, $C_R(t)$ is the receiver concentration at the timepoint the donor concentration is being determined for, and f is defined by:

$$f = 1 - \frac{V_S}{V_R} \quad (3)$$

Where, V_S is the sampling volume. The receiver concentration was calculated from the concentrations in each compartment at a given time:

$$C_R(t) = \frac{[b(t)] \times V_R + [c(t)] \times V_R + [d(t)] \times V_R}{V_R} \quad (4)$$

The cumulative transported fraction was calculated from the donor and receiver concentrations with the following equation:

$$CTF(t) = \frac{1}{A} \times \sum_{k=1}^{i} \frac{[C_R(t_k) - f \times C_R(t_{k-1})] \times V_R}{[C_D(t_{k-1}) + C_D(t_k)]/2} \quad (5)$$

Where, A is the area of the barrier. A linear curve fit of the cumulative transported fraction gives the permeability coefficient.

The receiver concentration was corrected for calculating basolateral to apical flow:

$C_R(t) = [a(t)]$ (6)

Transport Across the Endothelial Layer

The donor concentration for drug transport from b to c was calculated by:

$C_D(t) = C_D(t_{i-1}) - \frac{[C_O(t) - f \times C_O(t_{i-1})] \times V_R}{V_D}$ (7)

Where C_O is the total concentration in the other compartments at a given time calculated by:

$C_O(t) = \frac{[a(t)] \times V_R + [c(t)] \times V_R + [d(t)] \times V_R}{V_R}$ (8)

The receiver concentration was calculated from the concentrations in the receiving compartments c and d:

$C_R(t) = \frac{[c(t)] \times V_R + [d(t)] \times V_R}{V_R}$ (9)

The cumulative transported fraction was calculated from the receiver and donor concentration using equation (5) and the permeability coefficient was obtained from the curve of the cumulative transported fraction.

The receiver concentration was corrected for calculating basolateral to apical flow:

$C_R(t) = \frac{[a(t)] \times V_R + [b(t)] \times V_R}{V_R}$ (10)

Transport Across the Hepatic Layer

The donor concentration for drug transport from c to d was calculated by equation (7),

where C_O is calculated by:

$C_O = \frac{[a(t)] \times V_R + [b(t)] \times V_R + [d(t)] \times V_R}{V_R}$ (11)

The receiver concentration was calculated from the concentrations in the receiving compartment d at a given time:

$C_R(t) = [d(t)]$ (12)

From the receiver and donor concentration, the cumulative transported fraction was calculated using equation (5) and the permeability coefficient was obtained from the curve of the cumulative transported fraction.

4.8. Statistics

The data are presented as number of repetitions (n), mean±SD. Calculations were done using RStudio (Version 1.2.5001, RStudio, Inc.) and Microsoft Excel (Version 15.41, Microsoft Office, Seattle, Washington). P-values were obtained using a Two sample T-test and determined significant different when p-value<0.05.

Supporting Information ((delete if not applicable))

Supporting Information is available from the Wiley Online Library or from the author.

Acknowledgements

The authors would like to acknowledge the Danish National Research Foundation (DNRF122) and Villum Fonden (Grant No. 9301) for Intelligent Drug Delivery and Sensing Using Microcontainers and Nanomechanics (IDUN).

References

[1] P. V. Balimane, S. Chong, R. A. Morrison, *J. Pharmacol. Toxicol. Methods* **2000**, *44*,

301.

[2] P. Colombo, F. Sonvico, G. Colombo, R. Bettini, *Pharm. Res.* **2009**, *26*, 601.

[3] M. Dickson, J. P. Gagnon, *Nat. Rev. Drug Discov.* **2004**, *3*, 417.

[4] S. M. Paul, D. S. Mytelka, C. T. Dunwiddie, C. C. Persinger, B. H. Munos, S. R. Lindborg, A. L. Schacht, *Nat. Rev. Drug Discov.* **2010**, *9*, 203.

[5] A. Sivaraman, J. Leach, S. Townsend, T. Iida, B. Hogan, D. Stolz, R. Fry, L. Samson, S. Tannenbaum, L. Griffith, *Curr. Drug Metab.* **2005**, *6*, 569.

[6] J. Törnell, M. Snaith, *Drug Discov. Today* **2002**, *7*, 461.

[7] S. Venkatesh, R. A. Lipper, *J. Pharm. Sci.* **2000**, *89*, 145.

[8] G. Lazzari, V. Nicolas, M. Matsusaki, M. Akashi, P. Couvreur, S. Mura, *Acta Biomater.* **2018**, *78*, 296.

[9] C. Venter, C. Niesler, *Biotechniques* **2018**, *64*, 52.

[10] E. Dohle, I. Bischoff, T. Böse, A. Marsano, A. Banfi, R. E. Unger, C. J. Kirkpatrick, *Eur. Cells Mater.* **2014**, *27*, 149.

[11] P. Miranda-Azpiazu, S. Panagiotou, G. Jose, S. Saha, *Sci. Rep.* **2018**, *8*, 8784.

[12] R. A. M. Blom, S. T. Erni, K. Krempaská, O. Schaerer, R. M. Van Dijk, M. Amacker, C. Moser, S. R. R. Hall, C. Von Garnier, F. Blank, *PLoS One* **2016**, *11*, e0163539.

[13] F. An, Y. Qu, Y. Luo, N. Fang, Y. Liu, Z. Gao, W. Zhao, B. Lin, *Sci. Rep.* **2016**, *6*, 25022.

[14] I. Maschmeyer, A. K. Lorenz, K. Schimek, T. Hasenberg, A. P. Ramme, J. Hübner, M. Lindner, C. Drewell, S. Bauer, A. Thomas, et al., *Lab Chip* **2015**, *15*, 2688.

[15] S. J. Trietsch, G. D. Israëls, J. Joore, T. Hankemeier, P. Vulto, *Lab Chip* **2013**, *13*, 3548.

[16] Z. Abid, S. Strindberg, M. M. Javed, C. Mazzoni, L. Vaut, L. H. Nielsen, C. Gundlach, R. S. Petersen, A. Müllertz, A. Boisen, et al., *Lab Chip* **2019**, *19*, 2905.

[17] H. D. Chirra, L. Shao, N. Ciaccio, C. B. Fox, J. M. Wade, A. Ma, T. A. Desai, *Adv.*

Healthcare Mater. **2014**, *3*, 1648.

[18] K. J. McHugh, T. D. Nguyen, A. R. Linehan, D. Yang, A. M. Behrens, S. Rose, Z. L. Tochka, S. Y. Tzeng, J. J. Norman, A. C. Anselmo, et al., *Science* **2017**, *357*, 1138.

[19] J. R. Jørgensen, M. L. Jepsen, L. H. Nielsen, M. Dufva, H. M. Nielsen, T. Rades, A. Boisen, A. Müllertz, *Eur. J. Pharm. Biopharm.* **2019**, *143*, 98.

[20] H. J. Kim, D. Huh, G. Hamilton, D. E. Ingber, *Lab Chip* **2012**, *12*, 2165.

[21] J. D. Wang, N. J. Douville, S. Takayama, M. Elsayed, *Ann. Biomed. Eng.* **2012**, *40*, 1862.

[22] D. Huh, H. J. Kim, J. P. Fraser, D. E. Shea, M. Khan, A. Bahinski, G. A. Hamilton, D. E. Ingber, *Nat. Protoc.* **2013**, *8*, 2135.

[23] K. Y. Chumbimuni-Torres, R. E. Coronado, A. M. Mfuh, C. Castro-Guerrero, M. F. Silva, G. R. Negrete, R. Bizios, C. D. Garcia, *RSC Adv.* **2011**, *1*, 706.

[24] M. W. Toepke, D. J. Beebe, *Lab Chip* **2006**, *6*, 1484.

[25] D. T. Butcher, T. Alliston, V. M. Weaver, *Nat. Rev. Cancer* **2009**, *9*, 108.

[26] B. Geiger, A. Bershadsky, *Curr. Opin. Cell Biol.* **2001**, *13*, 584.

[27] M. J. Paszek, N. Zahir, K. R. Johnson, J. N. Lakins, G. I. Rozenberg, A. Gefen, C. A. Reinhart-King, S. S. Margulies, M. Dembo, D. Boettiger, et al., *Cancer Cell* **2005**, *8*, 241.

[28] N. Annabi, S. M. Mithieux, P. Zorlutuna, G. Camci-unal, A. S. Weiss, A. Khademhosseini, *Biomaterials* **2013**, *34*, 5496.

[29] Y. Li, G. Huang, B. Gao, M. Li, G. M. Genin, T. J. Lu, F. Xu, *NPG Asia Mater.* **2016**, *8*, e238.

[30] R. Pimentel C., S. K. Ko, C. Caviglia, A. Wolff, J. Emnéus, S. S. Keller, M. Dufva, *Acta Biomater.* **2017**, *65*, 174.

[31] S. Hong, D. Sycks, H. F. ai Chan, S. Lin, G. P. Lopez, F. Guilak, K. W. Leong, X. Zhao,

Adv. Mater. **2015**, *27*, 4035.

[32] R. L. DiMarco, D. R. Hunt, R. E. Dewi, S. C. Heilshorn, *Biomaterials* **2017**, *129*, 152.

[33] D. B. Gunasekara, J. Speer, Y. Wang, D. L. Nguyen, M. I. Reed, N. M. Smiddy, J. S. Parker, J. K. Fallon, P. C. Smith, C. E. Sims, et al., *Anal. Chem.* **2018**, *90*, 13331.

[34] J. Susewind, C. De Souza Carvalho-Wodarz, U. Repnik, E. M. Collnot, N. Schneider-Daum, G. W. Griffiths, C. M. Lehr, *Nanotoxicology* **2016**, *10*, 53.

[35] M. Djabourov, J. Leblond, P. Papon, *J. Phys.* **1988**, *49*, 319.

[36] T. Heck, G. Faccio, M. Richter, L. Thöny-Meyer, *Appl. Microbiol. Biotechnol.* **2013**, *97*, 461.

[37] C. Canali, C. Mazzoni, L. B. Larsen, A. Heiskanen, Ø. G. Martinsen, A. Wolff, M. Dufva, J. Emnéus, *Analyst* **2015**, *140*, 6079.

[38] K. Kuwahara, Z. Yang, G. C. Slack, M. E. Nimni, B. Han, *Tissue Eng. Part C Methods* **2010**, *16*, 609.

[39] G. Yang, Z. Xiao, X. Ren, H. Long, H. Qian, K. Ma, Y. Guo, *PeerJ* **2016**, *4*, e2497.

[40] M. L. Jepsen, L. H. Nielsen, A. Boisen, K. Almdal, M. Dufva, *Biopolymers* **2019**, *110*, e23241.

[41] Z. Wei, S. Kale, R. El Fatimy, R. Rabinovsky, A. M. Krichevsky, *Front. Neurosci.* **2019**, *13*, 1.

[42] J. H. Sung, M. L. Shuler, *Lab Chip* **2009**, *9*, 1385.

[43] B. M. Maoz, A. Herland, E. A. Fitzgerald, T. Grevesse, C. Vidoudez, A. R. Pacheco, S. P. Sheehy, T. E. Park, S. Dauth, R. Mannix, et al., *Nat. Biotechnol.* **2018**, *36*, 865.

[44] H. Y. Tan, S. Trier, U. L. Rahbek, M. Dufva, J. P. Kutter, T. L. Andresen, *PLoS One* **2018**, *13*, e0197101.

[45] L. G. Griffith, M. A. Swartz, *Nat. Rev. Mol. Cell Biol.* **2006**, *7*, 211.

[46] M. Pinto, S. R. Leon, M. D. Appay, *Biol. Cell* **1983**, *47*, 323.

[47] G. E. Striker, J. M. Harlan, S. M. Schwartz, *Methods Cell Biol.* **1980**, *21*, 135.

[48] R. L. Nachman, E. A. Jaffe, *J. Clin. Invest.* **2004**, *114*, 1037.

[49] M. T. Donato, L. Tolosa, M. J. Gómez-Lechón, in *Protoc. Vitr. Hepatocyte Res.*, Springer, New York, **2015**, pp. 77–93.

[50] F. Leonard, E. M. Collnot, C. M. Lehr, *Mol. Pharm.* **2010**, *7*, 2103.

[51] P. Balimane, S. Chong, *Drug Discov. Today* **2005**, *10*, 335.

[52] P. Artursson, A. L. Ungell, J. E. Löfroth, *Pharm. Res.* **1993**, *10*, 1123.

[53] I. J. Hidalgo, T. J. Raub, R. T. Borchardt, *Gastroenterology* **1989**, *96*, 736.

[54] B. Srinivasan, A. R. Kolli, M. B. Esch, H. E. Abaci, M. L. Shuler, J. J. Hickman, *J. Lab. Autom.* **2015**, *20*, 107.

[55] R. Zhang, N. B. Larsen, *Lab Chip* **2017**, *17*, 4273.

[56] H. Lee, W. Park, H. Ryu, N. L. Jeon, *Biomicrofluidics* **2014**, *8*, 054102.

[57] S. C. Ramaiahgari, M. W. Den Braver, B. Herpers, V. Terpstra, J. N. M. Commandeur, B. Van De Water, L. S. Price, *Arch. Toxicol.* **2014**, *88*, 1083.

[58] P. C. Georges, J.-J. Hui, Z. Gombos, M. E. McCormick, A. Y. Wang, M. Uemura, R. Mick, P. A. Janmey, E. E. Furth, R. G. Wells, *AJP Gastrointest. Liver Physiol.* **2007**, *293*, G1147.

[59] M. Yin, J. A. Talwalkar, K. J. Glaser, A. Manduca, R. C. Grimm, P. J. Rossman, J. L. Fidler, R. L. Ehman, *Clin. Gastroenterol. Hepatol.* **2007**, *5*, 1207.

[60] A. Asthana, W. S. Kisaalita, *Drug Discov. Today* **2012**, *17*, 810.

[61] F. Hirschhaeuser, H. Menne, C. Dittfeld, J. West, W. Mueller-Klieser, L. a. Kunz-Schughart, *J. Biotechnol.* **2010**, *148*, 3.

[62] E. M. Brunt, A. S. H. Gouw, S. G. Hubscher, D. G. Tiniakos, P. Bedossa, A. D. Burt, F.

Callea, A. D. Clouston, H. P. Dienes, Z. D. Goodman, et al., *Histopathology* **2014**, *64*, 907.

[63] L. Perioli, G. D'Alba, C. Pagano, *Eur. J. Pharm. Biopharm.* **2012**, *80*, 621.

[64] C. Li, T. Liu, X. Cui, A. S. Uss, K. C. Cheng, *J. Biomol. Screen.* **2007**, *12*, 1084.

[65] V. Pade, S. Stavchansky, *Pharm. Res.* **1997**, *14*, 1210.

[66] C. Hilgendorf, H. Spahn-Langguth, C. G. Regårdh, E. Lipka, G. L. Amidon, P. Langguth, *J. Pharm. Sci.* **2000**, *89*, 63.

[67] L. H. Nielsen, A. Melero, S. S. Keller, J. Jacobsen, T. Garrigues, T. Rades, A. Müllertz, A. Boisen, *Int. J. Pharm.* **2016**, *504*, 98.

[68] B. D. Rege, X. Yu Lawrence, A. S. Hussain, J. E. Polli, *J. Pharm. Sci.* **2001**, *90*, 1776.

[69] A. M. Al-Mohizea, *Saudi Pharm. J.* **2010**, *18*, 97.

[70] V. Abet, F. Filace, J. Recio, J. Alvarez-Builla, C. Burgos, *Eur. J. Med. Chem.* **2017**, *127*, 810.

[71] A. E. Thomsen, G. M. Friedrichsen, A. H. Sørensen, R. Andersen, C. U. Nielsen, B. Brodin, M. Begtrup, S. Frokjaer, B. Steffansen, *J. Control. Release* **2003**, *86*, 279.

[72] T. Imai, M. Imoto, H. Sakamoto, M. Hashimoto, *Drug Metab. Dispos.* **2005**, *33*, 1185.

[73] S. Tavelin, J. Gråsjö, J. Taipalensuu, G. Ocklind, P. Artursson, in *Epithel. Cell Cult. Protoc.*, Humana Press, Totowa, NJ, **2002**, pp. 233–272.

[74] J. Schindelin, I. Arganda-Carreras, E. Frise, V. Kaynig, M. Longair, T. Pietzsch, S. Preibisch, C. Rueden, S. Saalfeld, B. Schmid, et al., *Nat. Methods* **2012**, *9*, 676.

[75] L. H. Nielsen, S. Gordon, R. Holm, A. Selen, T. Rades, A. Müllertz, *Eur. J. Pharm. Biopharm.* **2013**, *85*, 942.

[76] G. E. Granero, G. L. Amidon, *Int. J. Pharm.* **2006**, *317*, 14.

((Supporting Information can be included here using this template))

Supporting Information

3D-Printed Stackable Titer Plate Inserts Supporting Three Interconnected Tissue Models for Drug Screening

Morten Leth Jepsen, Andreas Willumsen, Chiara Mazzoni , Anja Boisen, Line Hagner Nielsen and Martin Dufva

MSc M. L. J., BSc A. W., Dr. C. M., Prof. A. B., Dr. L. H. N., Dr. M. D.,
The Danish National Research Foundation and Villum Foundation's Center for Intelligent Drug Delivery and Sensing Using Microcontainers and Nanomechanics (IDUN), Department of Health Technology, Technical University of Denmark, Ørsteds Plads 345C, 2800 Kgs. Lyngby, Denmark.

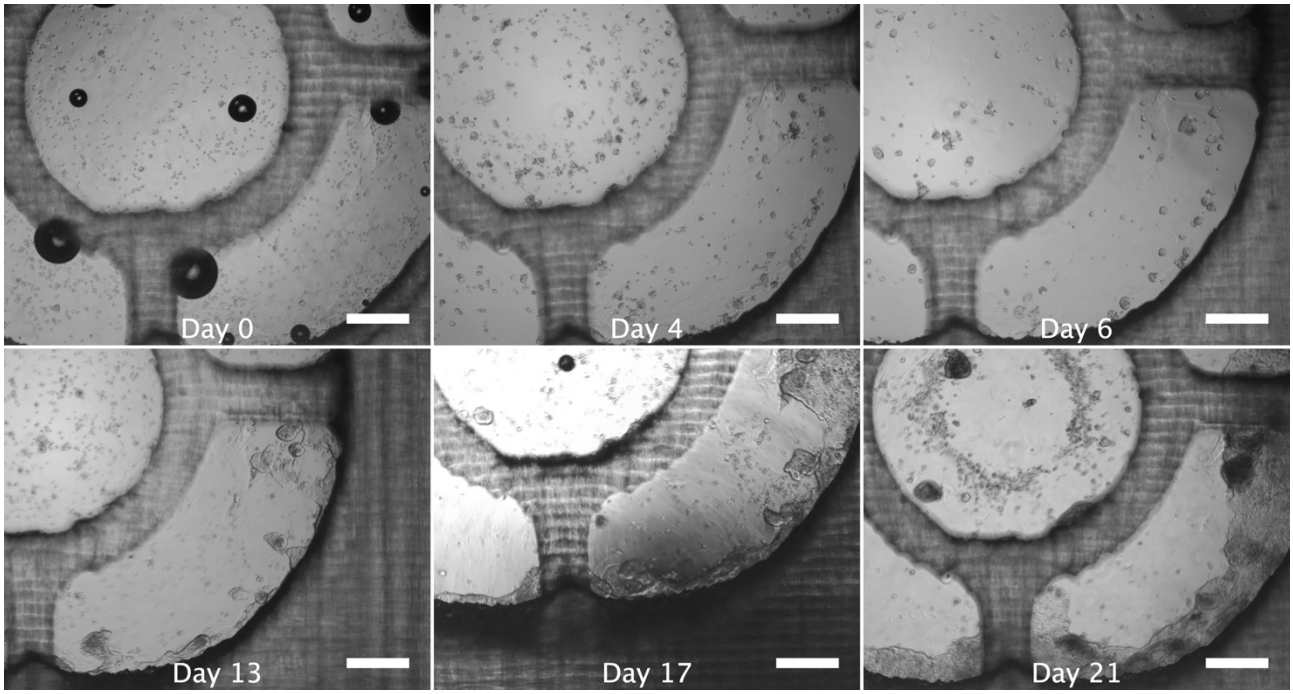

Figure S1: Growth of Caco-2 cells over 21 days on hydrogel growth-matrices when the 3D-printed inserts are not probably cleaned. Scalebars: 1000 μm.

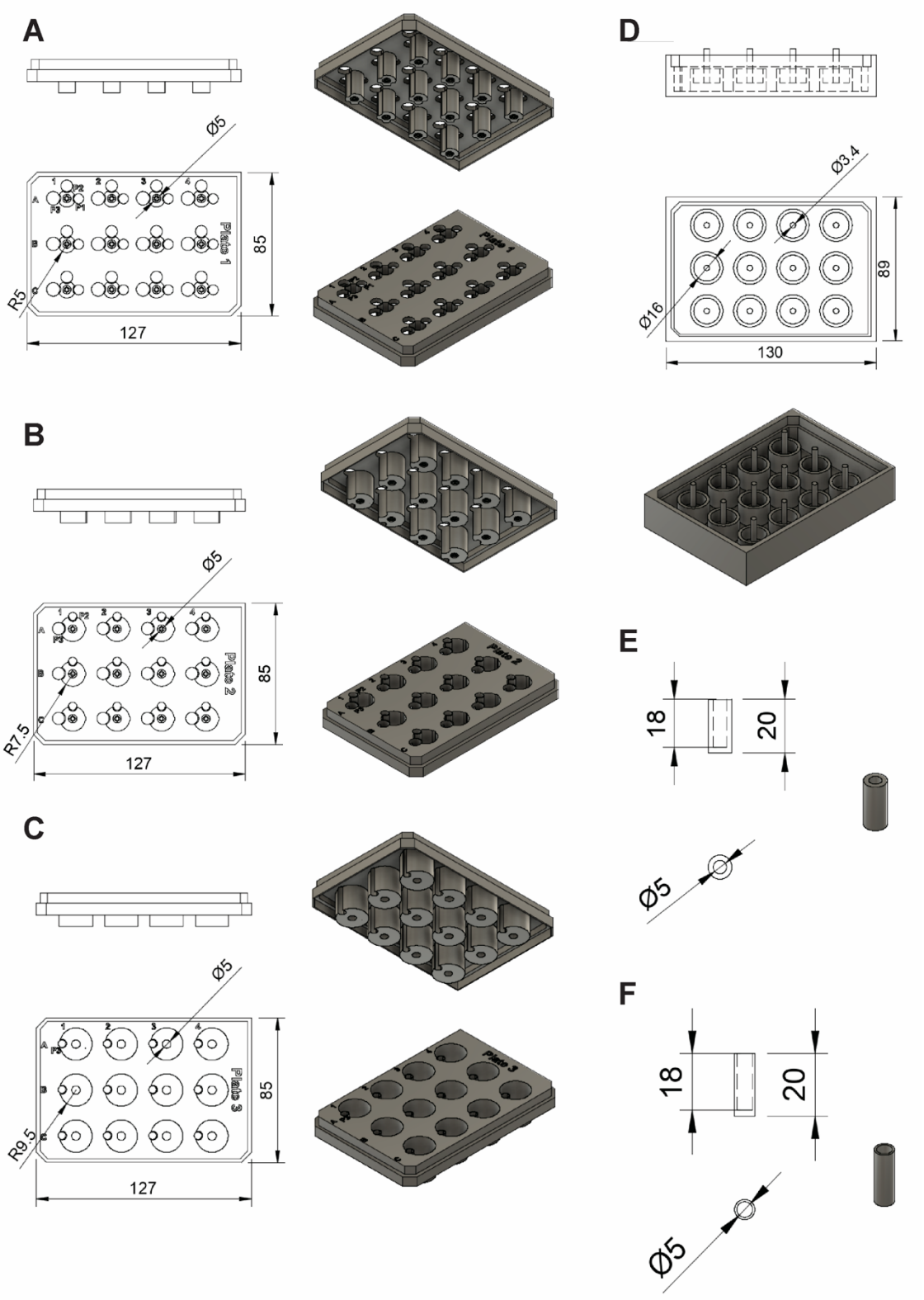

Figure S2: Technical drawing of 3D-printed inserts used for A) Caco-2, B) HUVEC, and C) HepG2 cells. D: Technical drawing of casting device. E: Technical drawing pillars used as

plugs for 3D-printed insert for Caco-2 cells. E: Technical drawing pillars used as plugs 3D-printed insert for HUVEC and HepG2 cells. Ø: Diameter, R: Radius. Measurements in mm.

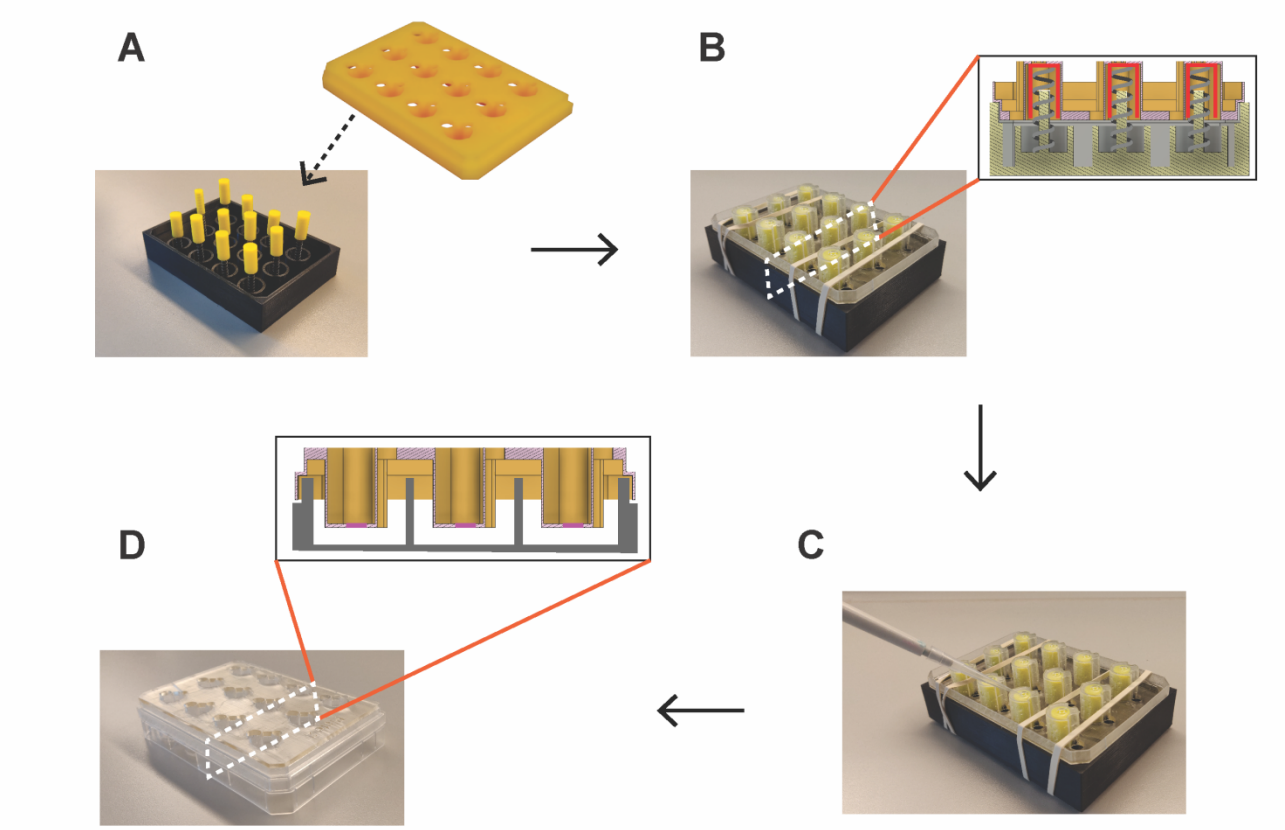

Figure S3: A: Springboard with pillars. B: Transport inserts clamped with rubber bands to the springboard. C: Casting of hydrogel in transport inserts. D: transport inserts removed from springboard and placed in a standard well plate.

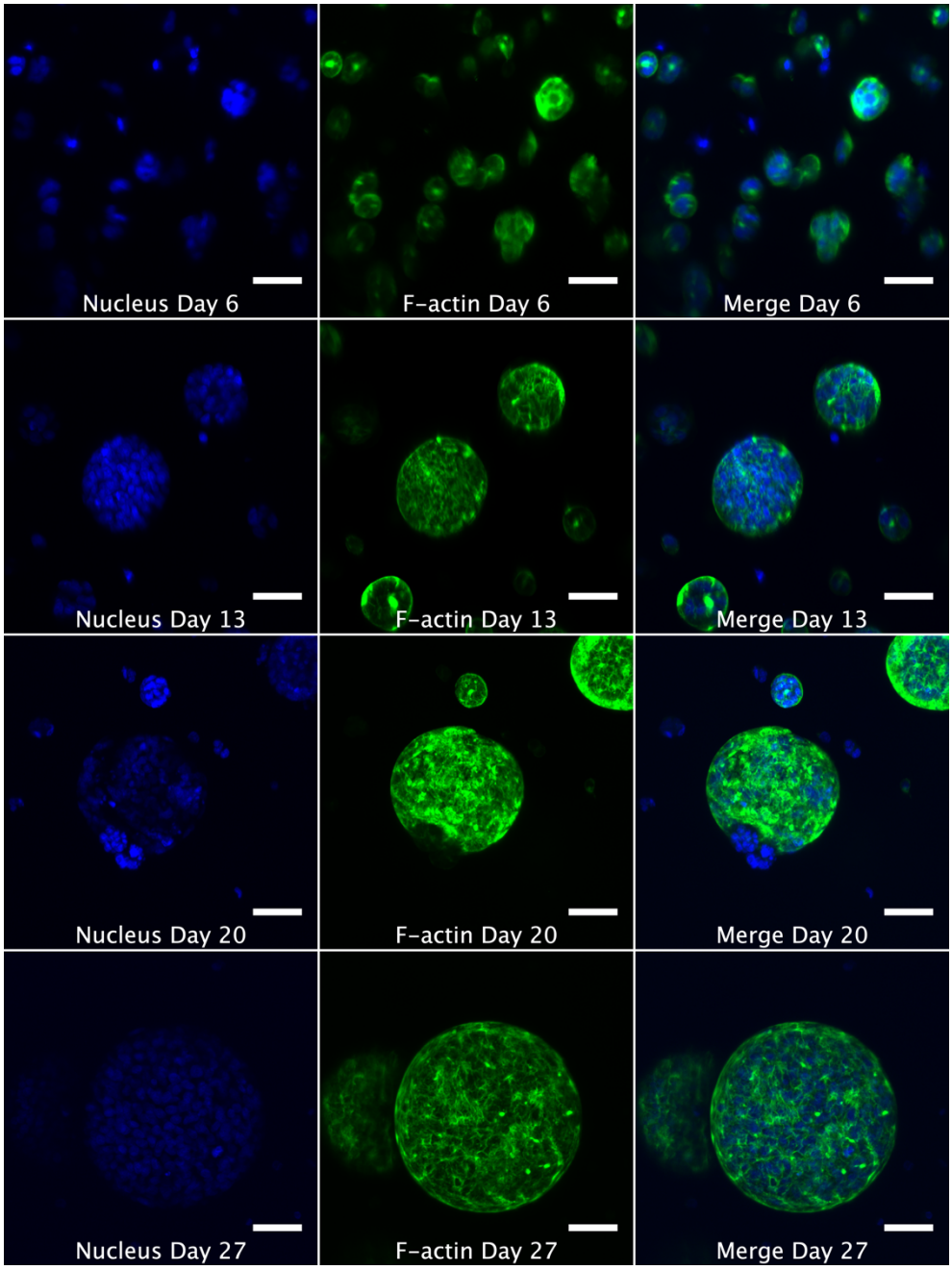

Figure S4: Images obtained by confocal microscopy representing growth of hepatic HepG2 spheroids over 6, 13, 20 and 27 days. Scalebars: 50 µm

Appendix B

Paper II

Characterization of thin gelatin hydrogel membranes with balloon properties for dynamic tissue engineering

M. L. Jepsen, L. H. Nielsen, A. Boisen, K. Almdal, and M. Dufva

Published in Biopolymers, vol. 100, no. 1, p. e23241, 2019

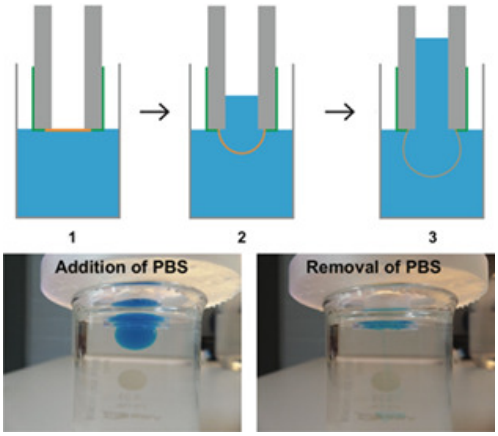

Received: 16 July 2018 | Revised: 12 October 2018 | Accepted: 2 November 2018

DOI: 10.1002/bip.23241

WILEY Biopolymers

ORIGINAL ARTICLE

Characterization of thin gelatin hydrogel membranes with balloon properties for dynamic tissue engineering

Morten Leth Jepsen | Line Hagner Nielsen | Anja Boisen | Kristoffer Almdal | Martin Dufva

Department of Micro- and Nanotechnology, The Danish National Research Foundation and Villum Foundation's Center for Intelligent Drug Delivery and Sensing Using Microcontainers and Nanomechanics (IDUN), Technical University of Denmark, Kongens Lyngby, Denmark

Correspondence
Martin Dufva, Department of Micro- and Nanotechnology, The Danish National Research Foundation and Villum Foundation's Center for Intelligent Drug Delivery and Sensing Using Microcontainers and Nanomechanics (IDUN), Technical University of Denmark, Ørsteds Plads 345C, 2800 Kongens Lyngby, Denmark.
Email: martin.dufva@nanotech.dtu.dk

Funding information
Danish National Research Foundation, Grant/Award Number: DNRF122; Danish Council for Independent Research Sciences, Technology and Production, Grant/Award Number: DFF 4004-00120B; Villum Foundation, Grant/Award Number: 9301

Abstract

Cell or tissue stretching and strain are present in any in vivo environment, but is difficult to reproduce in vitro. Here, we describe a simple method for casting a thin (about 500 μm) and soft (about 0.3 kPa) hydrogel of gelatin and a method for characterizing the mechanical properties of the hydrogel simply by changing pressure with a water column. The gelatin is crosslinked with mTransglutaminase and the area of the resulting hydrogel can be increased up 13-fold by increasing the radial water pressure. This is far beyond physiological stretches observed in vivo. Actuating the hydrogel with a radial force achieves both information about stiffness, stretchability, and contractability, which are relevant properties for tissue engineering purposes. Cells could be stretched and contracted using the gelatin membrane. Gelatin is a commonly used polymer for hydrogels in tissue engineering, and the discovered reversible stretching is particularly interesting for organ modeling applications.

KEYWORDS

biomimetics, gelatin, hydrogels, rheology

1 | INTRODUCTION

Hydrogels are polymeric solids swelled in substantial amounts of water, either of synthetic or natural origin.[1] Hydrogels can be crosslinked in numerous ways, including enzymatic protein crosslinking,[2] ionic gelation,[3] self-assembly,[4] and chemical crosslinking.[5]

In this work, we have utilized an enzymatically crosslinked gelatin hydrogel. Gelatin is derived from collagen, which is a major component of various connective tissues. Gelatin is denatured collagen fragments with a broad molecular weight distribution.[6] Gelatin will structurally transit from a helix structure to a coil at a temperature around 36°C, thereby phase transition from solid to liquid will occur.[6,7] Cell cultures are normally grown at 37°C, and therefore the gelatin needs to be crosslink to be utilized as a hydrogel in a cell culture. The coil formations can be crosslinked by mTransglutaminase (mTG) resulting in a gelatin hydrogel that retain the coil structure of the gelatin at 37°C. mTG crosslinked gelatin hydrogels are less tightly packed than a hydrogel resulting from cooling of dissolved gelatin forming a helix structured hydrogel.[8] However, gelatin is just one out of many polymers which hydrogels can be made of. Depending on the type of polymer, the fabrication method, and the crosslinking method, hydrogels' physical and/or chemical properties can be tuned to suit various fields such as biomedicine, soft electronics, sensors, and actuators.[9–11]

Hydrogels have a potential use in the field of tissue engineering. Since the microenvironment of in vivo tissues is mechanically flexible, cells are exposed to mechanical forces of various durations, frequencies, and amplitudes.[12] This work mainly focuses on mechanical flexibility in terms of a stretchable and contractible matrix. We use the term "dynamic surface" for this phenomenon, which resemble hollow organs for example, the motions of alveoli in lungs. The mechanical properties of hydrogels are tunable for example, the Young's modulus (E) and can vary greatly. Hydrogels have been reported from very soft with E = 1.5 kPa[13] to very stiff with E > 600 kPa.[14] By tuning the stiffness of hydrogel it is possible to tune them for the specific tissue of interest.

Previous publications have presented various approaches to achieve hydrogels with 2-dimensional (2D) dynamic surface behaviors. One approach is to expose cells to equibiaxial stretch by functionalizing hydrogels on top of a stretchable material such as polydimethylsiloxane (PDMS)[15] or stretching coated parafilm or PDMS.[16–19] However, permeable hydrogels supported by neither synthetic materials nor impermeable materials have closer resemblance with connective tissue more. Unsupported dynamic cell-laden hydrogels have been achieved by adding cells in a collagen hydrogel into a 3-dimensional (3D) printed mesh of a stretchable poly(ethylene glycol)-alginate-nanoclay hydrogel.[20] Other approaches include integration of magnets that could be used for stretching the hydrogel[21,22] or by seeding cells on top of a hydrogel for uniaxial stretch by moving the ends of the hydrogel apart.[23] However, all these approaches solely achieve a 2D stretch whereas we aim for achieving a 3D expandable hydrogel balloon.

Mechanical characterization of hydrogels is not straight forward due to their low Young's modulus making them difficult to clamp and most mechanical characterization equipment is optimized for measurements in the range of MPa and GPa[24]. Furthermore, hydrogels in the swollen state have rubbery mechanical behavior, and the Young's modulus of hydrogels is dependent on the degree of swelling.[25,26] Thus, hydrogels should be fully immersed (completely covered by a relevant medium) during characterization. Characterizations performed in air rather than liquid typically reduces the swelling due to evaporation. One approach to ensure the conditions of the hydrogel is by letting it swell before measuring, [27]but it can dry during measurements for example, in a rheometer.

One method of mechanical characterization methods preformed with immersed and fully swelled hydrogels is indentation, where a probe is pressed into and retracted from the material.[24] However, using indentation does not give information about stretchability nor contractability of the hydrogel. A method of stretching fully immersed hydrogels using a stainless steel ball has previously been published.[26] By measuring the central displacement caused by the stainless steel ball to the hydrogel membrane Young's modulus could be determined. However, by this approach, the force is centered to the middle of a hydrogel. Here, we present a method of stretching gelatin hydrogels fully submerged where the pressure comes from a liquid rather than a solid object causing a close to spherical inflation of the hydrogel. The stiffness, stretch, contraction, and durability were characterized. Furthermore, an epithelial and an endothelial cell line was stretched using the presented method.

2 | MATERIALS AND METHODS

2.1 | 3D printing of gelatin hydrogel membrane holder

3D designs were drawn using Fusion 360 (version 1.28.2, Autodesk, San Rafael, California) and print files were exported as STL format and processed in PreForm (version 2.12.0, Formlabs, Somerville, Massachusetts). The 3D printed holder was designed with a small ring at the opening tube for the membrane to attach when casted (Supporting Information Figures S1 and S2). All prints was done using a a Formlabs Form 2 3D printer (Formlabs).

Prints for demonstration of the stretch principle were printed in Clear resin (Clear V2 FLGPCL02, Formlabs) with a layer thickness of 0.1 mm followed by cleaning in isopropanol 2 times for 10 minutes and ultraviolet (UV) crosslinked for 60 minutes at room temperature. Prints for cell cultures were printed in Dental SG resin (Dental SG DGOR01, Formlabs) with a layer thickness of 0.05 mm, and were subsequently cleaned as described above. Support structures were cutoff, and the structures were UV crosslinked for 60 minutes at 60°C and autoclaved at 121°C.

2.2 | Casting of expandable hydrogel membrane

For casting expandable hydrogel membranes, 3D prints with a 10 mm diameter opening were dipped in a solution, if not stated otherwise, consisting of mTG (5 U/ml; Ajinomoto Activa T1, Hamburg, Germany) and gelatin (5% [w/v]) (Fluka, 48 723) in phosphate buffered saline (PBS) (D8537, Sigma, St. Louis, Missouri) and incubated for 30 minutes for cell cultures, and 120 minutes for expansion experiments, both at 37°C (Supporting Information Figure S2). Incidentally, it has been shown that gelatin film display highest elongation when crosslinked at 35°C.[28] Stock solution of mTG was made by dissolving mTG in PBS in final concentration of 15 U/ml. Stock solution of gelatin was made by dissolving gelatin in PBS to a final concentration of 7.5% (w/v). For sterilisation purposes, chloroform was added to the gelatin solution with final concentration of 0.5% [v/v] of the stock solution. Whereas mTG was sterile filtered using a 0.45 μm filter prior to use. The solutions were subsequently mixed in ratios giving 5% gelatin (w/v) and mTG 5 mTG U/ml in final concentrations. The procedure was the same for 2.5% (w/v) and 7.5% (w/v) gelatin membrane, but with either a 3.75% (w/v) or 11.25% (w/v) stock solution of gelatin, respectively.

For calculation of the membrane thickness, 4-membrane samples were weighed and found to be 45.18 ± 3.32 mg (n = 4, mean ± SD). The thickness was calculated from the weight, the radius of the gel (5 mm), and specific gravity of 5% gelatin (1.012)[29]:

$$h = \frac{V}{\pi r^2} \quad (1)$$

where, h is the thickness, V is the volume, and r is the radius.

2.3 | Rheological measurements

Measurements were performed using a Discovery Hybrid Rheometer 2 (TA instruments, New Castle, Delaware) with a 40 mm parallel plate and a steel Peltier plate. A mixture of gelatin/mTG (500 μl) was added to the Peltier plate set at 37°C. When the parallel plate was at the geometry gap of 250 μm, mineral oil (M5310, Sigma) was added around the plate to avoid evaporation. For investigation of gelation time, a strain of 1.5% was used with a frequency of 5 Hz. For measurements of oscillation frequency dependence, a logarithmic sweep was done with a strain of 1.5% with frequencies increasing from 0.02 to 15.92 Hz. For measurements of strain breaking point, a logarithmic sweep was performed with a frequency of 5 Hz while increasing the strain from 0.1% to 3000%.

Shear modulus was calculated by:

$$G^2 = G'^2 + G''^2 \quad (2)$$

where, G is the shear modulus, G' is the storage modulus, and G'' is the loss modulus. Since G'' is close to 0 $G \approx G' \approx 360$ Pa. A Poisson's ratio of 0.5 was assumed, as the hydrogel is regarded as an incompressible material. Therefore, the Young's modulus is calculated by:

$$E = 2G(1+\mu) \quad (3)$$

where, E is Young's modulus, G is the shear modulus, and μ is Passion's ratio giving a Young's modulus of ~1080 Pa.

2.4 | Stretch of fully immersed hydrogels

The hydrogel membranes were placed in a beaker of PBS in a 37°C heating oven and more PBS (colored with food dye) was added in steps of 200 µl. Pictures were taken using a Samsung WB32F compact camera. The pictures were subsequently fitted to a circle using a Plugin for Fiji[30] (Contact_Angle.jar, version December 7, 2006, Marco Brugnara) from which the radius and length of the base of the circle segment was obtained and normalized to a ruler in the beaker (Supporting Information Figure S5).

From this, the chord length, a, of a circular segment and radius, R, of the circle were obtained. From this the central angle, θ, was calculated by[31]:

$$\theta = 2\sin^{-1}\left(\frac{a}{2R}\right) \quad (4)$$

From which the arc length, s, could be calculated by[31]:

$$s = R\theta \quad (5)$$

However, when the circle segment of interest is the majority of the circle the arc length was calculated by:

$$s = 2\pi R - R\theta \quad (6)$$

The Equations (5) and (6) gives the arc length of the small circle segment, which is the stretched length (s). The stretch ratio (A) is defined as the ratio of s to the original diameter of the gel:

$$A = \frac{s}{\text{Original diameter}} \quad (7)$$

The stretch ratio and the force acting, calculated from the centimeter of water of the water column, on the membrane were fitted into the following equation for equibiaxial stretching[32]:

$$f = \mu_r\left[A^{\alpha_r - 1} - A^{-(1+2\alpha_r)}\right] \quad (8)$$

Where f is the force per unit undeformed area, A is the stretch ratio, and μ_r and α_r are constants. The fitting was done in RStudio (Version 1.0.136, RStudio, Inc., Boston, Massachusetts) using a nonlinear least squares fit.

From the fitted μ_r and α_r, the shear modulus was calculated by[32]:

$$G = \frac{\mu_r \alpha_r}{2} \quad (9)$$

where, G is the shear modulus. G was inserted in Equation (3) to obtain the Young's modulus.

The surface area of the spherical cap, was calculated by[33]:

$$S_{\text{cap}} = 2\pi RH \quad (10)$$

where, S_{cap} is the surface area, R is the radius, and H is the height of the circle segment, which is calculated by[33]:

$$H = R \pm \sqrt{R^2 - b^2} \quad (11)$$

where, H is the height of the circle segment, R is the radius of the circle, and b is the radius of the base of the circle segment. When the circle segment of interest was the majority of the circle, $\sqrt{R^2 - b^2}$ is added to R, when the circle segment is the minority $\sqrt{R^2 - b^2}$ is subtracted.

When having the surface area from Equation (10) was used to calculated the stretch area ratio with the following equation:

$$\text{Stretch area ratio} = \frac{S_{\text{cap}}}{\text{Original area}} \quad (12)$$

2.5 | Fatigue test and breaking strength of hydrogel membranes

Hydrogels prepared as described were tested for fatigue by adding 4 ml of PBS and removing and re-adding 1 ml of the solution 100 times. A picture was taken after every 10 pipetting steps.

The breaking strength was defined as the last point at which the membrane was intact and addition of 200 µl buffer more resulted in rupture of the membrane.

2.6 | Cell growth on stretchable hydrogel membranes

Caco-2 cells (ATCC HTB-37, LGC Standards GmbH, Wesel, Germany) p27-32 were grown in T-75 cell culture flaks (Starstedt, Nümbrecht, Germany) along with 13 ml of Dulbecco's Modified Eagle's medium (DMEM) – high glucose (Sigma-Aldrich Denmark A/S Broendby, Denmark) with heat inactivated fetal bovine serum (FBS; 20% [v/v]; Biowest SAS, Nuaillé, France), non-essential amino acids (1% [v/v]; Gibco, Fisher Scientific, Slangerup, Denmark), and penicillin–streptomycin (P/S; 100 U/ml penicillin and 100 µg/ml streptomycin; Sigma-Aldrich Denmark A/S Broendby, Denmark).

EA.hy926 cells (ATCC CRL-2922, LGC Standards GmbH, Wesel, Germany) p20-25 were grown in T-75 cell culture flaks (Starstedt, Nümbrecht, Germany) along with 13 ml of DMEM – high glucose (Sigma-Aldrich Denmark A/S Broendby) with heat inactivated FBS (20% [v/v]; Biowest SAS), and P/S (100 U/ml penicillin and 100 µg/ml streptomycin; Sigma-Aldrich Denmark A/S Broendby).

The cell culture medium was changed every other day and upon 80%-90% confluency, the cells were split. The cells were washed with PBS followed by incubation with trypsin-ethylenediaminetetraacetic acid (EDTA) solution (0.5 g/L porcine trypsin and 0.2 g/L EDTA-4Na) (Sigma-Aldrich Denmark A/S Broendby). Once the cells were detached, trypsin-EDTA were inhibited by addition of cell culture medium, and a sample was taken for counting the cells (counted with NucleoCounter NC-200). The rest of the suspension was collected and spun for 5 minutes (800 rpm), followed by washing the cells in PBS and spun again for 5 minutes (800 rpm). The cells were seeded (50 000 cells in 500 µl) on top of a casted stretchable hydrogel

membranes with 1 ml cell medium below. The cells were allowed to adhere to the membrane overnight at 37°C and 5% CO_2 before stretching by removal of basolateral medium.

2.7 | Microscopy on stretch hydrogels

Microscopy images were captured using a Zeiss Axio Observer Z1 inverted microscope (Carl Zeiss MicroImaging GmbH, 37 081 Gottingen, Germany), using an EC Plan-Neofluar 5×/0.16 Ph1 M27 or a LD Plan-Neofluar 40×/0.6 Korr M27 objective (Carl Zeiss MicroImaging GmbH). Initially 1000 µl medium was below the hydrogel membrane. For stretching and contraction 600 µl was removed and re-added.

2.8 | Scanning electron microscopy on dried stretch hydrogel membranes

Gelatin membranes in a 3D printed holder (Supporting Information Figure S1b) were inflated by air and dried for 66 hours before being mounted for scanning electron microscopy micrographs (SEM). The samples were scanned using a Hitachi TM3030 tabletop microscope (Hitachi High-Technologies Europe GmbH, Krefeld, Germany) in low vacuum mode at 15 kV operating voltage.

2.9 | Statistics

The data are presented as number of repetitions (n), mean ± SD. Calculations were done using RStudio (Version 1.0.136, RStudio, Inc.) and Microsoft Excel (Version 15.41, Microsoft Office, Seattle, Washington).

3 | RESULTS AND DISCUSSION

3.1 | Fully immersed Young's modulus characterization of the gelatin hydrogel membrane

The presented method allows for characterization of a stretched hydrogels while being fully immersed in a relevant medium, which to the authors' knowledge has not been previously presented. In the presented setup a thin gelatin membrane was casted in a 3D printed holder (Supporting Information Figure S1 and S2). The gelatin membrane attaches to the 3D printed holder during the casting and crosslinking reaction. Initial test showed that the gelatin membrane was firmly attached to the edges and did not easily detach when exposed to water pressure. In fact, overpressure resulted in rupture of the gelatin membrane with the remaining gelatin parts sticking to the rim of the 3D printed holder. We conclude that the gelatin membrane forms a very robust bond with the 3D printed holder.

The thin gelatin membrane was inflated as a balloon by increasing the pressure on it with a water column (Figure 1A). The hydrogel membrane could be stretched as a water column above the membrane exposed it to an increased pressure (Figure 1A). As the pressure increased an approximately spheroidal shaped inflated membrane was created which could be fitted as a circle (Supporting Information Figure S5). From this, the stretch of the membrane was determined as a stretch ratio from Equation (7), as described in Materials and Methods. Data points were plotted as pressure versus stretch ratio (Figure 1B). We fit both our small and large deformation data with Equation (8)[32] describing inflation in terms of stretch as a result of increased pressure on a circular balloon-like membranes into a spheroidal shape. For this the hydrogels are assumed as isotropic elastic solids, hence their strain only depends on stretch on the principal axis (X, Y, and Z) relative to the "ground state". We use the term elasticity as a description of the ability of a material to return to its original shape after deformation, which in principle can be of any magnitude.

Equation (8) is derived[32] assuming an incompressible material, thus, taking the thinning of the film at large deformation into account. From this fit the shear modulus can be extracted from Equation (9). The result of fitting is in principle the shear modulus, G, which is valid at all deformations. We have chosen to convert our numbers into Young's moduli to facilitate comparison with literature data although from the point of view of our measurements this conversion is not needed since we exclusively deal with shear moduli. The Young's modulus was calculated by inserting the obtained shear modulus in Equation (3), thereby characterizing the stiffness of a hydrogel while it was fully immersed.

When stretching a 5% gelatin hydrogel crosslinked for 2 hours with mTG, there was a lag phase at low pressure (<150 Pa) where the membrane was stretched only slightly. Above about 200 Pa, the pressure affected the stretching in linear fashion (Figure 2A). This inflation profile resembles inflation of a balloon where the polymer at a certain pressure allows inflation and further stretch requiring a smaller increase in pressure relative to the proportionally larger pressure increase required during the initial stetching phase.

A 5% gel could be stretched up to 4-fold in the length direction (increase of the perimeter of the gel). Eventually, the membrane would burst and the breaking strength was calculated to be 0.49 ± 0.09 kPa (n = 9, mean ± SD). A 7.5% gelatin hydrogel could be stretched but did not break even when filling up the test setup completely with water, hence the breaking strength is >0.89 kPa. (Figure 2A). A 2.5% membrane could be extended but no measurements were possible as no water column was formed due to the softness of this membrane (Supporting Information Figure S3f). Instead, the gel expanded until it bursted.

The Young's modulus for 5% gelatin hydrogel membranes was 0.35 ± 0.08 kPa (n = 9, mean ± SD), calculated as described above, whereas for 7.5% membranes, the Young's modulus was 0.75 ± 0.31 kPa (n = 5, mean ± SD; Figure 2B). A storage modulus of ~0.26 kPa, corresponding to a Young's modulus of ~0.78 kPa, was measured for the 5% gelatin hydrogel in a Discovery Hybrid Rheometer 2 (measured 2 hours after it had been crosslinked at 37°C inside the rheometer; Supporting Information Figure S6a). However, after about 8 hours the storage modulus settled on ~0.36 kPa (Supporting Information Figure S6a) corresponding to a Young's modulus of ~1.08 kPa. In summary, the stretch measurement gave a Young's modulus of 0.35 kPa, whereas measurements with a rheometer gave a higher Young's modulus of 0.78 kPa.

Previously, measurements of samples of 5% gelatin and comparable amounts of mTG as used here, have shown Young's modulus in the range of ~6 kPa measured on a Solid Analyzer at 37°C without having the sample immersed.[34] Others have shown Young's modulus

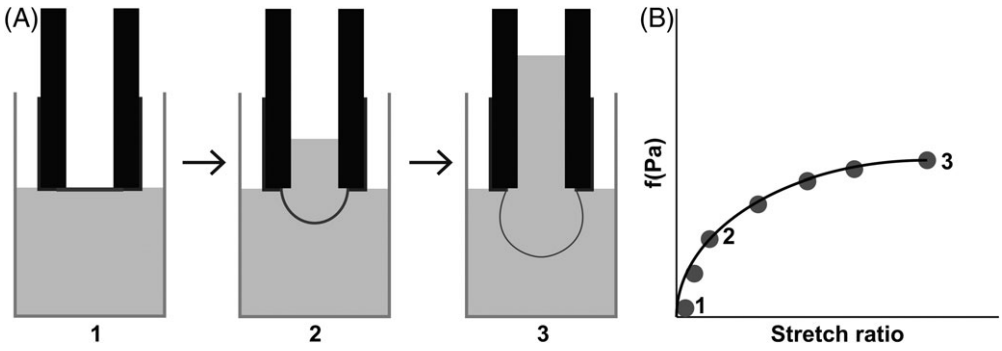

FIGURE 1 Schematic of the experimental setup. A, Gelatin hydrogel membrane (gray) in a 3D printed holder (black) was inflated as the pressure increases from a watercolumn (light gray). B, Corresponding plot of pressure vs stretch ratio. By fitting the data to Equation (8) the Young's modulus can be extracted

of 12.4 kPa of 5% gelatin hydrogels where the measurements were performed at room temperature.[35] The lower modulus measured in the stretch setup (Figure 2) compared to the rheometer and Solid Analyzer is believed to be caused by swelling of hydrogels in the immersed state.

Stretching by pressure from a liquid or a gas rather than a stainless-steel ball allows for functionalization of the hydrogel surface without disturbing the functionalization when inflating and/or stretching the surface. The inflation of the hydrogels in the presented setup does not result in a perfect sphere due to attachment at the rim. This causes inhomogeneous deformation with equibiaxial stretching at the pole and planar elongation at the rim.[36] The characteristics of the inflation resemble the inflation of a balloon, where in the presented setup the lumen of the hydrogel balloon acts as a dynamic surface.

3.2 | Characteristics of the gelatin hydrogel membrane

The hydrogel membrane was measured to be 0.58 ± 0.04 mm (n = 4 mean ± SD) thick (Figure 3A). The thickness of the presented hydrogel membrane is comparable to the previously published stretchable hydrogels which range from 0.13 mm[22] to 3 mm.[37] The hydrogel could be reversibly expanded and contracted (Figure 3B) which is important if for example, the lung is to be modelled. The gel typically was destroyed during handling where a pipette easily ruptures it. Stretch ratios of above 20 times have been published[37] for 1-dimensional (1D) stretches. By contrast, we observed stretch ratio of about 4 for a 5%, however, the area was stretchable up to 13-folds (Supporting Information Figure S6b). It is however unclear if 2D stretching compares to 3D stretching. A 2 to 4-fold stretching in the length scale and 13-fold stretching in the area is more than sufficient for modulating tissues (see below). Furthermore, the stretching was shown to be reversible with gelatin membranes being able to be stretched and contracted at least 100 times. These tests were done by pipetting water up and down forcing the gelatin membrane to oscillate between 2.8 and 3.2 stretch ratio (data not shown).

It was found that the hydrogel was inflatable when adding PBS (Figure 3B) and 70% (v/v) ethanol (Figure 3C), and when applying an air pressure (Figure 3C) indicating that the composition of the medium is not important for the expansion. Expansion of air as well as other liquids is essential for modelling various tissues like joints, skin, lungs, heart, intestine, and so forth.

Food dye could diffuse through the hydrogel gel over time. After 16 hours, the dye has diffused completely into the receiving volume of the beaker. Interestingly, after an overnight incubation, the water column of the buffer solution decreased to a level where the membrane was only slightly inflated (Figure 3D). This indicates that water has diffused through the gel into the receiving beaker. It is likely that this is due to the higher water pressure on the upper side of the gel due to the applied water column.

Other shapes and sizes of the gelatin hydrogel membranes were also feasible for example, a larger membrane with a diameter of 18 mm and a 16 × 16 mm square could easily be formed (Supporting Information Figure S3). Moreover, the membrane inflated with air

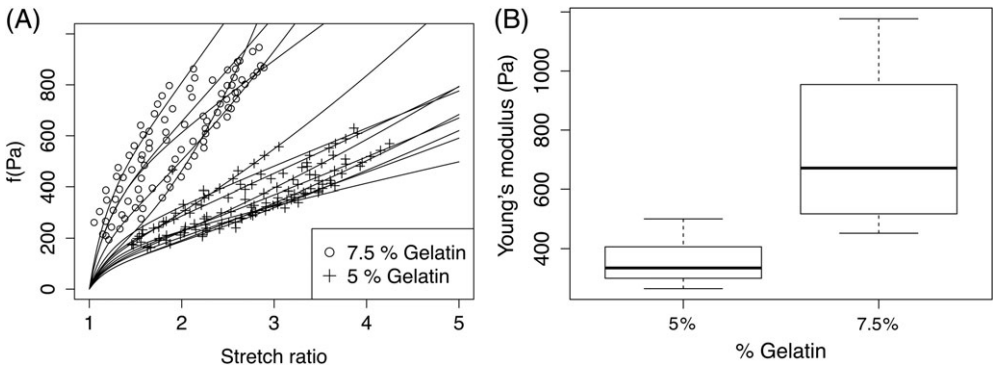

FIGURE 2 Immersed stretch of gelatin hydrogel membrane. A, Pressure as a function of stretch ratio for experiments with individual fits to Equation (8). B, The corresponding Young's modulus extracted from the immersed stretch experiments

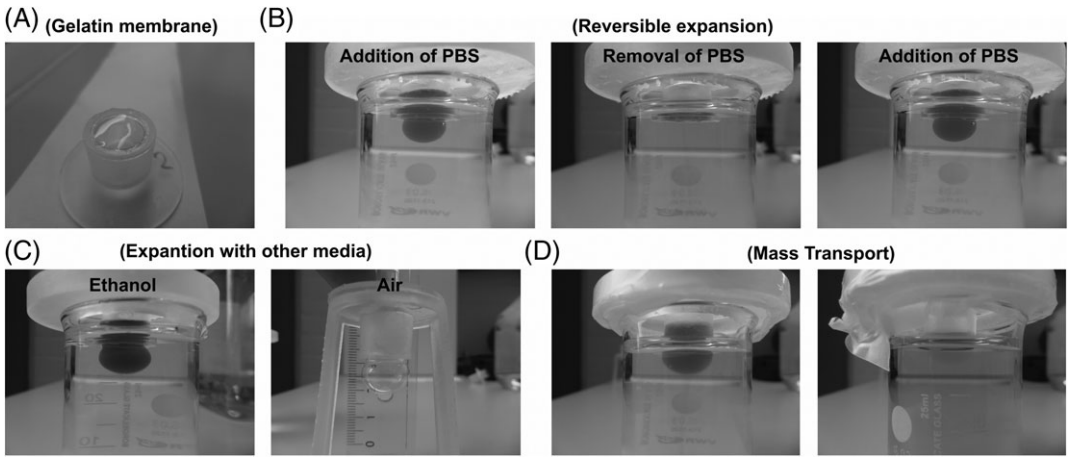

FIGURE 3 Characteristics of the stretchable gelatin hydrogel. A, Gelatin hydrogel membrane. B, Reversible expansion by addition and removal of 1 ml phosphate buffered saline (PBS) on top of the gelatin membrane in a beaker with PBS. C, Gelatin hydrogel membrane expanded with 1 ml 70% ethanol on top in a beaker with 70% ethanol and membrane expanded by addition of air pressure from a syringe. D, Difussion of blue food dye from 1 ml PBS food dye mixture thourgh the gelatin hydrogel into a beaker with PBS after 30 minutes and after 16 hours

could be dried in its inflated shape (Supporting Information Figure S4a-c), and once dried, SEM revealed a smooth surface of the gelatin hydrogel membrane (Supporting Information Figure S4d,e).

Prior published stretchable hydrogels rely on complicated casting procedures such as purification of proteins,[27,38] 3D printing,[20] integration of magnets,[21,22] nanopatterned hydrogels,[23] nanocomposition of clay nanosheets,[13,14] or a mixture of natural and synthetic polymers.[37] Whereas, the presented method only requires mixing gelatin and mTG. This reduces time and cost and diminishes the technical difficulties in when casting stretchable hydrogel. Furthermore, mTG is non-toxic, biocompatible, and is the most studied enzyme in protein-based crosslinked hydrogels in tissue engineering.[35] The mechanical behavior of gelatin crosslinking with mTG is dependent on the temperature at which the crosslinking is performed.

3.3 | Stretch of cell culture on a gelatin hydrogel membrane

The gelatin membranes was subsequently used to study stretching of non-confluent cell layers. Non-confluent cell layer was used to easily see if cells where stretched and move relative to each other. Caco-2 (an epithelial colorectal adenocarcinoma cell line), a cell line commonly used for intestine modelling,[39] cells were seeded on the membranes in a 3D printed holder placed in a well plate (Supporting Information Figure S2). Once the Caco-2 cells had attached to the membrane, they were stretched by changing the water pressure on the outside of the 3D printed membrane holder (Figure 4A). In the initial state, the cell islands were close to each other (Figure 4B), and by removal of medium from the basolateral side on the 3D printed holder, the cell islands were stretched apart (Figure 4C). The cell islands got closer together again by re-addition of the basolateral medium as the membrane re-contracted (Figure 4D). Observing cell islands being stretched apart would not be possible when stretching a hydrogel in a rheometer with a microscope extension, since the cells are on top of the hydrogel and the rheometer pushes a cylinder onto the sample.

The CRL-2922 human umbilical vein endothelial cell line was used to show morphological changes to cells when exposed to stretching of the gelatin membrane. CRL-2922 cells were allowed to attach to the gelatin membrane and the cells display typical endothelial cell morphology (Figure 4E) before stretching. Stretching the gelatin membrane resulted in stretching of the adhered endothelial cells (Figure 4F). This resulted in cells that got further elongated (one example is indicated by the black circle) or had one end detached from the surface (white circle). Cells that did not adhere well to the gelatin from start did not show stretching. CRL-2922 cells that kept adhering to the gelatin membrane could be re-contracted when contracting the gelatin membrane (Figure 4G, black marked cell). Also, cells that got partly released (white circle) showed contraction when the gelatin membrane was contracted. Hence, the gelatin membrane can be utilized to investigate individual cell reactions to stretching.

The mechanically stimulated deformation of the membrane is reversible; thus the membrane setup is suitable for mimicry of dynamic physiological movements. Moreover, the membrane mimics the extracellular matrix, since gelatin resembles collagen and connective tissue found in the body.[11,40] In addition, epithelial bending is essential for lumen morphogenesis,[41] hence the presented method could be applicable for tissue engineering of hollow organs. One lumen morphogenic pathway is apical constriction by which the epithelial cells undergo apical shrinkage while keeping their volume constant. The apical constriction must be followed by an increase of the height of the cells and/or basal expansion.[41,42] By stretching the cells on the presented gelatin hydrogel, it would be possible to cause both apical constriction and basal expansion. One such organ is the lung where it has been shown that apical constriction initiate new branching of lung tissue in chicken embryos.[43] The lung tissue is exposed to cyclic stretch and contraction with a rate of ~12 cycles/min in humans, as a result of breathing.[44] For rat lungs, a 40% increase in the surface area of the alveolar epithelial basement membrane was found at 100% total lung capacity.[45] The presented gelatin hydrogel is suitable as an alveolar epithelial basement membrane substrate, since it can easily be stretched 40% (Figure 2A)

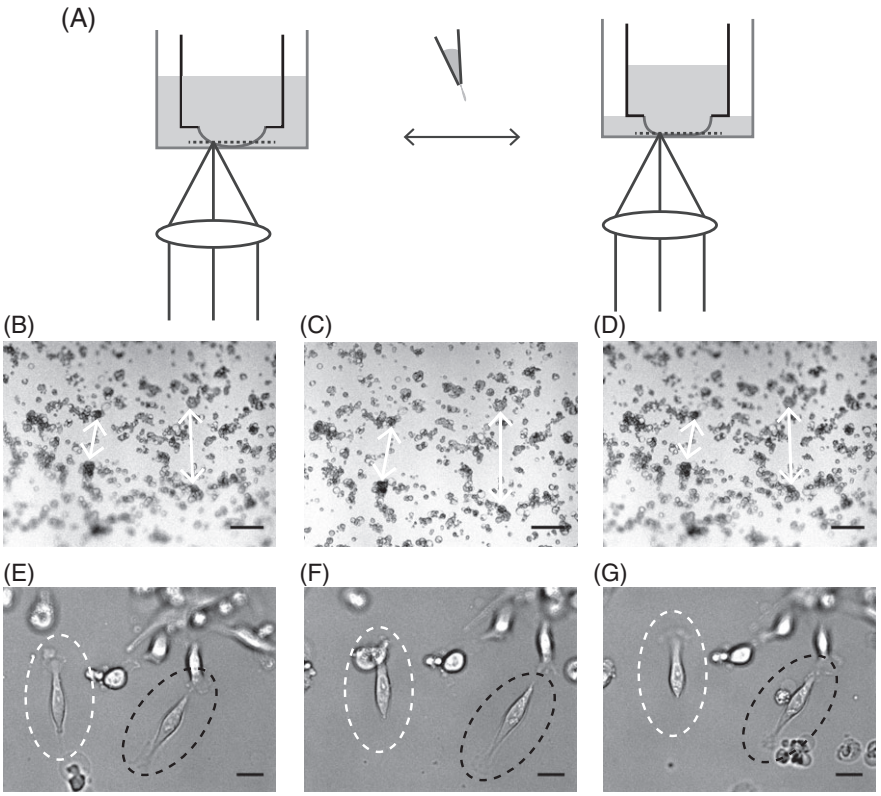

FIGURE 4 Streching of Caco-2 and CRL-2922 on gelatin hydrogel membrane. A, By removing medium from the outside of the inset with the membrane the membrane is stretch and by re-adding medium the membrane recontracts. B, Caco-2 cells on gelatin hydrogel membrane after 1 day incubation. Scale bar: 200 μm. C, Caco-2 cells on gelatin hydrogel membrane stretched by removing 600 μl medium basolaterally. Scale bar: 200 μm. D, Caco-2 cells on gelatin hydrogel membrane re-contracted by addition of 600 μl medium basolaterally. Scale bar: 200 μm. E, CRL-2922 cells on gelatin hydrogel membrane after 1 day incubation. Scale bar: 20 μm. F, CRL-2922 cells on gelatin hydrogel membrane stretched by removing 600 μl medium basolaterally. Scale bar: 20 μm. G, CRL-2922 cells on gelatin hydrogel membrane re-contracted by addition of 600 μl medium basolaterally. Scale bar: 20 μm

and subsequently contracted with cells attached (Figure 4D). However, the increase of 40% surface area was achieved by increasing the pressure transpulmonary pressure from 2 cmH_2O (~0.2 kPa) to 25 cmH_2O (~2.5 kPa),[45] comparing this to the pressure required to stretch the gelatin hydrogel (Figure 2A) the gelatin hydrogel is much softer. On the other hand, the alveolar epithelial basement membrane is supported by a layer of epithelial cells, endothelial cells, and elastic fibers making the alveoli strong.[46,47] Therefore, the in vivo tissue has more support than then presented gelatin hydrogel. The gelatin hydrogel can be tuned in strength by increasing the percentage of gelatin as was shown with 7.5% gelatin (Figure 2). Normally, a barrier consists of a confluent cell layer. However, in the current setup it was not possible to change medium without disturbing the cells or rupturing the membrane. Thus, it is not possible to grow the cells for longer periods. Future studies will involve medium changes using pumps that gently can control expansion and contraction during medium changes to minimize stretching cell layer more than what is physiologically relevant.

4 | CONCLUSION

We present a method of measuring Young's modulus on soft hydrogels fully immersed in buffer only by changing the pressure of a water column on top of the hydrogel. The Young's modulus measurements from the presented method were lower than that of benchmark techniques most likely caused by the hydrogel being fully immersed during measurements. We present a soft gelatin hydrogel with a Young's modulus around 0.35 kPa. The gelatin hydrogel composed of a natural polymer that is biocompatible and an extracellular matrix was utilized as a matrix for cells and stretching and contraction of the cells were done. The surface area of the gelatin hydrogel can be stretched by a factor of 13, which is beyond what is physiologically relevant. Moreover, the surface of the gelatin hydrogel can be functionalized with mammalian cell line cells for tissue engineering purposes.

ACKNOWLEDGMENTS

The authors would like to acknowledge the Danish National Research Foundation (DNRF122) and Villum Foundation (Grant No. 9301) for Intelligent Drug Delivery and Sensing Using Microcontainers and Nanomechanics (IDUN). Line Hagner Nielsen would like to acknowledge Danish Council for Independent Research Sciences, Technology and Production (FTP), Project DFF 4004-00120B for financial support.

MLJ contributed with design of and execution of experiment and analysis of data and writing of manuscript. LHN, AB, KA, and MD contributed with design of experiments and writing the manuscript.

ORCID

Morten Leth Jepsen https://orcid.org/0000-0001-9023-8706
Line Hagner Nielsen https://orcid.org/0000-0002-3789-4816
Anja Boisen https://orcid.org/0000-0002-9918-6567
Kristoffer Almdal https://orcid.org/0000-0002-5490-9303
Martin Dufva https://orcid.org/0000-0001-5449-0189

REFERENCES

[1] K. Almdal, J. Dyre, S. Hvidt, O. Kramer, *Polym. Gels Networks* **1993**, *1*, 5.
[2] T. Heck, G. Faccio, M. Richter, L. Thöny-Meyer, *Appl. Microbiol. Biotechnol.* **2013**, *97*, 461.
[3] W. R. Gombotz, S. Wee, *Adv. Drug Deliv. Rev.* **1998**, *31*, 267.
[4] L. E. R. O'Leary, J. A. Fallas, E. L. Bakota, M. K. Kang, J. D. Hartgerink, *Nat. Chem.* **2011**, *3*, 821.
[5] W. E. Hennink, C. F. van Nostrum, *Adv. Drug Deliv. Rev.* **2012**, *54*, 13.
[6] M. Djabourov, J. Leblond, P. Papon, *J. Phys.* **1988**, *49*, 319.
[7] H. Boedtker, P. Doty, *J. Phys. Chem.* **1954**, *58*, 968.
[8] J. S. Suwandi, R. E. M. Toes, T. Nikolic, B. O. Roep, *Clin. Exp. Rheumatol.* **2015**, *33*, 97.
[9] Y. S. Zhang, A. Khademhosseini, *Science* **2017**, *356*, eaaf3627.
[10] S. Lin, H. Yuk, T. Zhang, G. A. Parada, H. Koo, C. Yu, X. Zhao, *Adv. Mater.* **2016**, *28*, 4497.
[11] I. El-Sherbiny, M. Yacoub, *Glob. Cardiol. Sci. Pract.* **2013**, *38*, 316.
[12] S. Ahadian, R. Civitarese, D. Bannerman, M. H. Mohammadi, R. Lu, E. Wang, L. Davenport-Huyer, B. Lai, B. Zhang, Y. Zhao, S. Mandla, A. Korolj, M. Radisic, *Adv. Healthcare Mater.* **2017**, *7*, 1700506.
[13] K. Haraguchi, T. Takehisa, *Adv. Mater.* **2002**, *14*, 1120.
[14] Y. Hu, Z. Du, X. Deng, T. Wang, Z. Yang, W. Zhou, C. Wang, *Macromolecules* **2016**, *49*, 5660.
[15] L. Casares, R. Vincent, D. Zalvidea, N. Campillo, D. Navajas, M. Arroyo, X. Trepat, *Nat. Mater.* **2015**, *14*, 343.
[16] D. Wang, Y. Xie, B. Yuan, J. Xu, P. Gong, X. Jiang, *Integr. Biol.* **2010**, *2*, 288.
[17] A. Livne, E. Bouchbinder, B. Geiger, *Nat. Commun.* **2014**, *5*, 3938.
[18] X. Shi, L. Li, S. Ostrovidov, Y. Shu, A. Khademhosseini, H. Wu, *ACS Appl. Mater. Interfaces* **2014**, *6*, 11915.
[19] C. P. Ursekar, S. K. Teo, H. Hirata, I. Harada, K. H. Chiam, Y. Sawada, *PLoS One* **2014**, *9*, e90665.
[20] S. Hong, D. Sycks, H. F. ai Chan, S. Lin, G. P. Lopez, F. Guilak, K. W. Leong, X. Zhao, *Adv. Mater.* **2015**, *27*, 4035.
[21] Y. Li, G. Huang, M. Li, L. Wang, E. L. Elson, T. Jian Lu, G. M. Genin, F. Xu, *Sci. Rep.* **2016**, *6*, 19550.
[22] Y. Li, G. Huang, B. Gao, M. Li, G. M. Genin, T. J. Lu, F. Xu, *NPG Asia Mater.* **2016**, *8*, e238.
[23] J. Deng, C. Zhao, J. P. Spatz, Q. Wei, *ACS Nano* **2017**, *11*, 8282.
[24] M. L. Oyen, *Int. Mater. Rev.* **2014**, *59*, 44.
[25] K. S. Anseth, C. N. Bowman, L. Brannon-Peppas, *Biomaterials* **1996**, *17*, 1647.
[26] M. Ahearne, Y. Yang, A. J. El Haj, K. Y. Then, K.-K. Liu, *J. R. Soc. Interface* **2005**, *2*, 455.
[27] N. Annabi, S. M. Mithieux, P. Zorlutuna, G. Camci-unal, A. S. Weiss, A. Khademhosseini, *Biomaterials* **2013**, *34*, 5496.
[28] F. Liu, H. Majeed, J. Antoniou, Y. Li, Y. Ma, W. Yokoyama, J. Ma, F. Zhong, *Food Hydrocoll.* **2016**, *58*, 20.
[29] J. J. Emery, W. D. L. Finn, K. W. Lee, Uniformity of saturated sand specimens. in *Evaluation of Relative Density and its Role in Geotechnical Projects Involving Cohesionless Soils*, American Society for Testing and Materials, Philadelphia, PA **1973**, p. 182.
[30] J. Schindelin, I. Arganda-Carreras, E. Frise, V. Kaynig, M. Longair, T. Pietzsch, S. Preibisch, C. Rueden, S. Saalfeld, B. Schmid, J. Y. Tinevez, D. J. White, V. Hartenstein, K. Eliceiri, P. Tomancak, A. Cardona, *Nat. Methods* **2012**, *9*, 676.
[31] E. W. Weisstein, "Circular Segment". From MathWorld--A Wolfram Web Resource, http://mathworld.wolfram.com/CircularSegment.html (accessed: July 2018).
[32] R. W. Ogden, *Proc. R. Soc. A Math. Phys. Eng. Sci.* **1972**, *326*, 565.
[33] E. W. Weisstein, "Spherical Cap." From MathWorld--A Wolfram Web Resource, http://mathworld.wolfram.com/SphericalCap.html (accessed: July 2018).
[34] C. R. Pimentel, S. K. Ko, C. Caviglia, A. Wolff, J. Emnéus, S. S. Keller, M. Dufva, *Acta Biomater.* **2017**, *65*, 174.
[35] G. Yang, Z. Xiao, X. Ren, H. Long, H. Qian, K. Ma, Y. Guo, *Peer J* **2016**, *4*, e2497.
[36] O. Hassager, S. B. Kristensen, J. R. Larsen, J. Neergaard, J. Nonnewton, *Fluid Mech.* **1999**, *88*, 185.
[37] J.-Y. Sun, X. Zhao, W. R. K. Illeperuma, O. Chaudhuri, K. H. Oh, D. J. Mooney, J. J. Vlassak, Z. Suo, *Nature* **2012**, *489*, 133.
[38] M. A. Gonzalez, J. R. Simon, A. Ghoorchian, Z. Scholl, S. Lin, M. Rubinstein, P. Marszalek, A. Chilkoti, G. P. López, X. Zhao, *Adv. Mater.* **2017**, *29*, 1.
[39] P. Artursson, K. Palm, K. Luthman, *Adv. Drug Deliv. Rev.* **2001**, *46*, 27.
[40] K. Y. Lee, D. J. Mooney, *Chem. Rev.* **2001**, *101*, 1869.
[41] A. Navis, C. M. Nelson, *Semin. Cell Dev. Biol.* **2016**, *55*, 139.
[42] E. J. Pearl, J. Li, J. B. A. Green, *Philos. Trans. R. Soc. B Biol. Sci.* **2017**, *372*, 20150526.
[43] H. Y. Kim, V. D. Varner, C. M. Nelson, *Development* **2013**, *140*, 3146.
[44] C. M. Waters, E. Roan, D. Navajas, *Compr. Physiol.* **2012**, *2*, 1.
[45] D. J. Tschumperlin, S. S. Margulies, J. Daniel, *J. Appl. Physiol.* **1999**, *86*, 2026.
[46] A. L. Kierszenbaum, L. L. Tres, Respiratory system. in *Histology and Cell Biology: An Introduction to Pathology*, Elsevier, Philadelphia, PA **2012**, p. 387.
[47] W. F. Boron, E. L. Boulpaep, *Medical Physiology*, Elsevier, Philadelphia, PA **2012**, p. 685.

SUPPORTING INFORMATION

Additional supporting information may be found online in the Supporting Information section at the end of the article.

How to cite this article: Jepsen ML, Nielsen LH, Boisen A, Almdal K, Dufva M. Characterization of thin gelatin hydrogel membranes with balloon properties for dynamic tissue engineering. *Biopolymers*. 2018;e23241. https://doi.org/10.1002/bip.23241

Figure S1

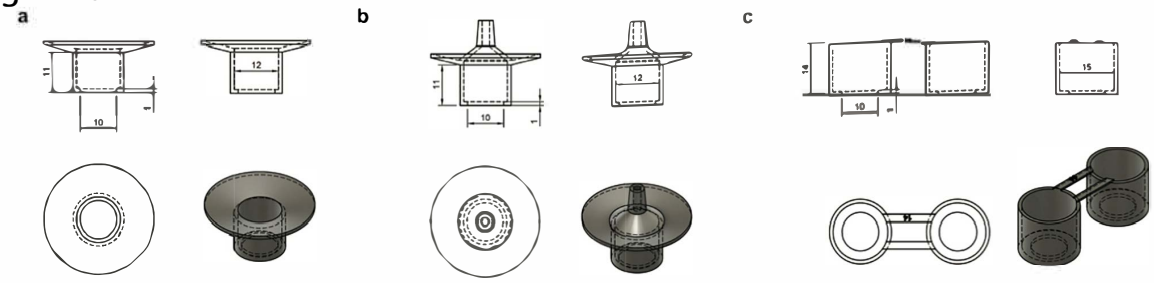

Figure S2

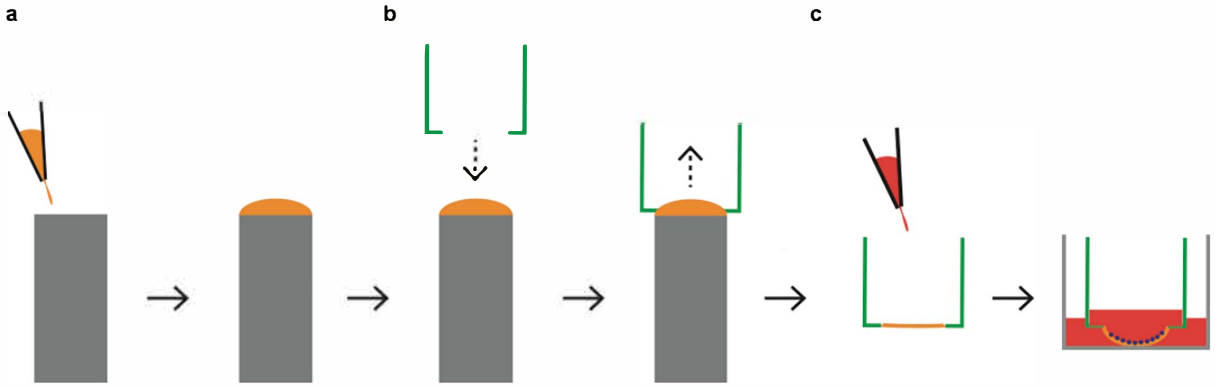

Figure S3

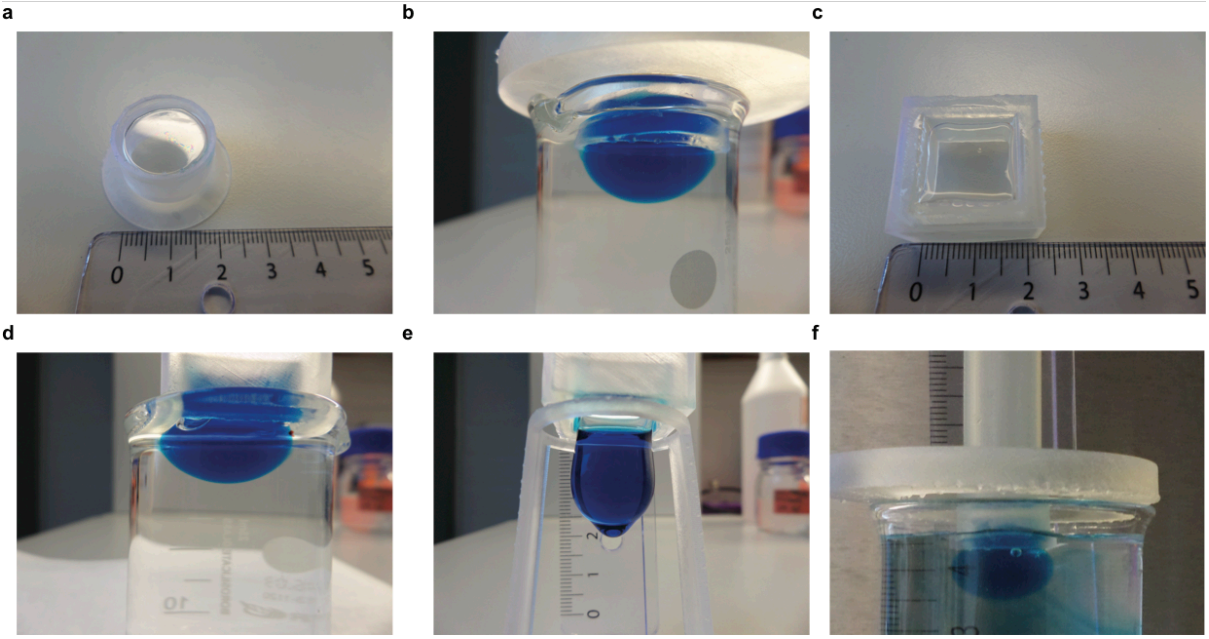

Figure S4

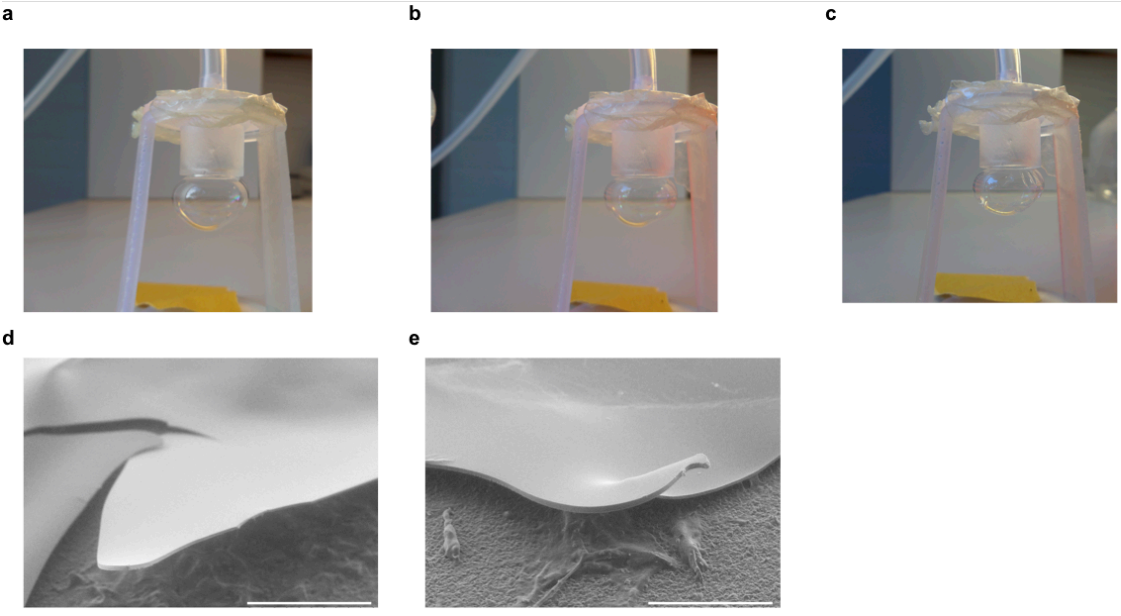

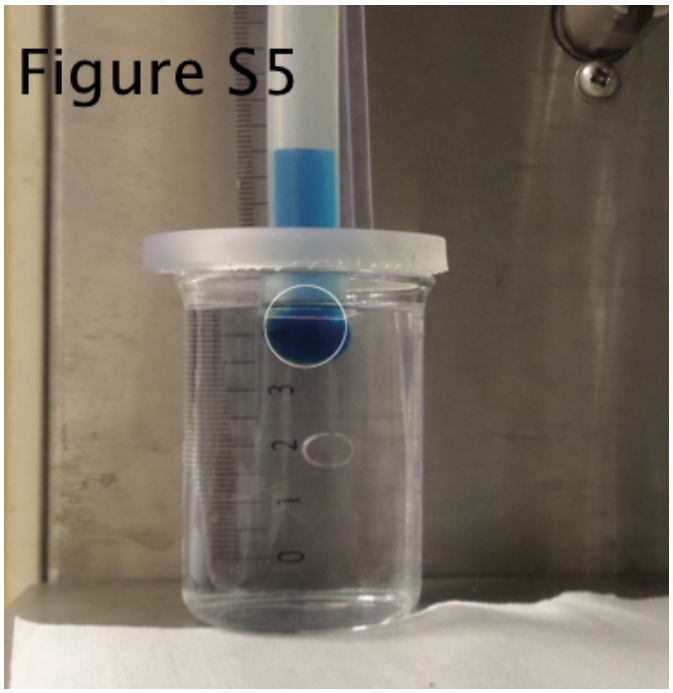
Figure S5

Figure S6

a

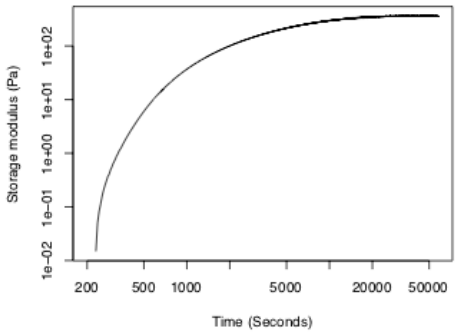
Storage modulus (Pa)
1e−02
1e−01
1e+00
1e+01
1e+02
200
500
1000
5000
20000
50000
Time (Seconds)

b

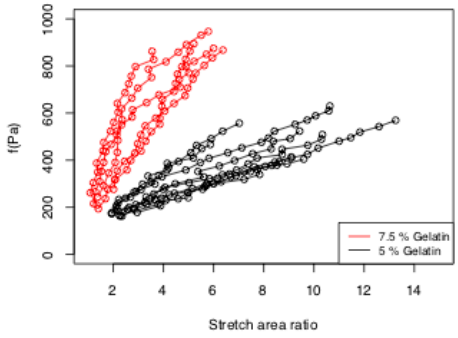
f(Pa)
0
200
400
600
800
1000
2
4
6
8
10
12
14
Stretch area ratio
7.5 % Gelatin
5 % Gelatin